HYDRAULIC PROPERTIES OF RECYCLED WOOD MATERIAL

by

VANDANA SUBROY

A Thesis submitted to the

Graduate School-New Brunswick

Rutgers, The State University of New Jersey

in partial fulfillment of the requirements

for the degree of

Master of Science

Graduate Program in Environmental Sciences

written under the direction of

Daniel Giménez

and approved by

_____

_____

_____

New Brunswick, New Jersey

[January, 2013]

ABSTRACT OF THE THESIS

HYDRAULIC PROPERTIES OF RECYCLED WOOD MATERIAL

By

VANDANA SUBROY

Thesis Director:

Daniel Giménez

Abstract

Leachate from ground wood stockpiled at recycling facilities may be detrimental to water quality. Although mathematical modeling of water movement through stockpiles may help estimate leachate quantity, information on water retention and unsaturated hydraulic conductivity of wood particles needed to run the models are unavailable. Our objectives were to (a) estimate the hydraulic properties of field stockpiled wood material, (b) assess performance of three models of pore structure in simulating water flow, and (c) determine relationships between optimized hydraulic parameters and particle size.

The particle size distributions (PSDs) of thirty samples collected from stockpiles of coarsely and finely ground wood were measured, and their geometric mean diameters (d_g) and distribution spreads (S_o) were used to establish two groups (I and II), with Group I samples having greater d_g values for any given S_o than Group II samples. Six samples

with PSDs representative of both groups were selected for hydraulic characterization. Material was packed in acrylic flow cells and outflow was induced by applying successive pressure potentials of -2, -10 and -40 cm to the bottom of the cells. Water retention data from outflow tests and from steady state measurements carried out in pressure extractors at potentials of -200, -500, -2000 and -10000 cm were fitted to unimodal and bimodal water retention functions. Inverse modeling of outflow data was performed using the software HYDRUS-1D and assuming (1) a unimodal pore-size distribution-SPM, (2) a bimodal pore-size distribution –DPM, (3) two distinct and interacting pore domains each with their own water retention and hydraulic conductivity functions-DPeM.

Wood material released almost 50% of their total water at -2 cm with Group I samples releasing significantly higher volumes than Group II. All models of pore structure captured outflow dynamics. Statistical tests indicated that the DPeM followed by the SPM were the best models for conductivity and the DPM for water retention. Parameters of hydraulic models could be estimated from PSD data. Predictions by all models indicate that hydraulic conductivity of the unsaturated material is very low (around 0.09 cm/hr at -10 cm), suggesting that water would move slowly through stockpiles except during intense rainfalls.

Acknowledgements

This thesis was only possible because of the essential support of many people whom I would like to gratefully acknowledge:

My advisor, Dr. Daniel Giménez, for his *infinite* patience, supportive suggestions and invaluable guidance throughout this research.

My committee members, Dr. Peter Strom and Dr. Uta Krogmann, for their belief in me, and support of my work and also their helpful recommendations for my thesis.

Dr. Robert Miskewitz (Rutgers University) and Mike Lusk (Intermountain Environmental Inc.,) for their help in computer programming and the wiring of instruments needed to run my experiments.

Kate Sullivan for her monumental assistance with field sampling, and Fernando Collazo, Natalie Pabon and Leonardo Calderón for their spirited assistance in the laboratory.

The New Jersey Department of Environmental Protection for their financial support without which this research would not have been possible.

Finally, and most importantly, my parents and my sister Varsha, for their love and support which enabled me to strive and see this work through.

Table of Contents

List of Tables

List of Figures

List of Appendices

List of Selected Symbols

Symbol	Description	Example of dimension
Symbols in pore models		
α	Parameter in the van Genuchten (1980) model	cm^{-1}
α_1 , α_2	Parameters in the Durner (1994) bimodal pore model for the 1st (1) and 2nd (2) subsystem of pores	cm^{-1}
α_M , α_m	Parameters in the dual permeability model for the macropore (M) and matrix (m) domains	cm^{-1}
K_s	Saturated hydraulic conductivity	cm/hr
K_{sM}, K_{sm}	Saturated hydraulic conductivities for the macropore (M) and matrix (m) domains	cm/hr
n	Parameter in the van Genuchten (1980) unimodal pore model	—*
n_1 , n_2	Parameters in the Durner (1994) bimodal pore model for the 1st (1) and 2nd (2) subsystem of pores	—
n_M , n_m	Parameters in the dual permeability model for the macropore (M) and matrix (m) domains	—
θ	Volumetric water content	cm^3/cm^3
θ_r, θ_s	Residual (*r*) and saturated (*s*) volumetric water contents	cm^3/cm^3
θ_{rM}, θ_{sM}	Residual (*rM*) and saturated (*sM*) volumetric water contents of the macropore region	cm^3/cm^3
θ_{rm}, θ_{sm}	Residual (*rm*) and saturated (*sm*) volumetric water contents of the matrix region	cm^3/cm^3
w_1, w_2	Weight of the 1st (1) and 2nd (2) subsystem of pores in the Durner (1994) bimodal pore model	—
w_M, w_m	Weight of the macropore (M) and matrix (m) pore domains in the dual permeability model	—
Other symbols		
A	Cross-sectional area of the flow cell	cm^2
d	Opening diameter in a sieve	µm
d_g	Geometric mean diameter	µm
d_{gi}	Geometric mean of material retained between the *ith* and *(i+1)th* sieves	µm
f_i	Mass fraction of particles with geometric mean d_{gi}	—
h	pressure potential	cm
H	Height of the flow cell	cm
η	Porosity of the packed column of wood particles	cm^3/cm^3
η_p	Porosity of an individual wood particle	cm^3/cm^3
Q	Flow rate at steady state	cm^3/hr
S_o	Sorting coeffieient	µm
v_p	Volume of an individual wood particle	cm^3

* non-dimensional

1. Introduction

In 2010, 57% of the 17 million metric tons of urban tree and woody yard residue generated was recovered for reuse and recycling in the United States (Falk and McKeever, 2004; USEPA, 2010). Wood recycling facilities that process tree and woody yard residue for landscape mulch typically grind up the incoming material twice, and stockpile it outdoors for periods of time ranging from weeks to months. Leachate from wood piles is of concern due to it toxicity to aquatic life, which has been attributed to low pH and high concentrations of organic compounds such as tannin, lignin, tropolone, terpene and lignan (Zenaitis and Duff, 2002; Tao et al., 2007; Hedmark and Scholz, 2008). Environmental impacts of leachate to surface and groundwater can be assessed with numerical models. For porous systems such as land-filled solid waste and waste rock piles from mines, numerical models have been used to simulate the flow, transport and distribution of water and contaminants and estimate leachate quantity, as well as provide guidance on the design of control and collection systems for leachate (El-Fadel et al., 1997, Fala et al, 2005; Molson et al, 2005, Khire and Mukherjee, 2007; Fellner and Brunner, 2010; Safari et al., 2012).

We have found only one published study on the simulation of water movement through wood chip media. The model in that study (Seng et al., 2012) however, focused only on the movement of water in a static cylindrical composting reactor containing wood chips through evaporation, diffusion and percolation and did not incorporate the

external addition of water into through precipitation which would be required to model fluid flow through field stockpiles of ground wood.

Solutions of non-linear flow equations needed to model fluid movement in unsaturated porous media require information on water retention and hydraulic conductivity functions of the material (Han et al., 2011). Hydraulic characterization of wood particle media has been limited to porosity and saturated hydraulic conductivity measurements on woody biofilter media (Table 1), which are highly porous with particle sizes and hydraulic conductivities being on the order of those of gravel with sizes of 2-80 mm (Gee and Bauder, 1986) and 108-10800 cm/hr, (Domenico and Schwartz, 1998), respectively.

There is, therefore, a need for information about the hydraulic properties of wood particles over a wide range of particle sizes. Field techniques to measure hydraulic conductivity of porous media such as soils (Amoozegar and Warrick, 1986; Green et al., 1986) and land filled municipal solid waste (Ettala, 1987; Oweis et al., 1990; Shank, 1993; Jain et al., 2006) are unsuitable for stockpiles of ground wood because of their irregular geometry, the low density of the material and the inability to control boundary conditions. Steady state laboratory techniques to measure the water retention curve (Dane et al., 2002) have been found to be inadequate to accurately measure near-saturation hydraulic properties of porous systems with large-sized pores (e.g. Logsdon et al., 1993) and the same may hold true for wood particle media as well.

The mathematical technique of inverse modeling estimates parameters of interest by minimizing an objective function between measured and predicted values of a process

that varies with time (Hopmans et al., 2002). Estimation of hydraulic parameters by inverse modeling involves selecting water retention and hydraulic conductivity functions and solving the governing flow model iteratively (Hopmans et al., 2002). The selection of the water retention and associated hydraulic conductivity functions should reflect the nature of the pore system of the material studied. Likewise, the process selected for simulation should be designed to augment the characteristics of the pore system to be characterized.

Hydraulic parameters for solid waste samples have been determined by inverse modeling data of cumulative drainage from saturated columns induced by pressures of increasing magnitude applied in multiple steps (Scicchitano, 2010; Han et al., 2011). The water retention and hydraulic conductivity functions of the unimodal pore model by van Genuchten (1980) have been widely used to describe water retention functions for a multitude of materials such as soils (Han et al., 2010), compost (Naasz et al., 2005; Londra, 2010; Al Naddaf et al., 2011), solid waste (Kazimoglu et al.,2006; Scicchitano, 2010; Han et al., 2011), land-filled municipal solid waste (Johnson et al., 2001; Haydar and Khire, 2005; Khire and Mukherjee, 2007; Fellner and Brunner, 2010) and waste rock piles (Fala et al, 2005; Molson et al, 2005). The assumption, however, of a unimodal distribution of pore sizes may not be valid and may not be able to account for preferential flow through large pores (e.g. Gärdenäs et al., 2006). Therefore, models incorporating a dual (bimodal) subsystem of pores with uniform flow and also assuming dual interacting pore domains with non-equilibrium flow need to be considered when modeling porous media with a wide range of particle sizes.

The objectives of this work therefore were to: 1) use multistep flow experiments to estimate hydraulic parameters of wood particle media with different size distributions representative of material stockpiled in the field, 2) assess the performance of different models of pore structure of increasing complexity for their ability to simulate the movement of water through the wood particles and 3) evaluate relationships between predicted hydraulic parameters of the models considered and particle size of the material. Inverse modeling was carried out using the software package HYDRUS-1D version 4.14 (Šimůnek et al., 2009).

2. Materials and methods

2.0. Overview of experiments

Physical characterization of bulk density and particle size distribution (PSD) was carried out on 30 samples. A composite of the 30 samples was used to determine water retention data at pressure potentials ranging from -200 to -10000 cm. Based on PSD analyses a subset of six samples was selected for hydraulic characterization of porosity, saturated hydraulic conductivity and multistep outflow. Hydraulic parameters were obtained by inverse modeling flow data from the multistep outflow experiments using HYDRUS-1D.

2.1. Materials

A total of 30 samples consisting of both coarsely (once) and finely (twice) ground recycled wood material were obtained from material stockpiled at three facilities in New Jersey. A composite sample of material from the top middle, and bottom of piles was mixed on site and allowed to air-dry for one month at laboratory conditions. The moisture content of air-dried samples was on an average 7 (±5) %, and was used to correct bulk density and particle size distribution data to oven-dry (105±3°C for 24 hours) moisture content.

2.2. Sample characterization

2.2.1. Bulk density

One kilogram of air-dried material was loosely packed in a calibrated container and dropped 15 times from a height of 15 cm (ASAE S269.4, 1992) on to a rubber mat. The depth of the settled material after the 15th drop was measured at three points in the container, and the average depth after each of those drops was converted to volume and used to estimate bulk density (ρ_b). The changing bulk density with increasing number of drops for all samples is shown in Appendix I.

2.2.2. Particle size distribution

Particle size distribution (PSD) was determined in triplicate by mechanical sieving of 2 L samples (ASAE S424.1, 1992) through a set of 10 US Standard sieves with openings (μm) of 25400, 19050, 9525, 5660, 2830, 1410, 590, 297, 149, and 63. Non-wood materials were removed before sieving and results were expressed as mass percent of material retained on each sieve.

Triplicate measurements of cumulative masses expressed as percent of material retained on a sieve (*F(d)*) was fitted with either a power (Eq. 1) or a sigmoidal (Eq. 2) function using the Solver® software in Microsoft Excel® (Microsoft Corp., Redmond, WA).

$$F(d) = b(d)^a \quad (1)$$

$$F(d) = \frac{1}{\left[1+\left(\frac{I_d}{d}\right)^k\right]^{\left(1-\frac{1}{k}\right)}} \quad (2)$$

Where, d is the opening diameter in a sieve, and b, a, I_d and k are fitting parameters. The 1st (d_{25}) and the 3rd (d_{75}) quartile diameters of a PSD, were estimated with either Eq. (1) or Eq. (2) and used to calculate the sorting coefficient (S_o) of the distribution as (Lotspeich and Everest, 1981):

$$S_o = \sqrt{\frac{d_{75}}{d_{25}}} \quad (3)$$

The geometric mean diameter (d_g) was calculated as:

$$d_g = \prod_{i=1}^{n} {d_{gi}}^{f_i} \quad (4)$$

Where d_{gi} is the geometric mean of material retained between the *ith and (i+1)th* sieves and f_i is the mass fraction of particles with geometric mean d_{gi}.

2.2.3. Steady state measurements of water retention at pressure potentials between -200 and -10000 cm

A composite of all samples was made by mixing 1 L of each of the 30 samples and its PSD determined in triplicate. The composite was sieved into six size classes with upper bounds of 9525 µm, 5660 µm, 2830 µm, 1410 µm, 590 µm and 297 µm. [Note: each size class was obtained by passing material through a single sieve and not sequentially through a set of sieves]. Four replicate samples in each size class were packed into rings (1 cm in height and 5 cm in diameter) and placed in a pressure plate extractor (Soilmoisture Equipment Corporation, Santa Barbara, CA) at pressure potentials of -200 cm and -500 cm for 31 days and at -2000 cm and -10000 cm for 66 days to ensure equilibration. Samples removed from the pressure extractors were oven-dried at 105°C for 24 hours to determine their water content at the end of the experiment.

The geometric mean diameter of each size class was calculated with Eq. (4) considering only the size classes mixed. For each pressure potential, the relationship between volumetric water content (θ) and the calculated d_g of a size class was given by:

$$\theta = p{d_g}^q \quad (5)$$

where, p and q are fitted parameters (Table 2). The fitted θ-d_g curves (Fig. 1) were extrapolated to the d_g values of the samples used in outflow experiments to estimate their volumetric water contents in the range of pressure potentials measured with pressure extractors (-200 cm to -10000 cm).

2.2.4. Water absorption and porosity measurements in individual wood particles

A total of 33 air-dried wood particles greater than 297 µm in diameter were weighed, saturated in de-ionized water and weighed periodically for 15 days. The volume of each particle of wood was determined using an Elcometer® 1800 Densimeter (Elcometer Inc., MI) and used to determine the porosity of a particle calculated as the ratio of the volume of water absorbed in that period to the volume of the particle.

2.3. Flow experiments

Measurements of porosity (η), saturated hydraulic conductivity (K_s) and outflow rate of packed columns of wood mulch were carried out in acrylic flow cells (Soil Measurement Systems, Tuscon, AZ) 15 cm in height and 12 cm in internal diameter (Fig. 2). Each cell had two 1.5 cm diameter ports located 3 cm from the top and bottom, that were used to accommodate ceramic tensiometers, 3 cm long and 1cm in diameter with a bubbling pressure of ½ bar. Each tensiometer was connected to a pre-calibrated pressure

transducer (model 26PCAFA6D, Honeywell Sensing and Control, Morristown, NJ) monitored with a CR1000 data logger (Campbell Scientific Inc., Logan, UT). Samples were held between perforated metal-plate assemblies with the upper metal-plate used only during outflow measurements.

Air-dried material was packed directly on top of the lower metal-plate and incrementally around the saturated tensiometer-transducer systems to a target dry bulk density of 240 kg/m^3 which was the average determined for the 30 samples. Packed flow cells were saturated with deionized and deaerated water for 24 hours (Christianson et al., 2010). The amount of water added was determined by differences in mass before and after saturation. Porosity was calculated as the ratio of the volume of the water added to that of the empty flow cell.

After the measurement of porosity, saturated hydraulic conductivity was determined for the same sample by the constant head method (Chun et al., 2009; Christianson et al., 2010) by maintaining a constant pressure head of about 4 cm at the upper end of the flow cell by a Mariotte system. The outflow from the flow cell was collected every 30 seconds in a container placed on a balance (PB403-S/FACT, Mettler-Toledo Inc., Columbus OH) connected to a computer through RS-232 data acquisition software (WinWedge® version 3.X, TAL Technologies Inc., Philadelphia, PA) . The value of K_s (cm/hr) was calculated from (Jury et al., 1991):

$$K_s = \frac{Q\,H}{A(h+H)} \tag{6}$$

where, Q is the flow rate (cm^3/hr) at steady state (constant for an hour), A is the area (cm^2) and H is the height of the flow cell (cm) and h is the head (cm)]. The procedure

was repeated by decreasing *h* in two consecutive steps of approximately 1 cm and determining the corresponding *Q* values at equilibrium.

After determining K_s the flow cell was closed at the upper end with the perforated metal plate. At the lower end a disc of saturated sponge cloth (Spontex Inc., Columbia, TN) was placed in contact with the wood mulch and a filter paper #40 (Whatman, Clifton, NJ) was inserted between the sponge and the lower metal plate (Young et al., 2002). The K_s of the sponge cloth/filter paper combination was determined by the constant head method to be 0.6 cm/hr. The column was re-saturated and left overnight. During outflow experiments, the upper end of the flow cell was kept at atmospheric pressure and the lower end was equilibrated at successively decreasing pressure potentials of -2 cm, -10 cm and -40 cm for all samples but one, in which pressure potentials of -2 cm, -5 cm and -50 cm (replicate 1), and of -2 cm, -10 cm and -50 cm (replicate 2) were applied. The samples were kept at the pressure potential of -2 cm for about 5-7 days, at -5 or -10 cm for about 7- 10 days and at -40 or -50 cm for about 10-14 days to ensure that outflow was negligible at every pressure step. Data from the pressure transducers connected to the tensiometers were collected every 60 seconds for the first 3 hours after a change in pressure potential and thereafter every 15 minutes. Water draining from the flow cell was collected in a burette, which was emptied and weighed periodically to determine the cumulative outflow.

Once equilibrium was reached at the final pressure potential of -40 (or -50) cm, the water content of the material was determined from three sections in the flow cell comprising material between the two tensiometers, and above and below the upper and lower tensiometers, respectively. The water content remaining in the column was

expressed as the average of the water content in the three sections. The saturated water content of the material in a column was calculated by adding the cumulative volume of water drained during the experiment to the volume of water remaining after the final pressure step. Water retention at intermediate pressure potentials was determined by subtracting the cumulative volume of water that drained at a given pressure potential from the water content at saturation.

Water retention data from the outflow experiment (-2 to -40 or -50 cm) was supplemented with corrected data from the pressure extractor system (-200 to -10000 cm) and fitted with both unimodal (van Genuchten, 1980) and bimodal (Durner, 1994) functions (Table 3) using the SWRC Fit web interface (Seki, 2007) [http://seki.webmasters.gr.jp/swrc/].

2.4. Inverse modeling

Experimental observations of cumulative outflow and pressure head data from the multistep outflow procedures were inversely modeled to obtain the hydraulic parameters using the software package HYDRUS-1D (Šimůnek et al., 2009). Three different models of pore structure were considered (Table 3 and Fig. (3)): (1) a single porosity model (SPM) which assumes that the pore size distribution is unimodal and the water retention function is described by the van Genuchten (1980) model, (2) a dual porosity model (DPM) characterized by a bimodal distribution of pore sizes consisting of two overlapping subsystems of pores. The water retention function of each subsystem is described by the van Genuchten (1980) model linearly added to give the function for the total pore system (Durner, 1994), and (3) a dual permeability model (DPeM) in which the

pore system consists of two overlapping and interacting pore *domains*, each assumed to have an unimodal pore size distribution with their own water retention and hydraulic conductivity functions (Gerke and van Genuchten, 1993).

Both the SPM and the DPM are characterized by a single flow domain with the porous medium consisting of impervious particles separated by pores through which flow and transport takes place (Šimůnek and van Genuchten, 2008). The DPeM on the other hand assumes that the particles of the porous medium are also permeable, with water moving relatively fast in the inter-particle pore domain or macropore when close to saturation and slowly in the intra-particle pore domain or matrix (Šimůnek and van Genuchten, 2008). Differences in permeabilities between the two domains give rise to non-equilibrium flow in the DPeM. In this study, the macropore domain in the DPeM was assumed to retain water in the pressure potential range from 0 to -2 cm.

To ensure that the solution of the inverse problem exists and is unique and stable, the number of parameters that need to be estimated to solve the continuity equation(s) (Table 3) should be limited (Hopmans et al., 2002). The strategy used to fit the outflow and pressure plate data for different models is summarized in Table 3. The sponge-cloth filter paper combination placed at the lower end of the flow cell was accounted for as a second material during inverse modeling. To ensure that the combination remained saturated during inverse modeling, α and n were fixed at $1x10^{-20}$ cm^{-1} and 1.001 (Šimůnek et al., 2009), respectively; while its residual and saturated water contents were fixed at 0 (complete dryness) and 1 (complete saturation), respectively.

2.5. Goodness-of-fit

The goodness-of-fit of the models was determined by partitioning the sum of the squares of the residuals (SSR) [$\sum_{i=1}^{n}(y_i - x_i)^2$] as (Whitmore, 1991):

$$\sum_{i=1}^{n}(y_i - x_i)^2 = \sum_{i=1}^{n}\left((y_i - x_i) - (\bar{y} - \bar{x})\right)^2 + \sum_{i=1}^{n}(\bar{y} - \bar{x})^2 \quad (7)$$

Where, y_i are the observations and x_i are the corresponding predictions by the model, and $\bar{y}$ and $\bar{x}$ are the mean of the n observations and predictions, respectively. The first term on the right hand side measures the *error* or random variation between observations and predictions (ERR), and the second term measures the *lack of fit* or systematic variation that can be attributed to the model (LOFIT). The model is considered to be reliable if the LOFIT is not significantly larger than the ERR (Whitmore, 1991).

Considering that the three models used have different number of parameters (Table 3), the best model for the observed data was selected using the Akaike's Information Criterion (AIC_c) calculated as (Burnham and Anderson, 1998):

$$AIC_c = N[\ln\left(\frac{SSR}{N}\right)] + 2K + \frac{2K(K+1)}{(N-K-1)} \quad (8)$$

Where, N is the number of data points or observations and K is the number of estimable parameters in the model. Equation (8) is used when N/K has a value of less than 40 to correct for small sample bias. The model with the lowest AIC_c value (AIC_{cmin}) or the model with $\Delta = 0$ is chosen as the best from the set of models tested, where

$$\Delta = AIC_c - AIC_{cmin} \quad (9)$$

Whitmore's (1991) test and the AIC_c analysis were carried out separately for cumulative outflow data and pressure head data for a sample.

3. Results and Discussion

3.1. Physical and hydraulic characterization

Two distinct groups of wood mulch samples were identified based on the values of their sorting coefficient (S_o) and geometric mean diameter (d_g), with samples in Group I having greater d_g values for any given value of S_o than samples in Group II (Fig. 4). The mass percentages of particles passing the sieve with 2800 µm opening (i.e., fines) in samples of Group I (66±14%) and Group II (40±6%) in this study were higher than in those reported in the literature (Table 1). The shape of the particle size distributions was different between groups, with Eq. (1) fitting Group I and Eq. (2) Group II samples (Fig. 5). The measured and fitted particle size distributions of the 30 samples are given in Appendix I.

The distribution of particle sizes in a mix influenced the volumetric water content θ retained at a given pressure potential (Fig. 1). The increase in θ with d_g may be due to the decrease in porosity of wood particles (η_p) with decrease in particle size (Table 4, Fig. 6). Wood particles smaller than 590 µm were observed to be slightly hydrophobic.

Six duplicate samples with particle size distributions representative of Group I and II were selected for hydraulic characterization (Fig. 4). There was no significant difference (P>0.05) between the average porosity of the selected Group I (0.73 cm^3/cm^3) and Group II (0.76 cm^3/cm^3) samples or of their average measured K_s values of 58 cm/hr and 63 cm/hr, respectively (Table 5). Measured porosities were in the range reported by other studies with woodchips, but measured K_s values were much lower than those

reported (Table 1). This possibly may be due to the higher amount of fines, which were observed to settle at the bottom of the flow cell during K_s measurements, resulting in reduced conductivity (Schälchli, 1992). Porosity values measured before the outflow experiments were on an average 6.1(±4.4)% lower than the water content at saturation back-calculated from the outflow experiment. It is likely that wood particles had continued to absorb water in the approximately 48 hour period between the measurement of porosity and the start of the outflow experiment. In fact from the water absorption study on individual wood particles, particles >9500 µm absorbed water over the 15 day period of saturation while smaller particles were fully saturated within 24 hours. Porosity values of packed columns of wood particles measured after 24 hour saturation therefore, may not be representative of the actual porosity of the material, and must be made after allowing the material to saturate for a longer period of time, especially if the material is comprised of large particles.

3.2. Multistep outflow and inverse modeling

The outflow characteristics of the two groups were different, with Group I samples releasing a significantly greater (P= 0.00007) amount of the total water at the first pressure potential of -2 cm (56±2%) compared to Group II samples (43±5%). During the outflow experiment, differences in pressure potential between the upper and lower tensiometers were roughly equal to their differences in height as expected for near saturation systems (Fig. 7). For the first two pressure steps, the deviation between the expected values of pressure potentials based on the position of the tensiometers and their readings at equilibrium were between 0 and 3 cm for samples of Group I, and 0 and 5 cm for samples of Group II (Fig. 7). The deviation at the third step increased to an average of

8 cm for Group I and 16 cm for Group II. There is no explanation for the larger deviation in samples of Group II, but there is a possibility that deviations in general were caused by the decrease in contact area between the ceramic tensiometer cup and the irregularly-shaped wood particles, leading to an increase in tensiometer response time (Watson, 1965). The outflow and pressure head data for the six duplicate samples are given in Appendix II.

Water retention data from outflow experiments and pressure extractors were fitted with the van Genuchten (1980) and the Durner (1994) functions (Tables 6a and 6b). Fitted parameters from both models showed great variation between sample replicates and also between samples, and when used as inputs in HYDRUS-1D they did not simulate the outflow dynamics well. Therefore, inverse modeling of cumulative outflow and pressure potential data were used to optimize parameters defining the shape of water retention functions over the entire range investigated (SPM) or near saturation (DPM and DPeM). For the DPM and DPeM, parameters defining the drier range of water retention functions obtained by fitting data from pressure extractors were used to limit the number of parameters optimized during inverse modeling (Table 3). Consequently, inverse modeling with models SPM, DPM and DPeM required the optimization of two, three and six parameters, respectively (Table 3). Water retention data between -2 and -10000 cm was only included for optimization in the objective function of the DPM since preliminary runs indicated that water retention did not improve the fitting in either the SPM or the DPeM. Also, since our focus was on outflow prediction, the weight given to cumulative outflow data was five times that given to pressure head data for inverse modeling.

All models fitted the measured data reasonably well with R^2 greater than 0.82 in most cases (Tables 7a, 7b and 7c). According to the Whitmore (1991) test, all three models reproduced the major features of outflow dynamics (Table 8). Among the models, the DPeM provided the best prediction of cumulative outflow (lowest AIC_c value) in eight of the twelve samples, and the SPM in the remaining four samples. For pressure head data predictions, the AIC_c analysis supported the SPM in 42% of the cases over other models (Table 8). However, the sum of square of the residuals (SSR) of the pressure head increased with sample d_g for all three models suggesting that the tensiometer measurements in columns with large d_g may have not captured the pressure potentials inside the column.

Since the particles of wood are porous, the assumption of the pore system in wood mulch as two overlapping and interacting flow domains with vastly different hydraulic properties by the DPeM would seem to be most favorable to represent the material. This characterization allows the DPeM to simulate macropore flow during saturated conditions and also base matrix flow during unsaturated conditions (Gärdenäs et al., 2006) making it suitable to capture the dynamics of flow through the wood mulch system as opposed to a single flow domain as assumed by the SPM and the DPM. The DPeM also outperformed the more commonly used SPM in a study to determine the hydraulic properties of paper waste of different sized particles from laboratory multistep outflow experiments (Han et al., 2011).

Defining two subsystems of pores for the hydraulic functions as in the DPM enabled it successfully replicate the measured water retentions with accuracy comparable to those obtained by fitting static water retention data (Fig. 8). On the other hand, the

SPM and the DPeM which assume a homogeneous distribution of pores in their domains (single and dual, respectively) overestimated the water content at -2 cm by an average of 21% and 14%, respectively, and under estimated the water contents at pressure potentials less than about -10 cm by an average of 8%. In a research using paper waste the SPM performed similarly to this study and underestimated the water content in the matrix domain (Han et al., 2011). The DPeM in this investigation additionally under estimated the saturated water contents by an average of 7%. In comparison the only noticeable deviation of the DPM occurred at -2 cm and was an average of 5%. Measured and predicted water retentions for the six duplicate samples are given in Appendix III.

Predictions by the models indicate that the hydraulic conductivity of the material will quickly drop with the application of pressure potentials less than -10 cm (Fig. 9 and Appendix III). Hydraulic conductivities at -10 cm were significantly (P=0.011) different between the two groups and were on an average 0.12 and 0.03 cm/hr for Groups I and II, respectively. This trend is expected since samples in Group I comprise of larger sized particles and therefore have fewer smaller sized pores available for conductivity than Group II samples at the same pressure potentials. The same analysis also explains the inverse trend observed between values of predicted saturated matrix conductivity (K_{sm}) and d_g by the DPeM (Table 7c) even though there was no significant (P=0.228) difference in K_{sm} values between Group I (0.16 cm/hr) and Group II (0.33 cm/hr).

Since field stockpiles of coarsely and finely ground wood material are unsaturated most of the time, the low values of predicted unsaturated conductivity suggest that water (and hence, contaminants) will move slowly through them. However, when there are extended and substantial rains the stockpiled wood material may retain a greater amount

of water leading to a preferential flow in regions of greater saturation (Molson et al., 2005) and perhaps an increase in leachate especially from piles of finely ground material.

3.3.Relationship between particle size and optimized hydraulic parameters

A way to assess whether the predicted hydraulic parameters have a physical meaning is to find a correlation with independently measured physical properties of the system such as parameters defining particle size distributions (PSD) like the geometric mean diameter (d_g) and the sorting coefficient (S_o).

The average value of parameter *n* predicted by the SPM demonstrated a direct relationship with d_g (Fig. 10). This trend is physically sound since *n* is regarded as the slope of the water retention curve and as such it is expected to be greater for samples with larger pores (larger d_g) to simulate the rapid drop in their water contents with small pressure changes near saturation. Models that consider a dual organization of pores (DPM and DPeM) have parameters that assign weights to the pore systems or pore domains. In the DPM, the parameter w_1 is a measure of the importance of the first subsystem of pores (near saturation). The values of parameter w_1 predicted by the DPM increased with d_g up to about 3000 µm and thereafter remained constant at 0.60 (Fig. 11), indicating that the system of larger pores was more important in samples of larger particles. This trend is consistent with the fact that samples with d_g > 3000 µm hold more water between saturation and -2 cm, and therefore have lower water contents at – 2 cm (0.38) than samples with d_g < 3000 µm (0.49). In samples with a d_g of about 2000 µm both pore systems were seen to be equally important (w_1=0.5). For the DPeM, the parameter w_M (Table 3) denotes the macroporosity in a sample. Unlike w_1 the predicted

w_M values did not show any relationship with d_g and it was not significantly (P=0.397) different between Groups I (0.48) and II (0.51). This result is expected since the predicted saturated macropore conductivities (K_{sM}) (Table 7c) did not show a trend with d_g themselves or a significant (P=0.535) difference between groups implying that the macropore system itself behaved in the same manner.

Both the hydraulic parameters of the second subsystem of pores i.e., α_2 and n_2, obtained by fitting the steady state retention data, decreased with increase in d_g (Figs. 12 and 13). This indicates that samples with larger sized particles have fewer small pores than samples with lower d_g values, and release water gradually at very low negative pressure potentials.

Predicted macropore inflection points (α_M) by the DPeM demonstrated a direct relationship with d_g. Since the inflection point is considered to be roughly the inverse of the air entry value (van Genuchten and Nielsen, 1985) the result indicates a decrease in the air entry pressure potential for the macropore region with increase in particle size (Fig. 14). Consequently stockpiles with larger sized particles will be expected to drain faster with small pressure potential changes near saturation. A similar result was obtained by Han et al. (2011) in their study on paper waste of different particle sizes.

An important finding in this study was that of a direct relationship between the ratio of the first to the second inflection point, I_R, with d_g for both the DPM and the DPeM (Fig. 15). The I_R-d_g relationship is significant in that it enables the inflection point of one pore system (or pore domain) to be calculated if the PSD of the material and the inflection point of the second pore system (or pore domain) is known.

4. Conclusions

Recycled wood material was found to have a complex pore system, requiring a dual subsystem of pores to describe its water retention and a dual flow domain model to describe its outflow characteristics. Hydraulic parameters estimated from inverse modeling using transient flow data were more representative of the pore system found in wood mulch than parameters estimated from static measurements of water retention. This validates the use of transient flow data over steady-state data to describe the hydraulic properties of the system. The geometric mean diameters of particle size distributions were correlated to several hydraulic parameters which opens the possibility to estimate them from particle size data.

Results of this investigation suggest that water movement through recycled wood stockpiles is slow except for periods of extended and substantial rain events which might lead to preferential flow through regions of higher saturation in the pile. Since smaller sized wood particles have lower porosities and higher water absorption rates than larger pieces, it may be necessary then to grind incoming material at wood recycling facilities only once for on-site storage to limit the amount of leachate. Simulations of 2D/3D movement of water through the stockpiles of different geometries may then help determine the pile geometry that leads to the least leachate as has been done for waste rock pile from mines (Fala et. al., 2005).

References

Al Naddaf, O., Livieratos, I., Stamatakis, A., Tsirogiannis, I., Gizas, G., Savvas, D., 2011. Hydraulic characteristics of composted pig manure, perlite, and mixtures of them, and their impact on cucumber grown on bags. Scientia Horticulturae 129, 135-141.

Amoozegar, A., Warrick, A.W., 1986. Hydraulic conductivity of saturated soils: Field methods, in: Klute, A. (Ed.), Methods of soil analysis. Part 1. Physical and mineralogical methods, 2nd ed. ASA and SSSA, pp. 735-770.

ASAE, 1992. S269.4. Cubes, pellets and crumbles-Definitions and methods for determining density, durability and moisture content., ASAE Standards 1992. American Society of Agricultural Engineers, St. Joseph, MI, USA, pp. 384-386.

ASAE, 1992. S424.1. Method of determining and expressing particle size of chopped forage materials by screening, ASAE Standards 1992. American Society of Agricultural Engineers, St. Joseph, MI, pp. 414-416.

Burnham, K.P., Anderson, D.R., 1998. Model selection and inference: A practical information theoretic approach. Springer-Verlag, New York.

Christianson, L., Castello, A., Christianson, R., Helmers, M., Bhandari, A., 2010. Hydraulic property determination of denitrifying bioreactor fill media. Applied Engineering in Agriculture 26, 849-854.

Chun, J.A., Cooke, R.A., Eheart, J.W., Kang, M.S., 2009. Estimation of flow and transport parameters for woodchip-based bioreactors: I. laboratory-scale bioreactor. Biosystems Engineering 104, 384-395.

Dane, J.H., Hopmans, J.W., Romano, N., Winfield, K.A., Nimmo, J.R., Spaana, E.J.A., Baker, J.M., 2002. Water retention and storage, in: Dane, J.H., Topp, G.C. (Eds.), Methods of soil analysis. Part 4. Physical methods. ASA and SSSA, Madison WI, pp. 671-720.

Domenico, P.A., Schwartz, F.W., 1998. Chemical and Physical Hydrogeology, 2nd ed. John Wiley and Sons, New York.

Durner, W., 1994. Hydraulic conductivity estimation for soils with heterogeneous pore structure. Water Resources Research 30, 211-223.

Eching, S.O., Hopmans, J.W., Wendroth, O., 1994. Unsaturated hydraulic conductivity from transient multistep outflow and soil-water pressure data. Soil Science Society of America Journal 58, 687-695.

Ettala, M., 1987. Infiltration and hydraulic conductivity at a sanitary landfill. Aqua Fennica 17, 231-237.

Fala, O., Molson, J.W., Aubertin, M., Bussiere, B., 2005. Numerical modelling of flow and capillary barrier effects in unsaturated waste rock piles. Mine Water and the Environment 24, 172-185.

Falk, R. H., McKeever, D. B. 2004. Recovering wood for reuse and recycling: a United States perspective. European COST E31 Conference: Management of Recovered Wood Recycling Bioenergy and other Options: Proceedings, 22-24 April 2004, Thessaloniki. Thessaloniki: University Studio Press, 2004: Pages 29-40. Accessed from: http://www.epa.gov/epawaste/nonhaz/municipal/msw99.htm

Fellner, J., Brunner, P.H., 2010. Modeling of leachate generation from MSW landfills by a 2-dimensional 2-domain approach. Waste Management 30, 2084-2095.

Gärdenäs, A.I., Simunek, J., Jarvis, N., van Genuchten, M.T., 2006. Two-dimensional modelling of preferential water flow and pesticide transport from a tile-drained field. Journal of Hydrology 329, 647-660.

Gee, G.W., Bauder, J.W., 1986. Particle-size analysis, in: Klute, A. (Ed.), Methods pf soil analysis. Part 1. Physical and mineralogical methods, 2nd ed. ASA and SSSA, Madison, WI, pp. 383-409.

Gerke, H.H., van Genuchten, M.T., 1993. A dual-porosity model for simulating the preferential movement of water and solutes in structured porous-media. Water Resources Research 29, 305-319.

Green, R.E., Ahuja, L.R., Chong, S.K., 1986. Hydraulic conductivity of unsaturated soils: Predictions and formulas, in: Klute, A. (Ed.), Methods of soil analysis. Part 1. Physical and mineralogical methods, 2nd ed. ASA and SSSA, pp. 771-798.

Han, B.H., Scicchitano, V., Imhoff, P.T., 2011. Measuring fluid flow properties of waste and assessing alternative conceptual models of pore structure. Waste Management 31, 445-456.

Han, X.W., Shao, M.A., Horton, R., 2010. Estimating van Genuchten model parameters of undisturbed soils using an integral method. Pedosphere 20, 55-62.

Haverkamp, R., Parlange, J.Y., 1986. Predicting the water-retention curve from particle size dictribution.1. Sandy soils without organic-matter. Soil Science 142, 325-339.

Haydar, M.M., Khire, M.V., 2005. Leachate recirculation using horizontal trenches in bioreactor landfills. Journal of Geotechnical and Geoenvironmental Engineering 131, 837-847.

Hedmark, A., Scholz, M., 2008. Review of environmental effects and treatment of runoff from storage and handling of wood. Bioresource Technology 99, 5997-6009.

Hopmans, J.W., Simunek, J., Romano, N., Durner, W., 2002. Inverse methods, in: Dane, J.H., Topp, G.C. (Eds.), Methods of soil analysis. Part 4.Physical methods. ASA and SSSA, Madison, WI, pp. 963-1008.

Jain, P., Powell, J., Townsend, T.G., Reinhart, D.R., 2006. Estimating the hydraulic conductivity of landfilled municipal solid waste using the borehole permeameter test. Journal of Environmental Engineering-ASCE 132, 645-652.

Johnson, C.A., Schaap, M.G., Abbaspour, K.C., 2001. Model comparison of flow through a municipal solid waste incinerator ash landfill. Journal of Hydrology 243, 55-72.

Jury, W.A., Gardner, W.R., Gardner, W.H., 1991. Soil Physics, 5th ed. John Wiley and Sons, New York.

Kazimoglu, Y.K., McDougall, J.R., Pyrah, I.C., 2006. Unsaturated hydraulic conductivity of landfilled waste, in: Miller, G.A., Zapata, C.E., Houston, S.L., Fredlund, D.G. (Eds.), Fourth International Conference on Unsaturated Soils. ASCE, Carefree, Arizona, pp. 1525-1534.

Khire, M.V., Mukherjee, M., 2007. Leachate injection using vertical wells in bioreactor landfills. Waste Management 27, 1233-1247.

Logsdon, S.D., McCoy, E.L., Allmaras, R.R., Linden, D.R., 1993. Macropore characterization by indirect methods. Soil Science 155, 316-324.

Londra, P.A., 2010. Simultaneous determination of water retention curve and unsaturated hydraulic conductivity of substrates using a steady-state laboratory method. Hortscience 45, 1106-1112.

Lotspeich, F.B., Everest, F.H. 1981. A new method for reporting and interpreting textural composition of spawning gravel**.** Pacific Northwest Forest and Range Experiment Station, Research Note PNW-369. USDA Forest Service, Corvallis,OR.

Molson, J.W., Fala, O., Aubertin, M., Bussiere, B. 2005. Numerical simulations of pyrite oxidation and acid mine drainage in unsaturated waste rock piles. Journal of Contaminant Hydrology 78, 343-371.

Mualem, Y., 1976. A new model for predicting the hydraulic conductivity of unsaturated porous media. Water Resources Research 12, 513-522.

Naasz, R., Michel, J.C., Charpentier, S., 2005. Measuring hysteretic hydraulic properties of peat and pine bark using a transient method. Soil Science Society of America Journal 69, 13-22.

Oweis, I.S., Smith, D.A., Ellwood, R.B., Greene, D.S., 1990. Hydraulic characteristics of municipal refuse. Journal of Geotechnical Engineering-ASCE 116, 539-553.

Robertson, W.D., Yeung, N., van Driel, P.W., Lombard, P.S., 2005. High-permeability layers for remediation of ground water; Go wide, not deep. Ground Water 43, 574-581.

Safari, E., Ghazizade, M.J., Abdoli, M.A., 2012. A performance-based method for calculating the design thickness of compacted clay liners exposed to high strength leachate under simulated landfill conditions. Waste Management & Research 30, 898-907.

Schälchli, U., 1992. The clogging of coarse gravel river beds by fine sediment. Hydrobiologia 235, 189-197.

Scicchitano, V., 2010. Estimating hydraulic properties of landfill waste using multistep drainage experiments. M.S. Thesis, University of Delaware, Newark, DE.

Seki, K., 2007. SWRC fit- a nonlinear fitting program with a water retention curve for soils having unimodal and bimodal pore structure. Hydrology and Earth System Sciences Discussions 4, 407-437.

Seng, B., Kaneko, H., Hirayama, K., Katayama-Hirayama, K., 2012. Development of water movement model as a module of moisture content simulation in static pile composting. Environmental Technology 33, 1685-1694.

Shank, K.L., 1993. Determination of the hydraulic conductivity of the Alachua County southwest landfill. M.S. Thesis, University of Florida, Gainesville, FL.

Šimůnek, J., van Genuchten, M.T., 2008. Modeling nonequilibrium flow and transport processes using HYDRUS. Vadose Zone Journal 7, 782-797.

Šimůnek, J., Šejna, M., Saito, H., Sakai, M., van Genuchten, M. T. 2009. The HYDRUS-1D software package for simulating the one-dimensional movement of water, heat, and multiple solutes in variably-saturated media (version 4.08), Department of Environmental Sciences, University of California Riverside, Riverside, California.

Tao, W.D., Hall, K., Hall, E., 2007. Laboratory study on potential mechanisms for treatment of woodwaste leachate in surface flow constructed wetlands. Journal of Environmental Engineering and Science 6, 85-94.

USEPA.2010. Municipal solid waste generation, recycling, and disposal in the United States. Tables and Figures for 2010. Accessed from: http://www.epa.gov/epawaste/nonhaz/municipal/msw99.htm.

van Driel, P.W., Robertson, W.D., Merkley, L.C., 2006. Denitrification of agricultural drainage using wood-based reactors. Transactions of the ASABE 49, 565-573.

van Genuchten, M.T., 1980. A closed-form equation for predicting the hydraulic conductivity of unsaturated soils. Soil Science Society of America Journal 44, 892-898.

van Genuchten, M.T., Nielsen, D.R., 1985. On describing and predicting the hydraulic properties of unsaturated soils. Annales Geophysicae 3, 615-627.

Watson, K.K., 1965. Some operating characterisics of a rapid response tensiometer system. Water Resour. Res. 1, 577-586.

Whitmore, A.P., 1991. A method for assessing the goodness of computer-simulation of soil processes. Journal of Soil Science 42, 289-299.

Young, M.H., Karagunduz, A., Simunek, J., Pennell, K.D., 2002. A modified upward infiltration method for characterizing soil hydraulic properties. Soil Science Society of America Journal 66, 57-64.

Zenaitis, M.G., Duff, S.J.B., 2002. Ozone for removal of acute toxicity from logyard run-off. Ozone-Science & Engineering 24, 83-90.

Table 1. Physical and hydraulic characteristics of woody biofilter media.

Reference	Particle size	Bulk density (ρ_b) (kg/m^3)	Porosity (η) (cm^3/cm^3)	Saturated hydraulic conductivity (K_s)(cm/hr)	Mass percent of fines [d]
Robertson et al. 2005 [a]	1-50 mm	NR[c]	NR	39600 ± 10800	NR
Van Driel et al. 2006 [a]	coarse (1- 50 mm) fine (1-5 mm)	NR	0.70 (coarse); 0.47 (fine)	4320 ± 3600 (coarse); 432 ± 252(fine)	NR
Ima and Mann. 2007 [b]	2-25 mm	286 ± 1.7	0.63 ± 0.013	NR	7.4
Christianson et al. 2009 [b]	0-30 mm	200 - 243	0.66 -0.78	34200 ± 5760	<2
Chun et al., 2009 [b]	0–510 mm	200	0.79	9720 - 17640	29.5 [e]

[a] Field study; [b] Laboratory study; [c] NR - Not reported; [d] particles ≤2800 µm; [e] mass percentage of particles < 6000 µm.

Table 2. Parameter values from (Eq. (5)) obtained by fitting data pairs of geometric mean diameter (d_g) and corresponding volumetric water contents (θ) retained at different pressure potentials by woodchip mixes of different sizes (see also Figure 2).

Pressure potential (cm)	Fitted *p*	Fitted *q*
-200	0.1983	0.0250
-500	0.1865	0.0095
-2000	0.1484	0.0281
-10000	0.0820	0.0558

Table 3. Continuity equations, water retention [θ(h)] and hydraulic conductivity [K(h)] functions and the inverse modeling strategies for the three pore models considered.

	Model		
	SPM	**DPM**	**DPeM**
Continuity Eqn.	$\frac{\partial \theta(h)}{\partial t} = \frac{\partial}{\partial z}\left[K(h)\left(\frac{\partial h}{\partial z}+1\right)\right]$ [a]		$\frac{\partial \theta_M(h_M)}{\partial t} = \frac{\partial}{\partial z}\left[K_M(h_M)\left(\frac{\partial h_M}{\partial z}+1\right)\right] - \frac{\Gamma_w}{w_M}$ [b] $\frac{\partial \theta_m(h_m)}{\partial t} = \frac{\partial}{\partial z}\left[K_m(h_m)\left(\frac{\partial h_m}{\partial z}+1\right)\right] - \frac{\Gamma_w}{1-w_M}$ [c]
θ (h)	$\theta(h) = \theta_r + \frac{\theta_s - \theta_r}{[1+(\alpha h)^n]^m}$ [d]	$\theta(h) = \theta_r + \frac{(\theta_s-\theta_r)}{\sum_{i=1}^{k} w_i[1+(\alpha_i h)^{n_i}]^{m_i}}$ [e]	$\theta_i(h) = \theta_{ri} + \frac{\theta_{si}-\theta_{ri}}{[1+(\alpha_i h)^{n_i}]^{m_i}}$ [f]
K(h)	$K(h) = K_s S_e^{0.5}\left[1-\left(1-S_e^{1/m}\right)^m\right]^2$ [g]	$K(h) = K_s \frac{(\sum_{i=1}^{2} w_i S_{ei})^{0.5}\left[\left\{\sum_{i=1}^{2} w_i \alpha_i [1-(1-S_{ei}{}^{1/m_i})^{m_i}\right\}\right]^2}{(\sum_{i=1}^{2} w_i \alpha_i)^2}$	$K_i(h) = K_{si} S_{ei}^{0.5}\left[1-\left(1-S_{ei}^{1/m}\right)^m\right]^2$ [f]
Fixed parameters	θ_s [h], θ_r [i], K_s = measured value	θ_s [h], θ_r [i], K_s = measured value, α_2 [j], n_2 [k]	$\theta_{sM} = 1$, $\theta_{rM} = 0$, θ_{sm} [l], θ_{rm} [i], α_m [j], n_m [k] $a = r_g$ [m] β=3, γ_w=0.4
Optimized parameters	α, n	α_1, n_1, w_1	K_{sM}, K_{sm}, α_M, n_M, w_M, K_a

[a] Richards' equation. θ(h) [L^3L^{-3}] and K(h) [LT^{-1}] are the volumetric water content and the hydraulic conductivity functions respectively, corresponding to pressure head h [L], t is time [T], and z is the vertical axis [L].

[b and c] The continuity eqn. for the macropore and matrix systems, respectively (Gerke and van Genuchten, 1993). The macropore system was assumed to cover the range 0 to -2 cm. w_M is the fraction of the total volume occupied by macropores ($0<w_M<1$). Γw [T^{-1}] describes water exchange between the pore systems, calculated using $\Gamma_w = \frac{\beta}{a^2} K_a \gamma_w (h_M - h_m)$ where K_a is the effective saturated hydraulic conductivity of the interface between the two pore systems [LT^{-1}], β [−] is the shape factor of the porous particles of the material, a is the characteristic length of a particle [L], and γ_w is the dimensionless scaling factor.

[d] van Genuchten (1980). θ_s and θ_r are the saturated and residual water contents, respectively, α [L^{-1}] and n [-] are curve fitting parameters and $m = \left(1-\frac{1}{n}\right)$.

[e] Durner (1994). k=2 for the DPM, $0<w_i<1$ and $\sum w_i = 1$.

[f] van Genuchten (1980) applied separately to each pore system. Subscript i =M for the macropore and i =m for the matrix system. For the overall system, $\theta(h) = w_M\theta_M(h) + (1-w_M)\theta_m(h)$ and $K(h) = w_M K_M(h) + (1-w_M)K_m(h)$. Numerical solutions of the DPeM were accepted only if the ratio of the predicted saturated hydraulic conductivity of the overall system ($K_{sP} = w_M K_{sM} + (1-w_M)K_{sm}$) to that of its measured value (K_s) was between 0.5 and 2.

[g] Mualem (1976). $S_e = \frac{\theta(h)-\theta_r}{\theta_s-\theta_r}$; $m = \left(1-\frac{1}{n}\right)$.

[h] Taken as the average of the measured porosity of the column (η) and water content at saturation ($\theta_{\acute{s}}$) calculated from the multistep outflow experiment.

[i] θ_r and θ_{rm} were kept fixed at the value of θ_r of the Durner (1994) function obtained by fitting steady state water retention measurements with the SWRC Fit program.

[j] α_2 and α_m were kept fixed at the value of α_2 of the Durner (1994) function obtained by fitting steady state water retention measurements with the SWRC Fit program.

[k] n_2 and n_{rm} were kept fixed at the value of n_2 of the Durner (1994) function obtained by fitting steady state water retention measurements with the SWRC Fit program.

[l] θ_{sm} fixed at the water content measured at -2 cm from the multistep outflow experiment.

[m] geometric mean radius = $d_g/2$ (cm).

Table 4. Average ± standard deviation of air-dried mass (m_p), volume (v_p), and porosity (η_p) of wood particles from different size classes saturated for 15 days.

Size class (µm)	m_p (g)	v_p (cm^3)	η_p (-)
>25400	5.712 ± 2.311	13.47 ± 4.094	0.59 ± 0.04
19050-25400	4.327 ± 1.680	8.617 ± 2.222	0.60 ± 0.05
9525-19050	1.333 ± 0.931	2.596 ± 1.783	0.47 ± 0.10
5660-9525	0.259 ± 0.217	0.933 ± 0.438	0.35 ± 0.16
2830-5660	0.185 ± 0.247	0.717 ± 0.378	0.24 ± 0.11
1410-2830	0.014 ± 0.008	0.423 ± 0.019	0.06 ± 0.01
297-1410	0.006 ± 0.001	0.399± 0.020	0.02 ± 0.01

Table 5. Physical properties of the six samples selected for hydraulic characterization. Values shown are the average ± standard deviation of geometric mean diameter (d_g) and sorting coefficient (S_o) calculated from particle size distribution data. Values of dry packing density (ρ_b), porosity (η), saturated water content from the multistep outflow experiment (θ_{so}) and saturated hydraulic conductivity (K_s) are provided for each duplicate sample.

d_g (µm)	S_o (µm)	ρ_b (kg/m^3)	η (cm^3/cm^3)	θ_{so}	K_s (cm/hr)
1403±208	2.77	230/ 230	0.79/ 0.78	0.83/ 0.86	61 ±1/ 55 ±4
2255±260	2.43	240/ 240	0.75/ 0.76	0.79/ 0.77	65 ±2/ 63 ±1
3482±457	2.21	250/ 240	0.73/ 0.74	0.82/ 0.77	63 ±2/ 62 ±1
4402±1852 [a]	4.74	230/ 220	0.73/ 0.76	0.73/ 0.75	64 ± 1/ 54 ±0
5512±632	1.76	240/ 240	0.74/ 0.75	0.82/ 0.85	51 ±1/ 80 ±2
8130±1354 [a]	2.83	240/ 240	0.72/ 0.72	0.79/ 0.79	61 ±1/ 53 ±0

[a] Group I

Table 6a. Parameters θ_r, α and n of the van Genuchten (1980) model (Table 3) obtained by fitting the model separately to duplicate samples selected for hydraulic characterization. Samples are identified by their average geometric mean diameter (d_g).

d_g (μm)	θ_r (cm^3/cm^3)	α(cm^{-1})	n (-)
1403	6.7E-07/1.2E-07	5.53/11.55	1.17/1.16
2255	2.8E-02/2.1E-06	4.37/26.85	1.18/1.14
3482	3.3E-07/6.7E-06	29.78/63.26	1.14/1.12
4402 [a, b]	2.1E-06/1.8E-06	2431.5/572050	1.09/1.09
5512	4.8E-06/9.7E-08	51.89/13.31	1.12/1.15
8130 [a]	5.9E-07/2.7E-06	1241.7/1036.9	1.09/1.10

[a] Group I.
[b] The van Genuchten (1980) function fitted the water retention data of replicates of sample 4402 poorly.

Table 6b. Parameters θ_r, α_1, n_1, w_1, α_2 and n_2 of the bimodal Durner (1994) model (Table 3) obtained by fitting the model separately to duplicate samples selected for hydraulic characterization. Samples are identified by their average geometric mean diameter (d_g).

d_g (µm)	θ_r (cm^3/cm^3)	α_1 (cm^{-1})	n_1(-)	w_1(-)	α_2(cm^{-1})	n_2 (-)
1403	0.08/0.02	571.83/0.66	1.64/7.31	0.36/0.44	0.198/0.195	1.295/1.187
2255	0.04/0.03	2.62/302.71	1.53/1.48	0.55/0.44	0.109/0.278	1.174/1.168
3482	0.05/2.1E-05	0.97/6.99	3.94/1.51	0.53/0.62	0.095/0.040	1.202/1.122
4402 [a]	0.00/6.2E-05	13.40/6.72	22.08/35.50	0.77/0.51	0.055[b]/0.029 [b]	1.150 [b]/1.135[b]
5512	0.10/0.10	0.65/0.64	8.55/6.62	0.61/0.57	0.022/0.034	1.345/1.337
8130 [a]	6.6E-07/0.00	626.50/86.10	1.24/129.00	0.66/0.56	0.026/0.048	1.121/1.137

[a] Group I.
[c] The Durner (1994) model was fitted poorly to the water retention data of replicates of sample 4402. For inverse modeling, parameters α_2 and n_2 were kept fixed at the values given in this table and not those fitted by the SWRC Fit software (Seki, 2007).

Table 7a. Optimized parameters α and n and the coefficients of determination (R^2) of duplicate samples obtained by inversely modeling cumulative outflow and pressure head data using the single porosity model (SPM) in HYDRUS-1D. The samples selected for hydraulic characterization are identified by their geometric mean diameter (d_g).

d_g (μm)	α(cm^{-1})	n(–)	R^2
1403	0.37/0.77	1.49/1.33	0.83/0.92
2255	0.46/0.37	1.34/1.48	0.94/0.82
3482	0.80/0.37	1.38/1.47	0.92/0.88
4402 [a]	0.38/0.39	1.49/1.59	0.88/0.87
5512	0.62/0.39	1.54/1.58	0.92/0.73
8130 [a]	0.92/0.79	1.38/1.45	0.90/0.83

[a] Group I.

Table 7b. Optimized parameters α_1, n_1 and w_1 and the coefficients of determination (R^2) of duplicate samples obtained by inversely modeling cumulative outflow and pressure head data using the dual porosity model (DPM) in HYDRUS-1D. The samples selected for hydraulic characterization are identified by their geometric mean diameter (d_g). The values of α_2 and n_2 were kept fixed during inverse modeling at values shown in Table 6b.

d_g (μm)	α_1 (cm^{-1})	n_1(-)	w_1(-)	R^2
1403	0.56/2.08	14.71/1.58	0.36/0.55	0.92/0.91
2255	0.65/0.63	1.69/7.35	0.54/0.45	0.97/0.95
3482	2.56/0.40	1.79/2.23	0.58/0.61	0.90/0.96
4402 [a]	0.62/0.71	9.34/6.00	0.57/0.62	0.93/0.93
5512	1.73/-[b]	2.24/-[b]	0.64/-[b]	0.95/-[b]
8130 [a]	4.07/1.61	1.83/3.28	0.62/0.58	0.79/0.93

[a] Group I.
[b] poor prediction for replicate 2 of sample 5512.

Table 7c. Optimized parameters α_M, n_M, w_M K_{sm}, K_{sM}, K_a and the coefficient of determination (R^2) of duplicate samples obtained by inversely modeling cumulative outflow and pressure head data using the dual permeability model (DPeM) in HYDRUS-1D. The samples selected for hydraulic characterization are identified by their geometric mean diameter (d_g). The values of α_m and n_m were kept fixed during inverse modeling at values of α_2 and n_2 shown in Table 6b.

d_g (μm)	α_M (cm^{-1})	n_M(-)	w_M(-)	K_{sm} (cm/hr)	K_{sM} (cm/hr)	K_a (cm/hr)[b]	R^2
1403	0.16/0.24	2.28/1.71	0.50/0.63	0.12/0.57	35/53	1.5/0.9	0.86/0.88
2255	0.16/0.27	2.71/2.84	0.43/0.39	0.75/11.9	60/195	1.0/0.02	0.94/0.94
3482	0.52/0.29	1.58/2.19	0.62/0.48	0.19/0.62	49/93	1.4/1.1	0.90/0.91
4402 [a]	0.45/0.34	2.39/2.74	0.45/0.50	0.36/0.10	12/107	1.9/1.0	0.94/0.86
5512	0.36/0.45	2.90/1.73	0.47/0.58	0.05/0.01	110/102	1.0/1.0	0.88/0.67
8130 [a]	0.87/1.17	2.08/2.64	0.50/0.48	0.03/0.13	81/77	1.1/3.9	0.88/0.97

[a] Group I.
[b] Multiply value given in the table by 10^{-4} to get the actual value of the effective saturated hydraulic conductivity of the interface between the two pore systems (K_a) (Refer to Table 3).

Table 8. Sum of the square of the residuals (SSR), lack of fit (LOFIT), and deviation from AIC_{min} value (Δ) for a given sample and model for the cumulative outflow and pressure head data.

Cumulative Outflow									
Sample	**SSR**			**LOFIT**			Δ		
	SPM	**DPM**	**DPeM**	**SPM**	**DPM**	**DPeM**	**SPM**	**DPM**	**DPeM**
1403 (1)	18	59	6	2.1E-01	5.4E-01	4.1E-04	40	98	0
1403 (2)	23	40	23	2.3E-01	1.5E-01	2.0E-01	0	29	9
2255 (1)	8	24	1	2.3E-01	5.1E+00	1.1E-02	168	255	0
2255 (2)	17	48	1	8.2E-04	2.8E+01	1.0E-02	199	271	0
3482 (1)	8	39	4	3.0E-01	1.0E-01	1.4E-01	61	194	0
3482 (2)	9	21	6	1.0E-02	3.0E+00	8.4E-02	17	76	0
4402 (1)	29	230	3	7.9E-01	1.2E+02	3.1E-01	131	260	0
4402 (2)	17	204	33	4.0E-01	1.2E+02	1.0E+01	0	157	52
5512 (1)	8	21	2	3.7E-02	1.7E-02	1.2E-01	101	180	0
5512 (2)	29	4841	34	6.6E-01	4.0E+03	8.6E+00	0	401	21
8130 (1)	17	40	17	1.5E-01	1.9E-02	1.2E+00	0	60	12
8130 (2)	40	35	3	1.0E-04	4.6E-02	3.8E-02	165	159	0
Pressure head									
Sample	**SSR**			**LOFIT**			Δ		
	SPM	**DPM**	**DPeM**	**SPM**	**DPM**	**DPeM**	**SPM**	**DPM**	**DPeM**
1403 (1)	3033	3641	3396	293	476	189	0	19	19
1403 (2)	2522	5353	1889	141	1625	9	16	83	0
2255 (1)	1973	1917	1853	700	680	117	2	0	1
2255 (2)	1553	1378	1368	469	33	323	10	0	6
3482 (1)	4486	12700	4389	47	3177	62	0	177	5
3482 (2)	3101	2595	1942	873	896	1043	41	24	0
4402 (1)	3507	1706	1852	2356	767	578	87	0	17
4402 (2)	2499	1383	2571	1535	124	748	71	0	84
5512 (1)	1277	3651	4812	186	1029	1836	0	164	213
5512 (2)	7656	313693511	9118	6597	114205306	5270	0	1659	36
8130 (1)	6772	30747	7335	507	10041	596	0	202	19
8130 (2)	4625	8408	2021	189	2023	31	106	190	0

Figure 1. Volumetric water content (θ) retained at a given pressure potential as a function of geometric mean diameter (d_g) for the different wood particle mixes placed in the pressure plate extractor. Eq. (5) has been fitted (lines) to the measurements (symbols). Parameters resulting from the fits are listed in Table 2.

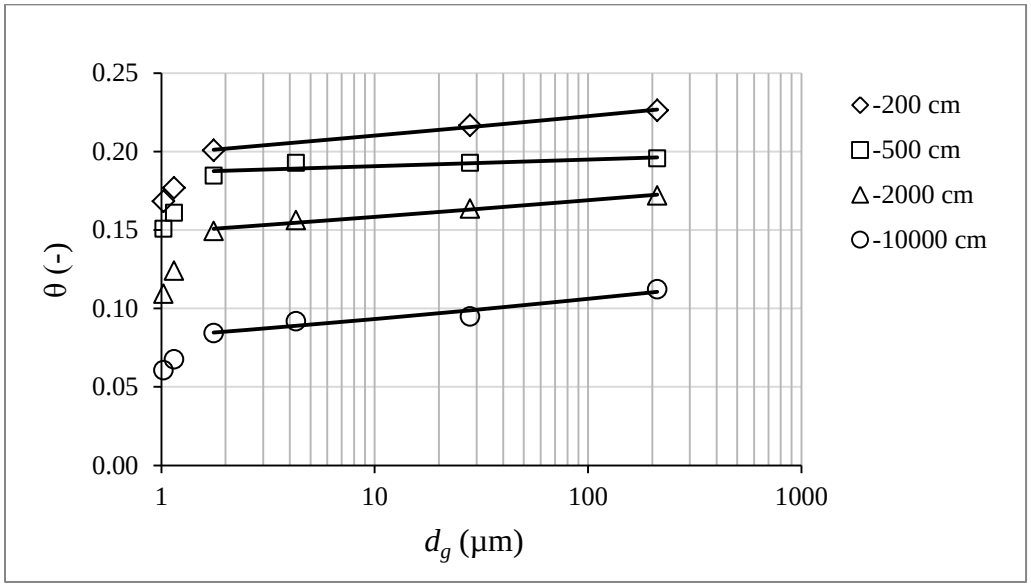

Figure 2. The flow cell with upper (T1) and lower (T2) tensiometers inserted. The pressure transducers attached to the tensiometers are not shown.

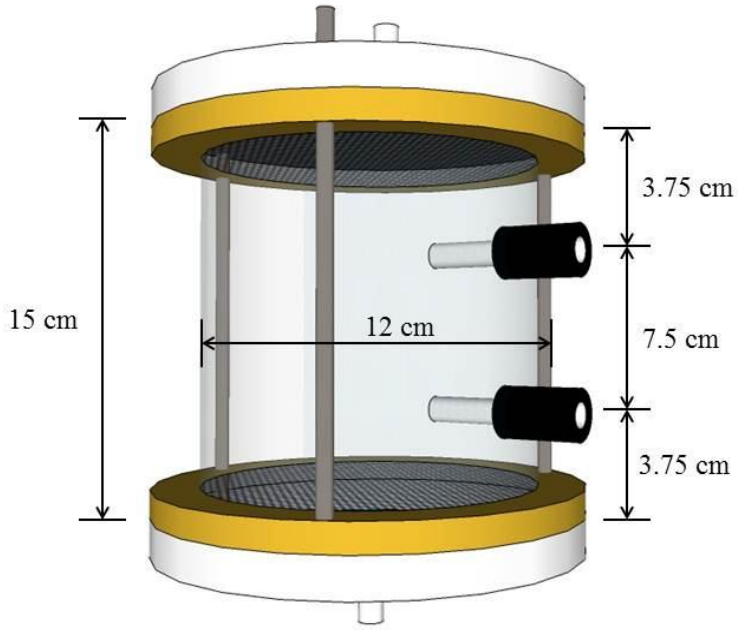

Figure 3. Graphical description of the pore system in wood particle media showing pores filled with air (white) and water (blue) and the pore models used to characterize it. In the *single porosity model* (SPM) and the *dual porosity model* (DPM) wood particles are impervious and fluid flow takes place only through inter particle pores. The SPM and DPM are characterized by unimodal and bimodal distributions of pore sizes, respectively. In the DPM one mode represents large pores (1) and the other smaller pores (2). In the *dual permeability model* (DPeM) wood particles are permeable leading to slower flow in the intra-particle domain or matrix (m) than in the interparticle domain or macropore (M). Both domains have unimodal pore systems, each with their own water retention [θ(h)] and hydraulic conductivity [K(h)] functions.

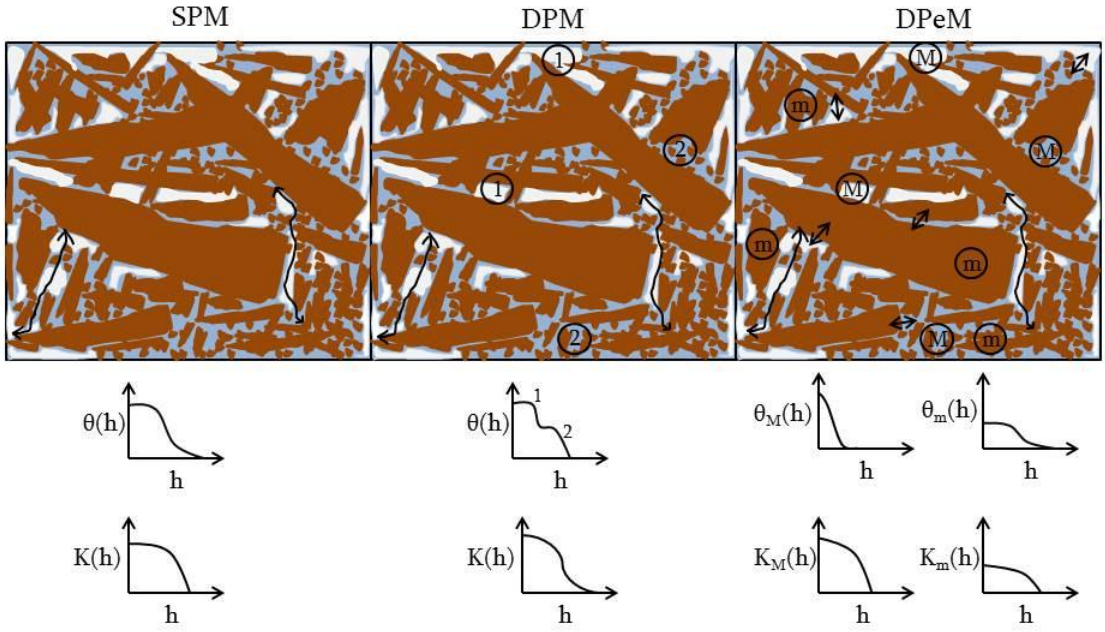

Figure 4. Sorting coefficient (S_o) as a function of geometric mean diameter (d_g) of particle size distributions of the 30 wood mulch samples (see Appendix I). The numbers alongside the filled data points denote the d_g of the samples selected for hydraulic characterization.

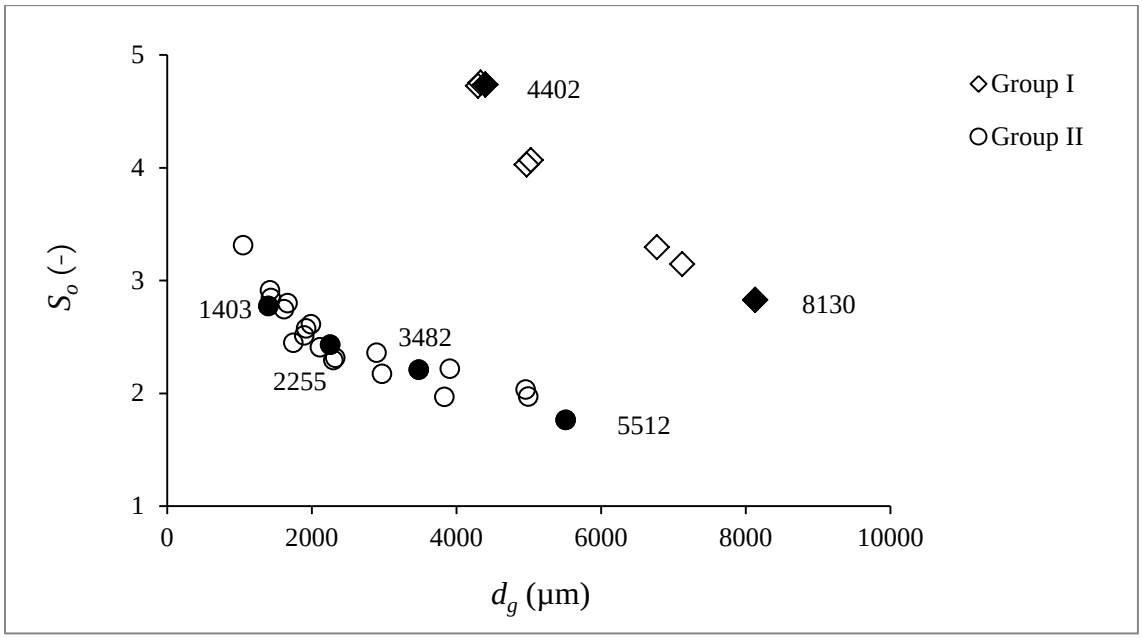

Figure 5. Particle size distributions of (a) Group I and (b) Group II samples selected for hydraulic characterization and identified by their geometric mean diameter (d_g) values (in μm). Symbols represent measurements and solid lines fits with Eq. 1 (Group I) and Eq. 2 (Group II).

(a)

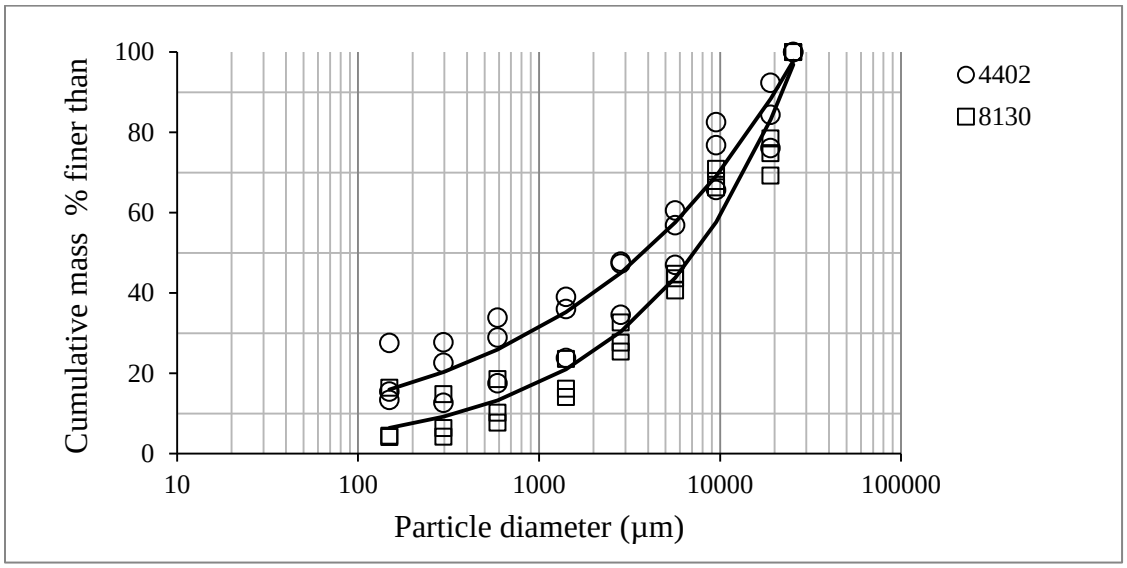

(b)

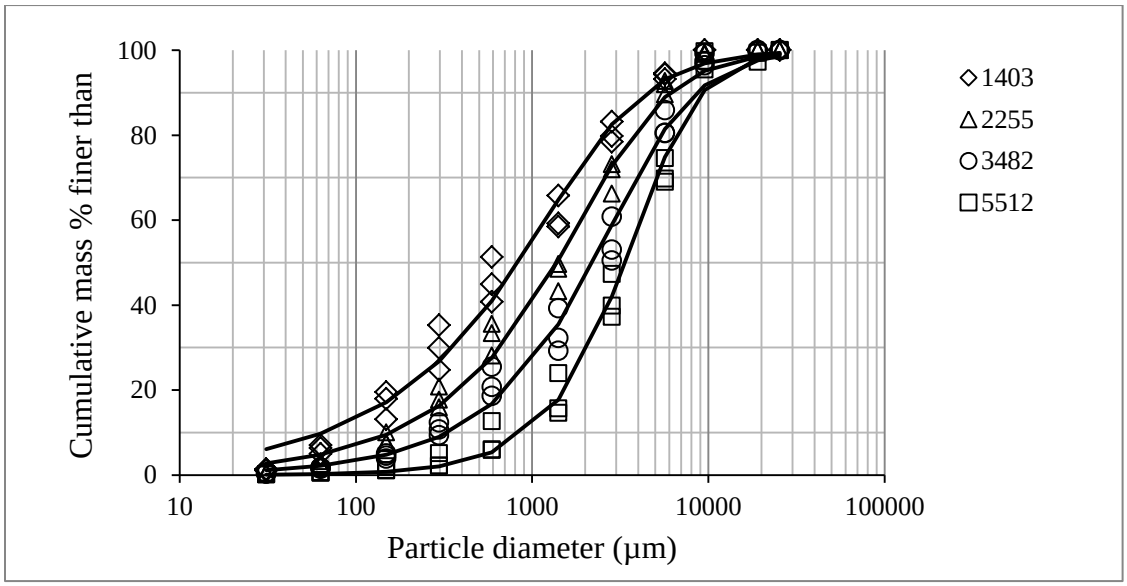

Figure 6. Volumetric water absorbed (Φ_t) as a function of time for woodchips of different sizes (in µm).

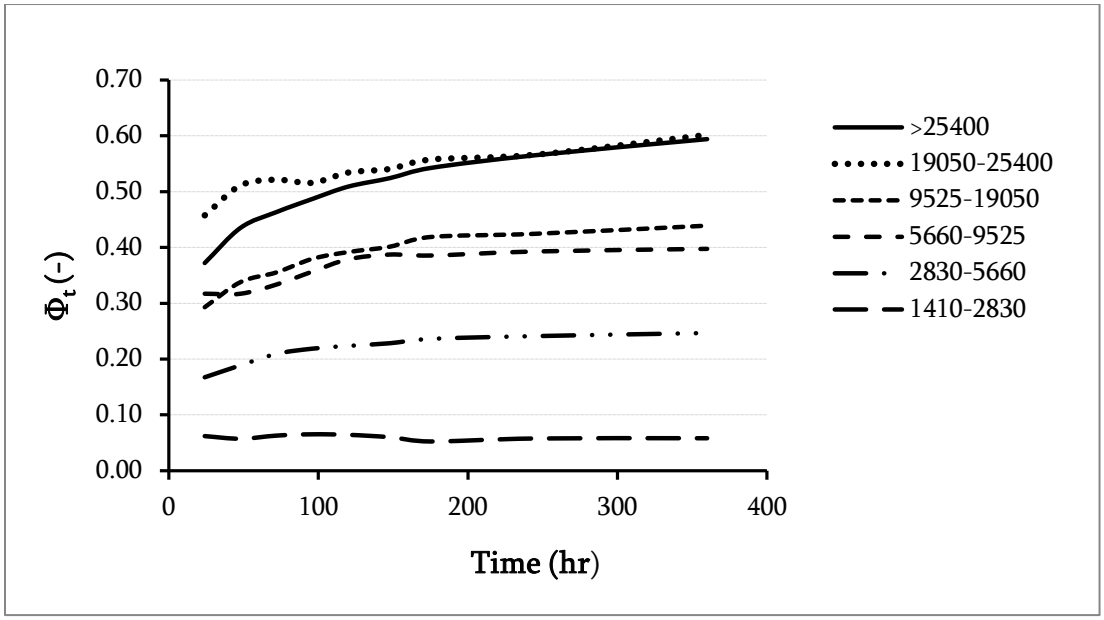

Figure 7. Measured (symbols) and predicted (lines) cumulative outflow and upper (T1) and lower (T2) pressure potentials of Group II samples 2255 and 5512 and Group I sample 8130. Models used are the single porosity (SPM), dual porosity (DPM) and dual permeability (DPeM).

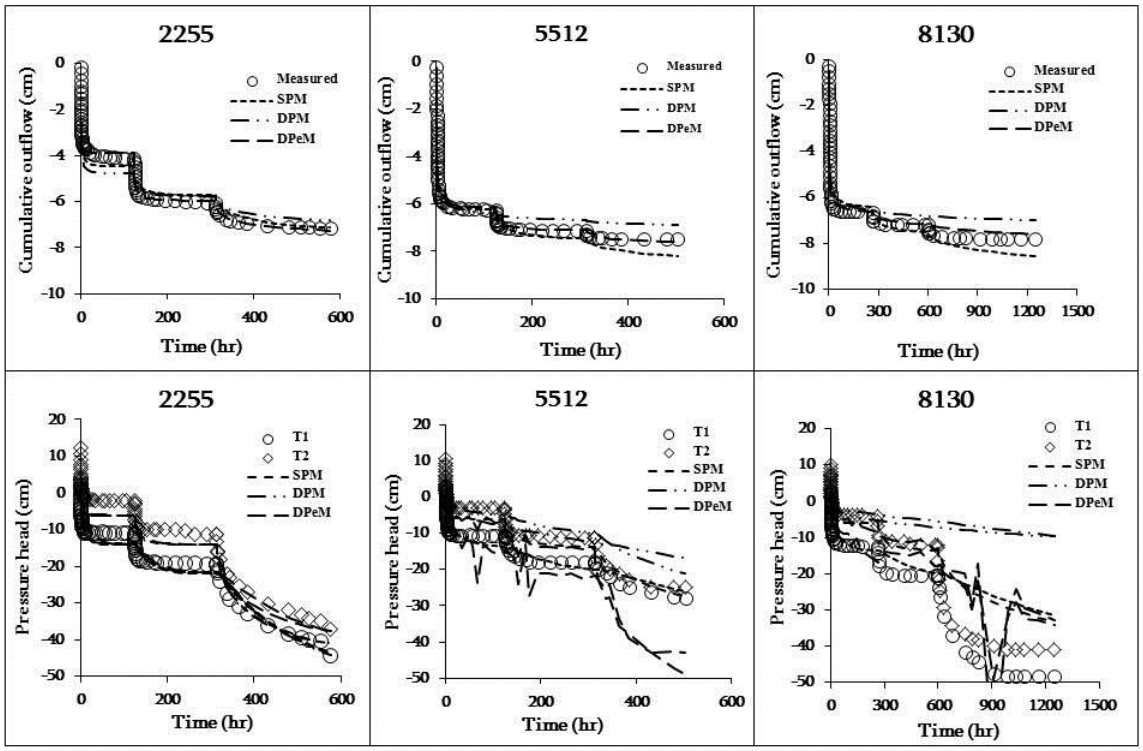

Figure 8. Measured and predicted water contents (θ) over the range of measured pressure potentials. Predicted water contents were obtained by fitting the: (a) van Genuchten (1980) model, (b) Durner (1994) model, or by inverse solution of cumulative outflow and pressure head data using models: (c) SPM, (d) DPM, and (e) DPeM as implemented in HYDRUS-1D. The line is the 1:1 line. Fitted equations are given below.

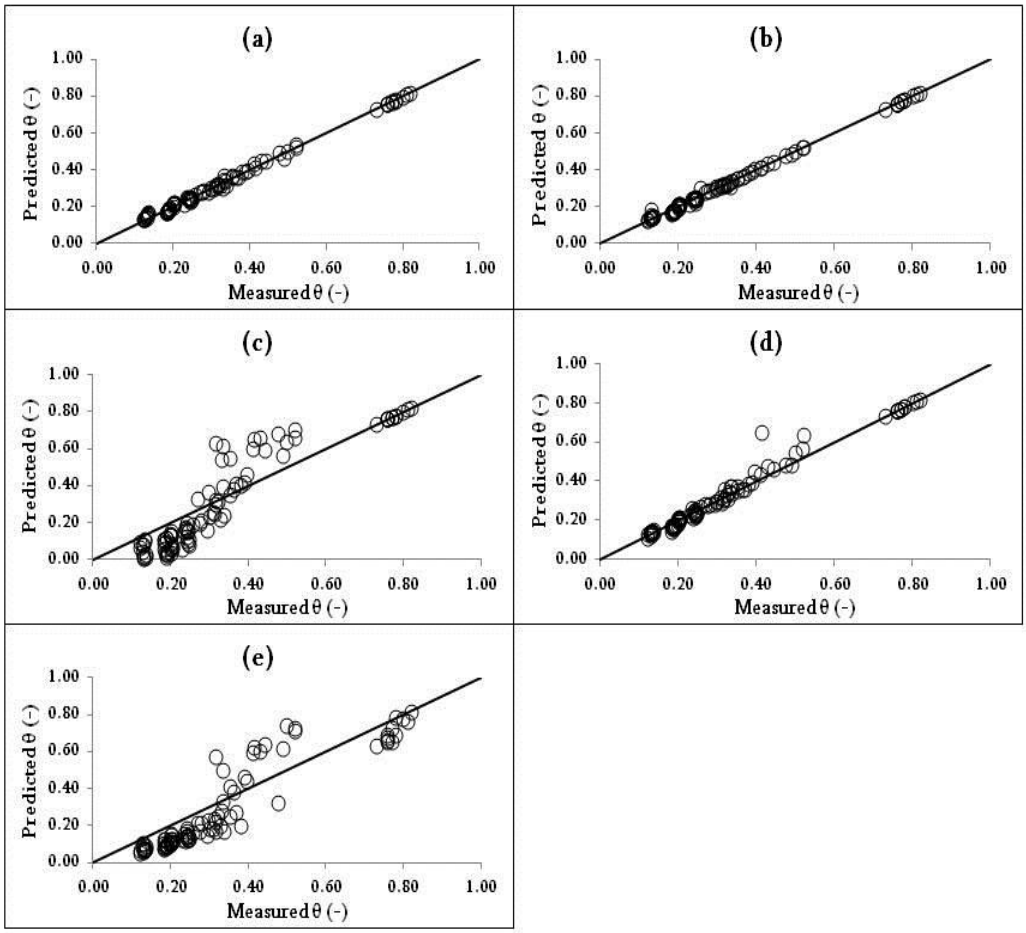

(a) $\theta_{predicted} = 0.9886\theta_{measured} + 0.0058$; $R^2 = 0.996$.
(b) $\theta_{predicted} = 0.9962\theta_{measured} + 0.0013$; $R^2 = 0.997$.
(c) $\theta_{predicted} = 1.2454\theta_{measured} - 0.1108$; $R^2 = 0.859$.
(d) $\theta_{predicted} = 1.0296\theta_{measured} - 0.0057$; $R^2 = 0.976$.
(e) $\theta_{predicted} = 1.1054\theta_{measured} - 0.084$; $R^2 = 0.846$.

Figure 9. Predicted hydraulic conductivity [K(h)] of Group II samples 2255 and 5512 and Group I sample 8130 by the single porosity (SPM), dual porosity (DPM) and dual permeability (DPeM) models. Note that the measured values of saturated hydraulic conductivity (K_s) is indicated in the log-scale at h= -0.1 cm instead of h=0 cm.

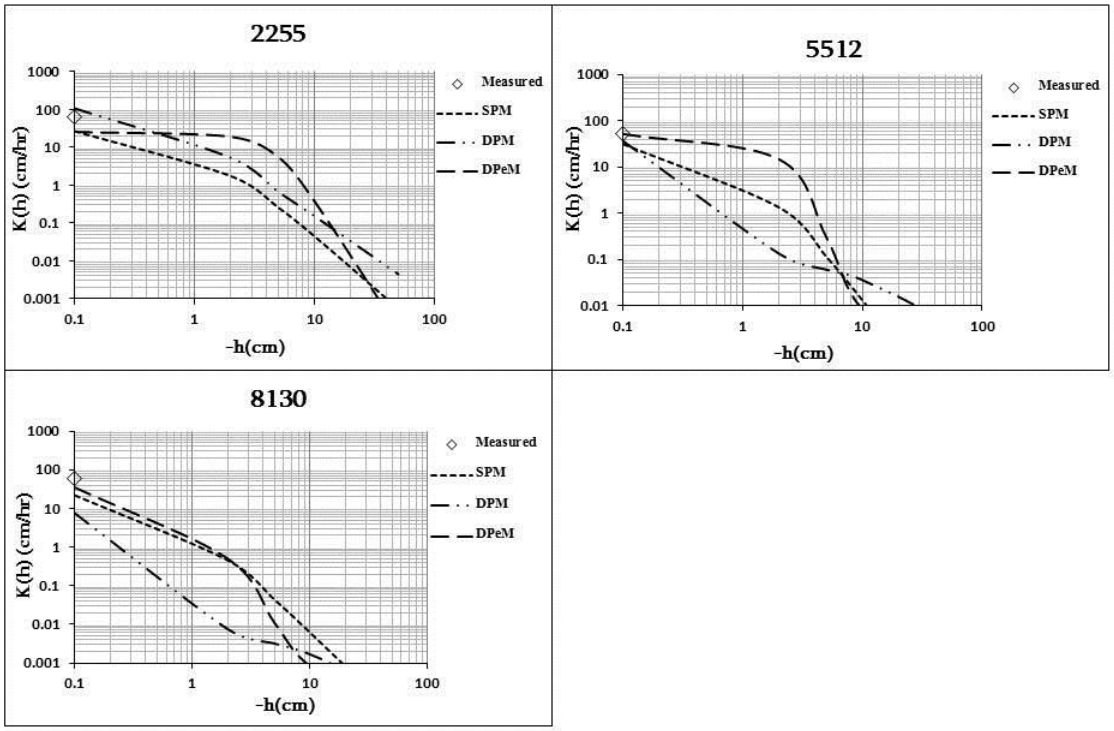

Figure 10. Relationship between the average values of *n* in the van Genuchten (1980) model obtained from the single porosity model (SPM) and the geometric mean diameter (d_g) of the samples chosen for hydraulic characterization. The filled data point was not considered for determining the relationship equation.

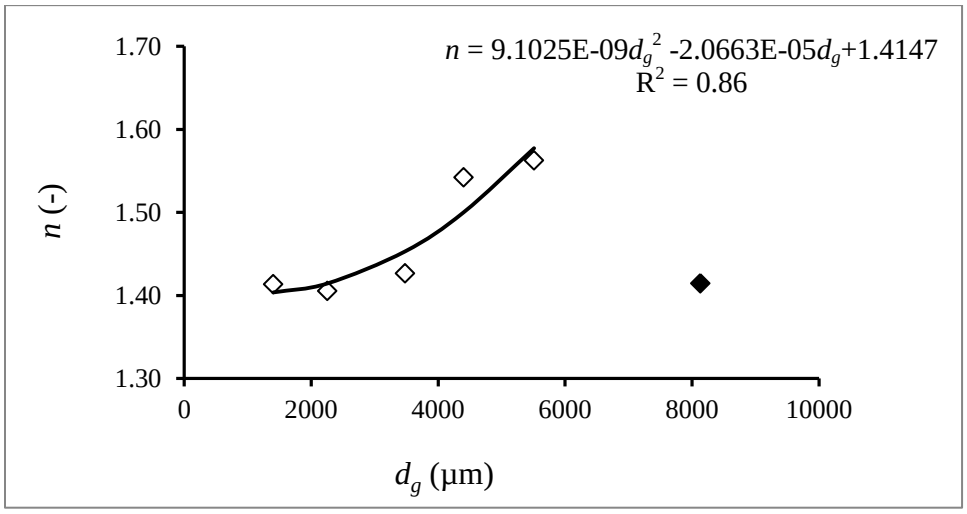

Figure 11. Relationship between the average values of w_1 in the Durner (1994) model obtained from the dual porosity model (DPM) and the geometric mean diameter (d_g) of the samples chosen for hydraulic characterization.

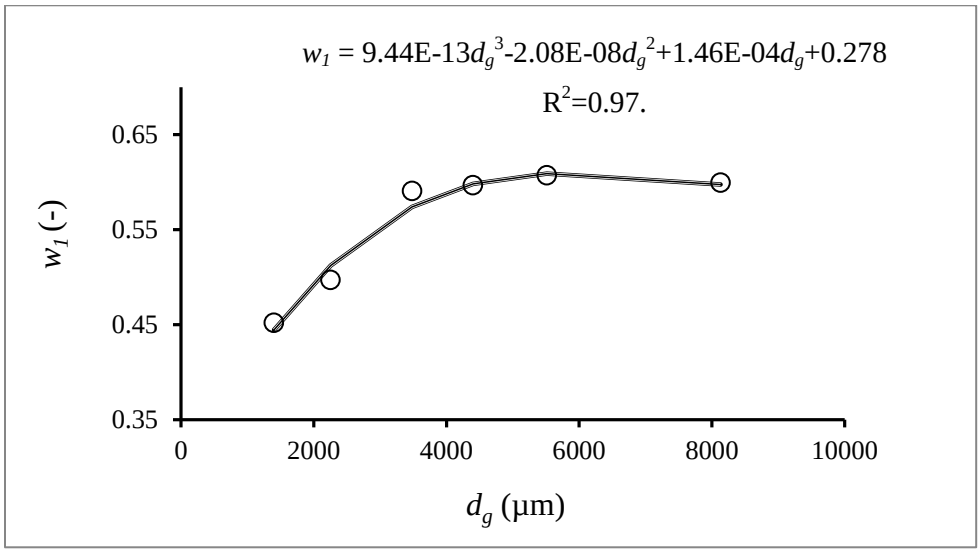

Figure 12. Relationship between the fitted average values of α_2 in the Durner (1994) model and the geometric mean diameter (d_g) of the six samples chosen for hydraulic characterization. The filled data point was not considered for determining the relationship equation.

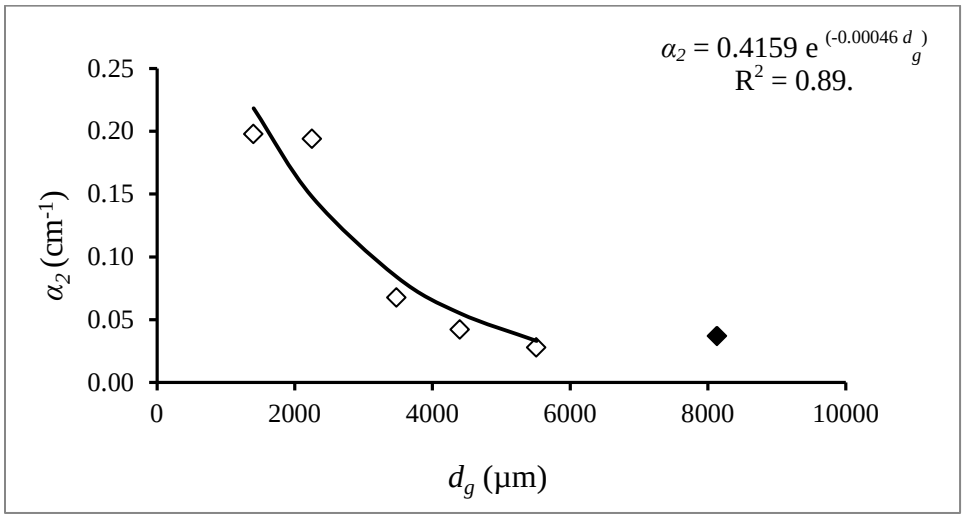

Figure 13. Relationship between the fitted average values of n_2 in the Durner (1994) model and the geometric mean diameter (d_g) of the six samples chosen for hydraulic characterization. The filled data point was not considered for determining the relationship equation.

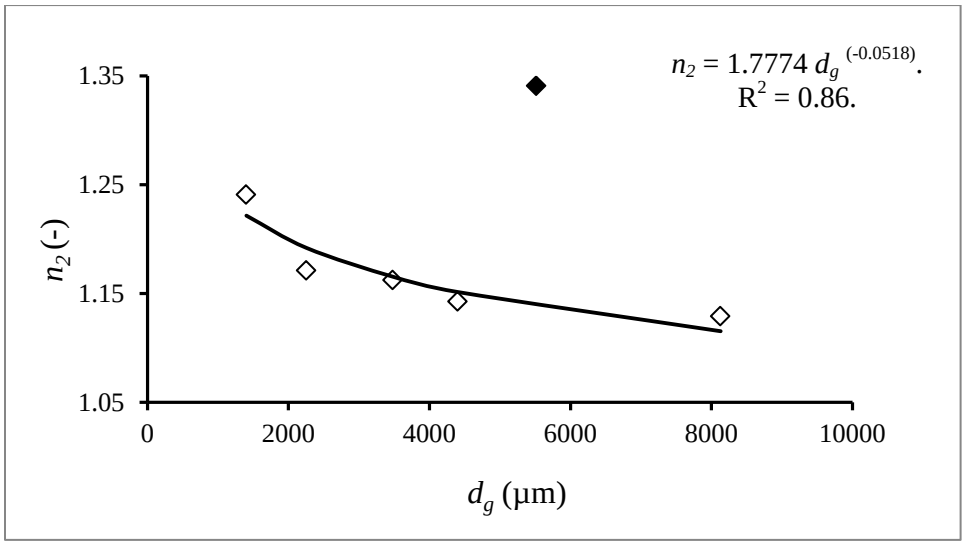

Figure 14. Relationship between the average macropore air entry pressure potential ($1/\alpha_M$) obtained from the dual permeability model (DPeM) and the geometric mean diameter (d_g) of the six samples chosen for hydraulic characterization.

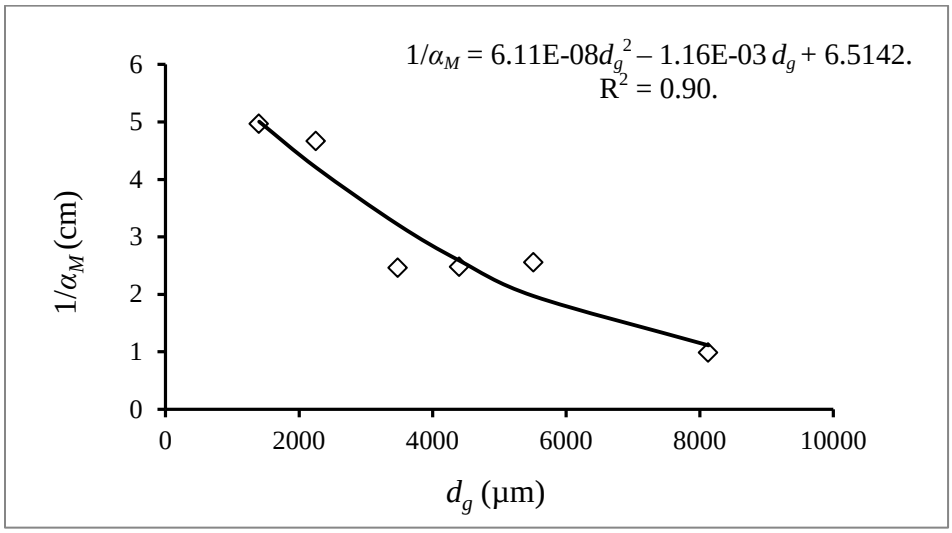

Figure 15. Relationship between the average inflection point ratio (I_R) and geometric mean diameter (d_g) for the dual porosity (DPM) and dual permeability (DPeM) models of the six samples chosen for hydraulic characterization. The relationship equations are given below.

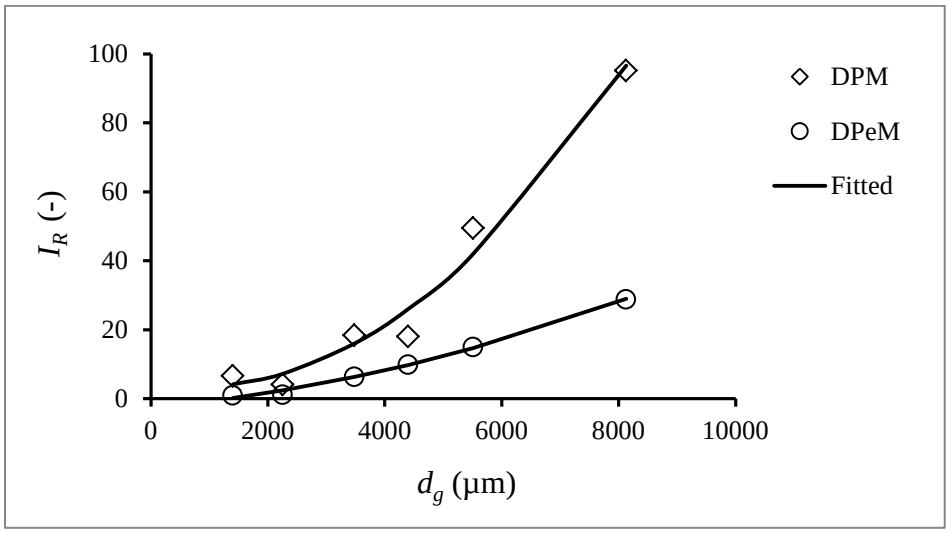

I_R=1.73E-06d_g^2 - 0.0027d_g +4.6541; R^2 = 0.976 (DPM).
I_R=2.91E-07d_g^2 + 0.0015d_g - 2.4563; R^2 = 0.996 (DPeM).

Appendices

Appendix I. Dry bulk density changes with increasing compaction as measured by the number of drops from a height of 15 cm and particle size distribution (PSD) curves for the 30 samples in this study. The chart titles refer to the geometric mean diameter of the sample, d_g (in µm). For bulk density the line denotes the average of the three replicates and for PSD it denotes the fit of either Eq. (1) or Eq. (2).

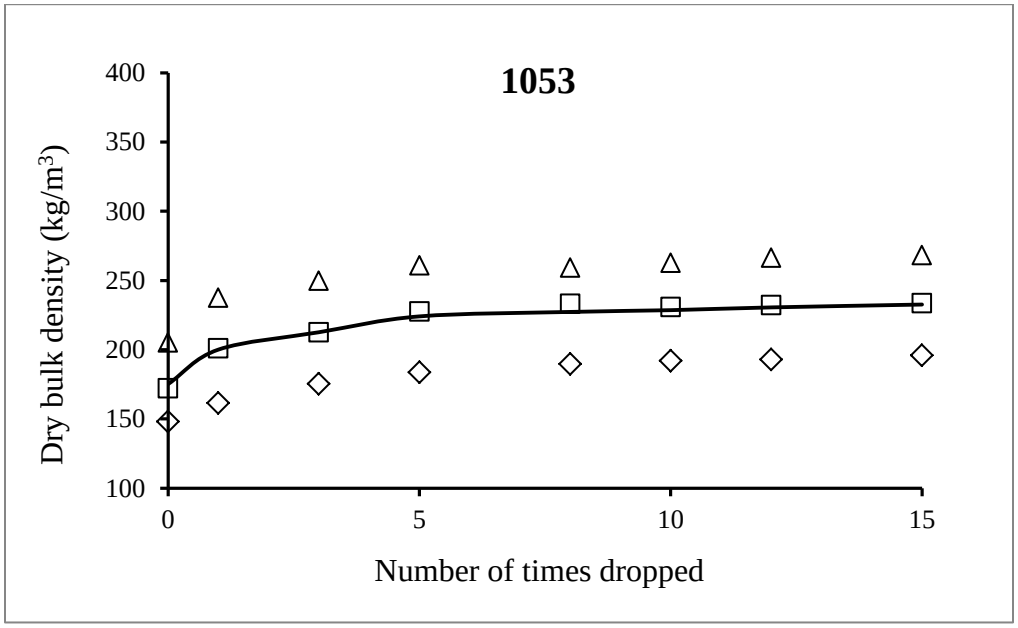

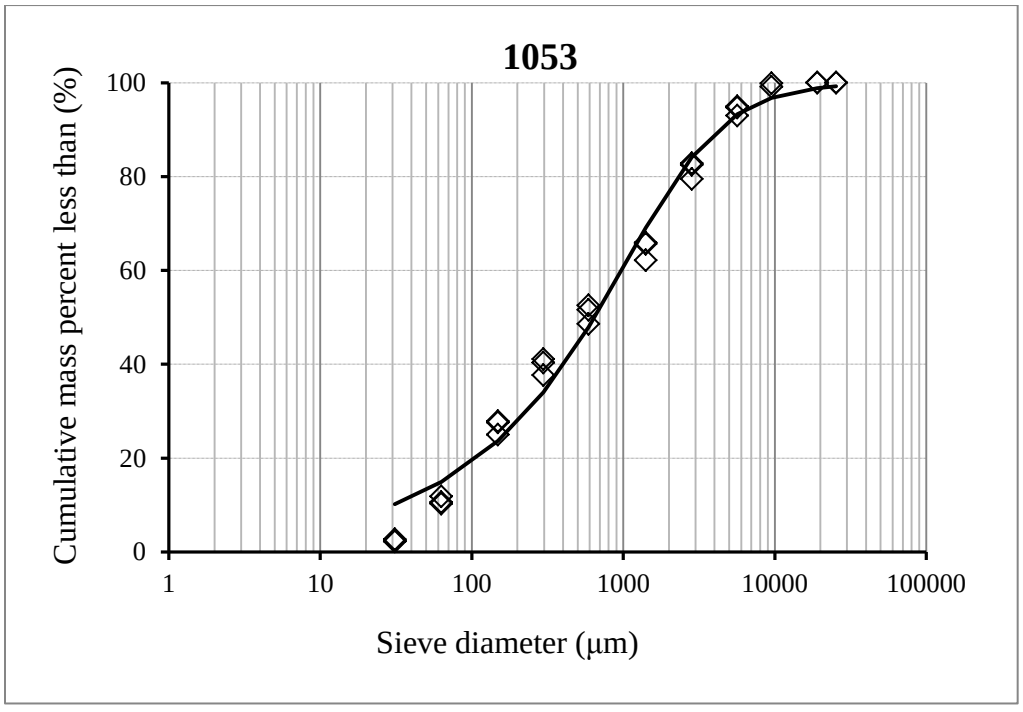

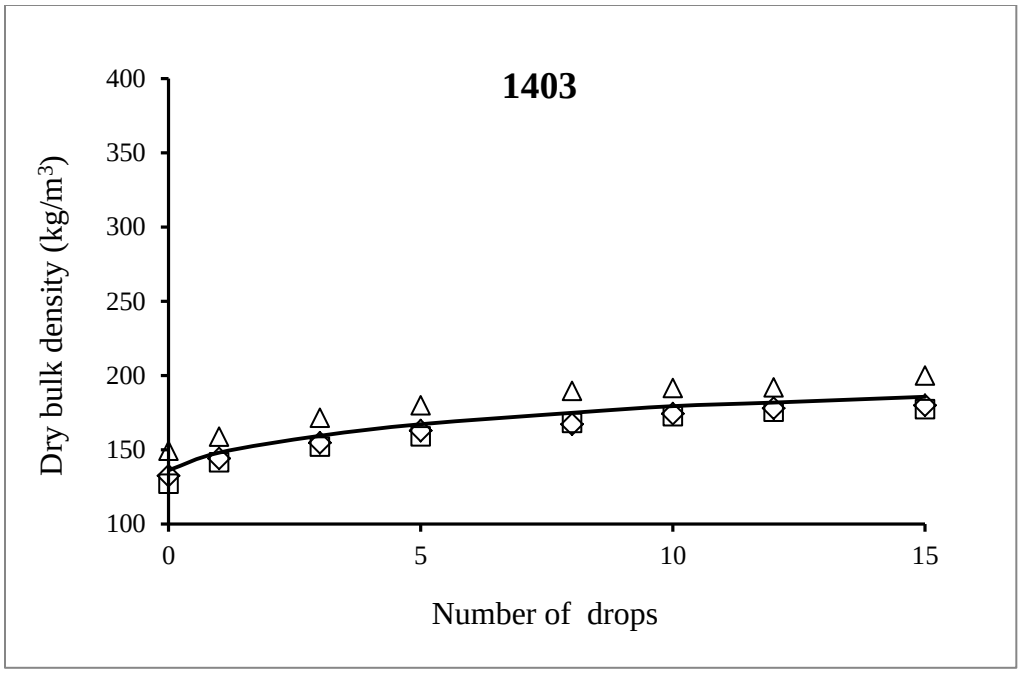
1403
Dry bulk density (kg/m3)
400
350
300
250
200
150
100
0
5
10
15
Number of drops

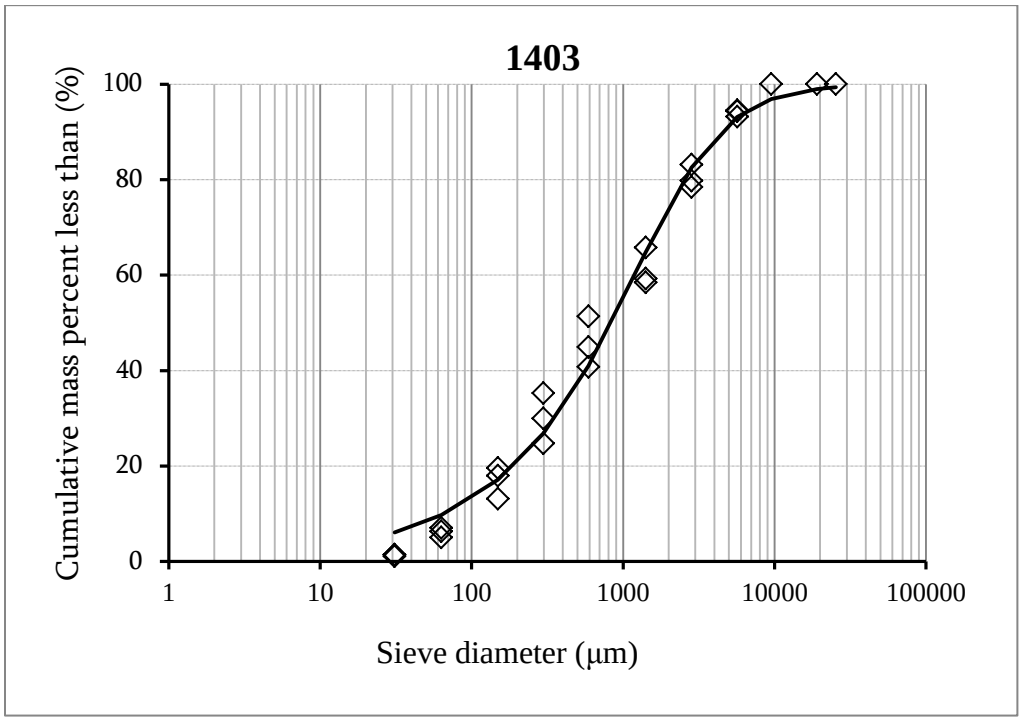
1403
Cumulative mass percent less than (%)
100
80
60
40
20
0
1
10
100
1000
10000
100000
Sieve diameter (μm)

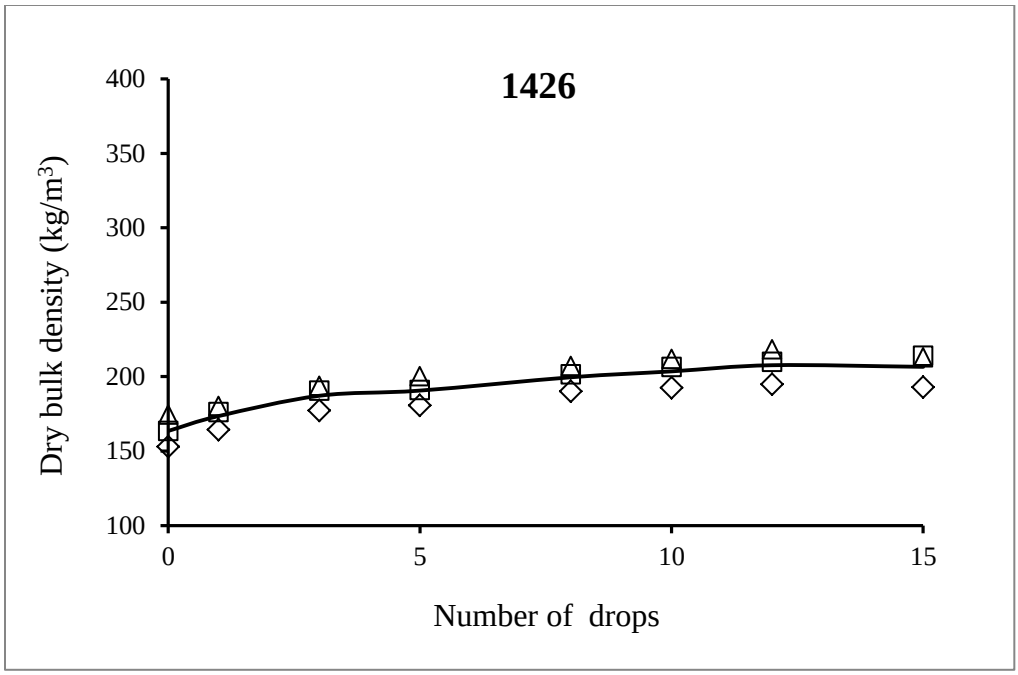
1426
Dry bulk density (kg/m3)
400
350
300
250
200
150
100
0
5
10
15
Number of drops

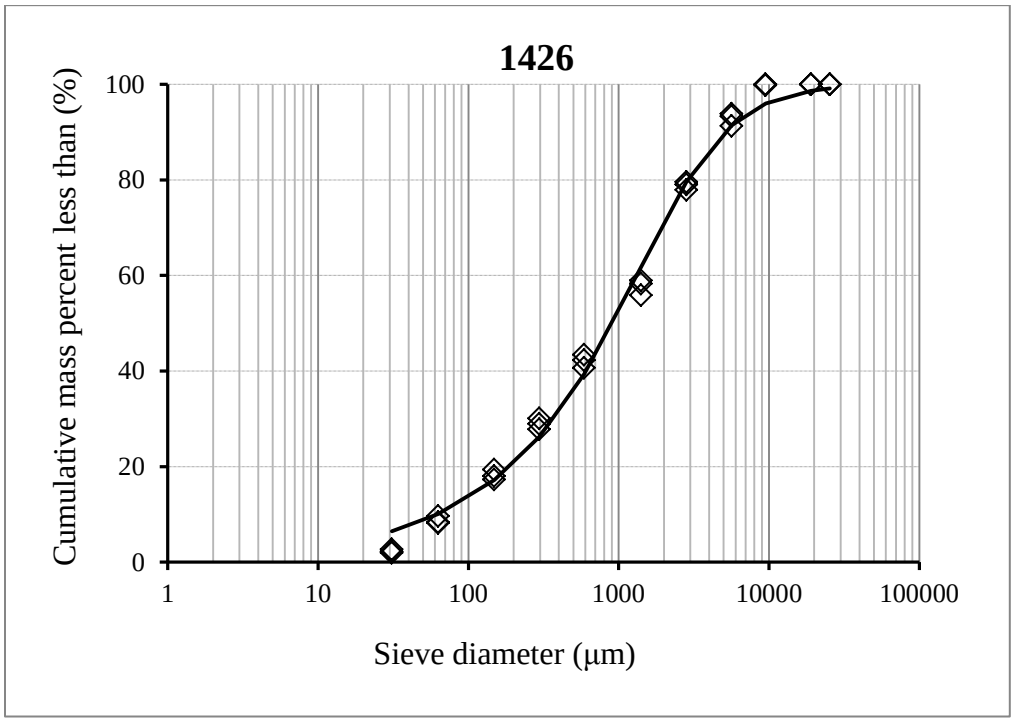
1426
Cumulative mass percent less than (%)
100
80
60
40
20
0
1
10
100
1000
10000
100000
Sieve diameter (μm)

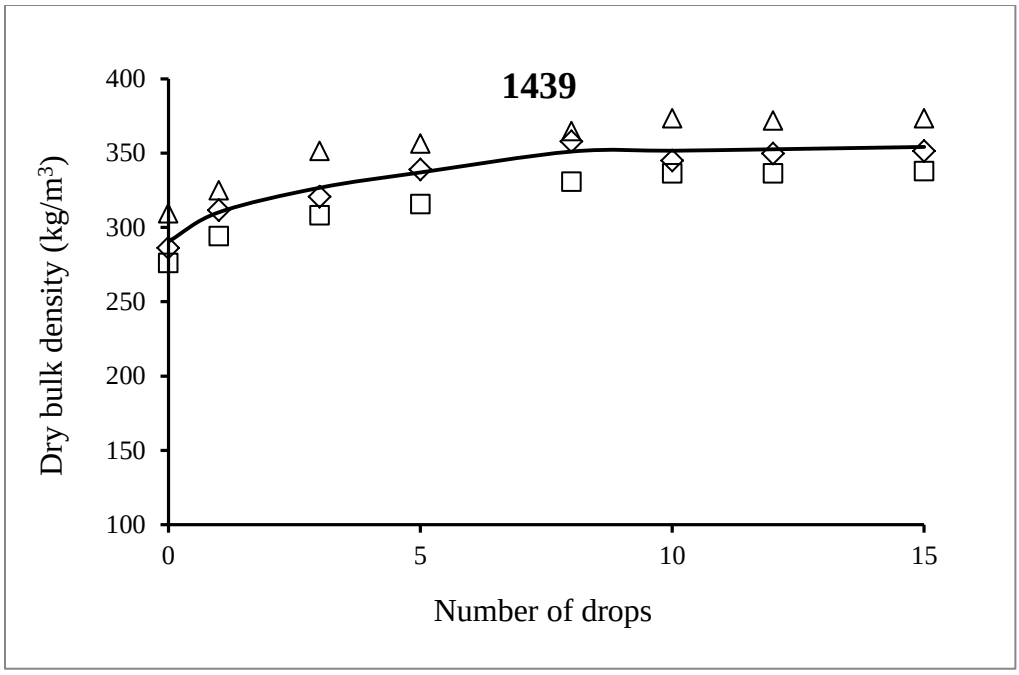
1439
Dry bulk density (kg/m3)
400
350
300
250
200
150
100
0
5
10
15
Number of drops

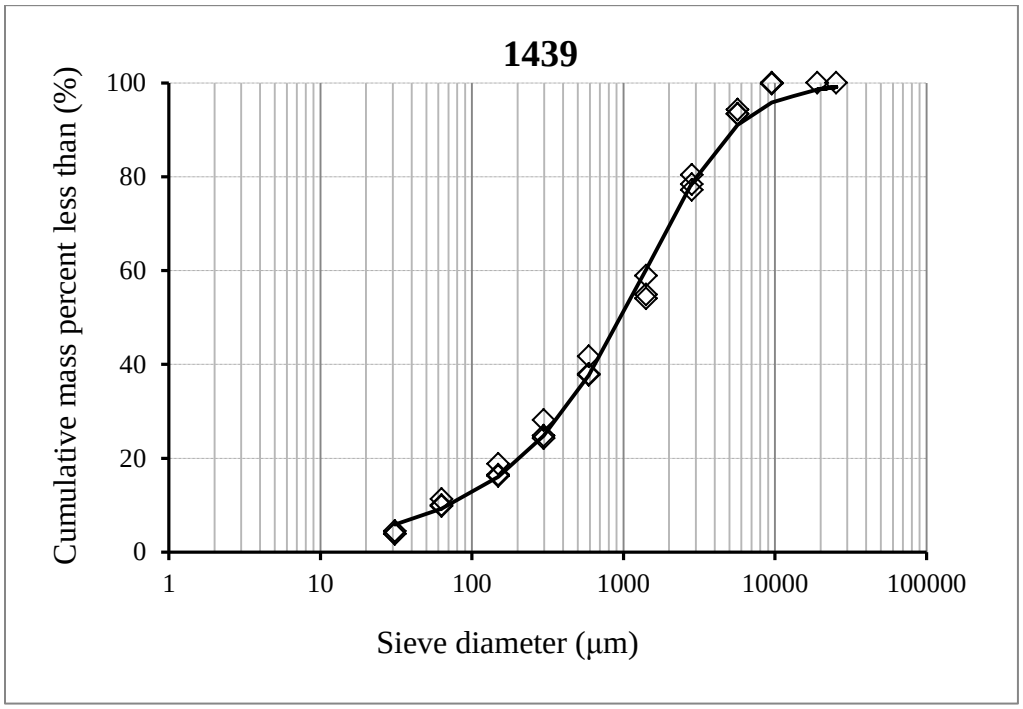
1439
Cumulative mass percent less than (%)
100
80
60
40
20
0
1
10
100
1000
10000
100000
Sieve diameter (μm)

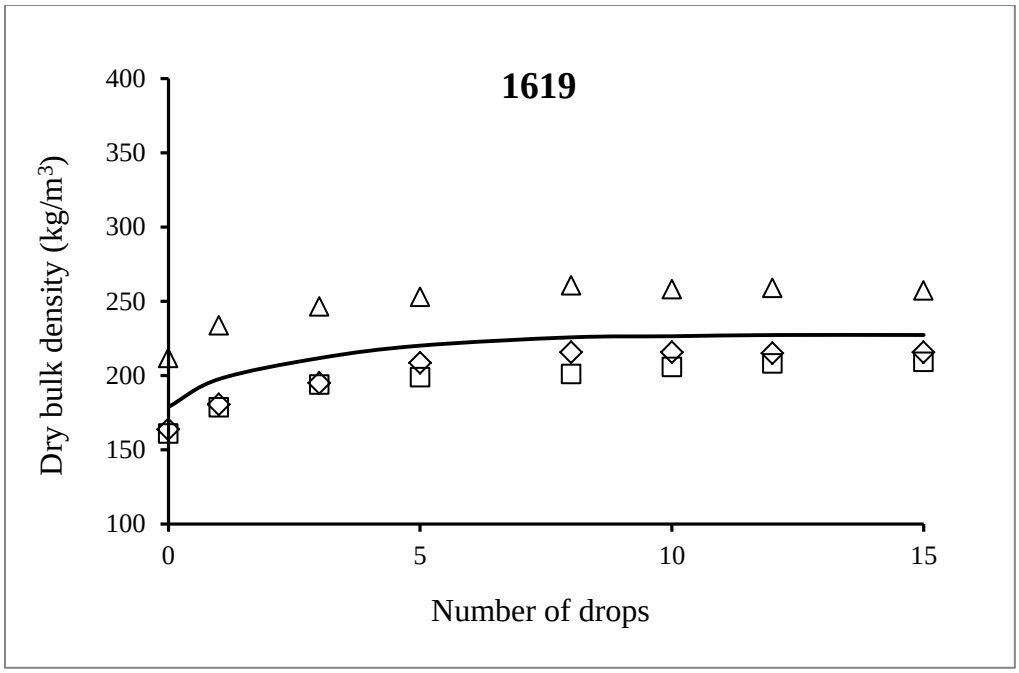
1619
Dry bulk density (kg/m3)
400
350
300
250
200
150
100
0
5
10
15
Number of drops

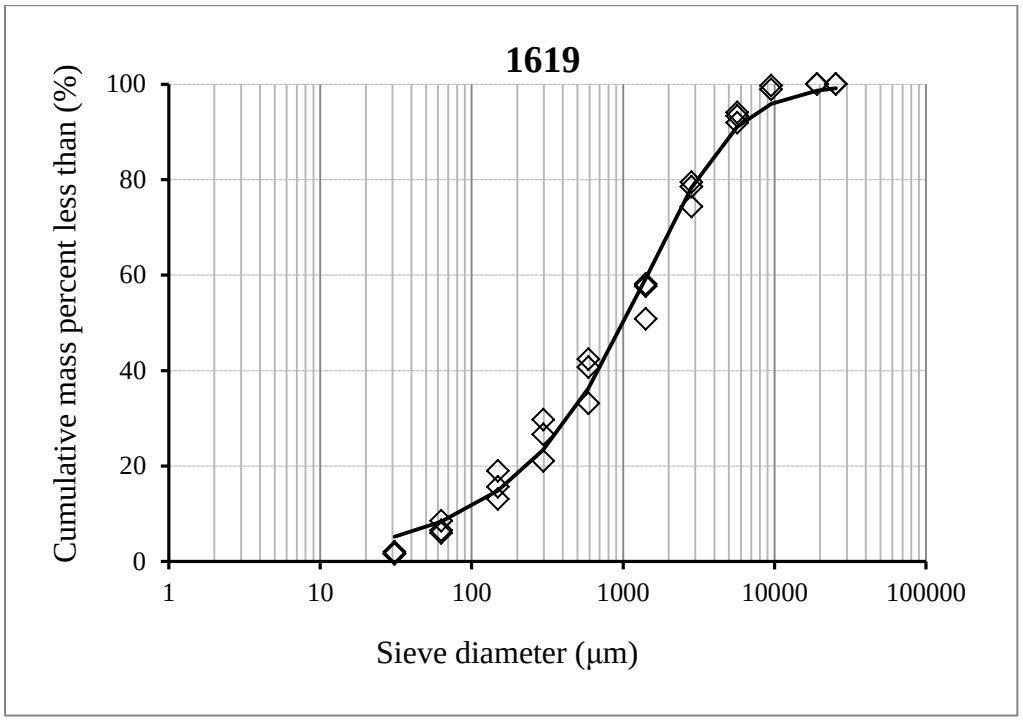
1619
Cumulative mass percent less than (%)
100
80
60
40
20
0
1
10
100
1000
10000
100000
Sieve diameter (μm)

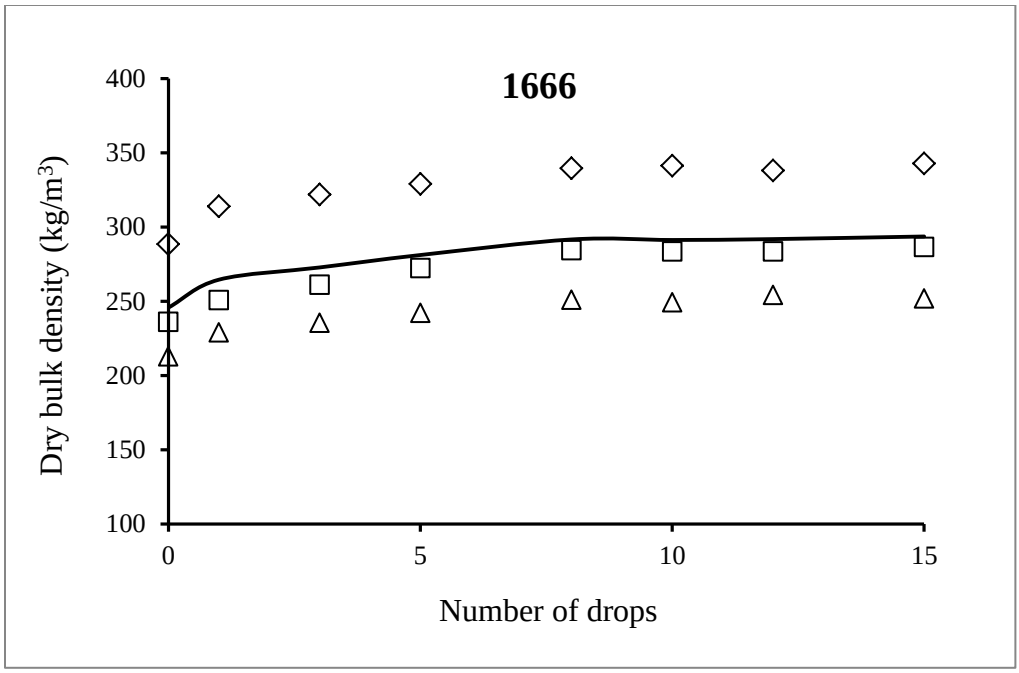
1666
Dry bulk density (kg/m3)
400
350
300
250
200
150
100
0
5
10
15
Number of drops

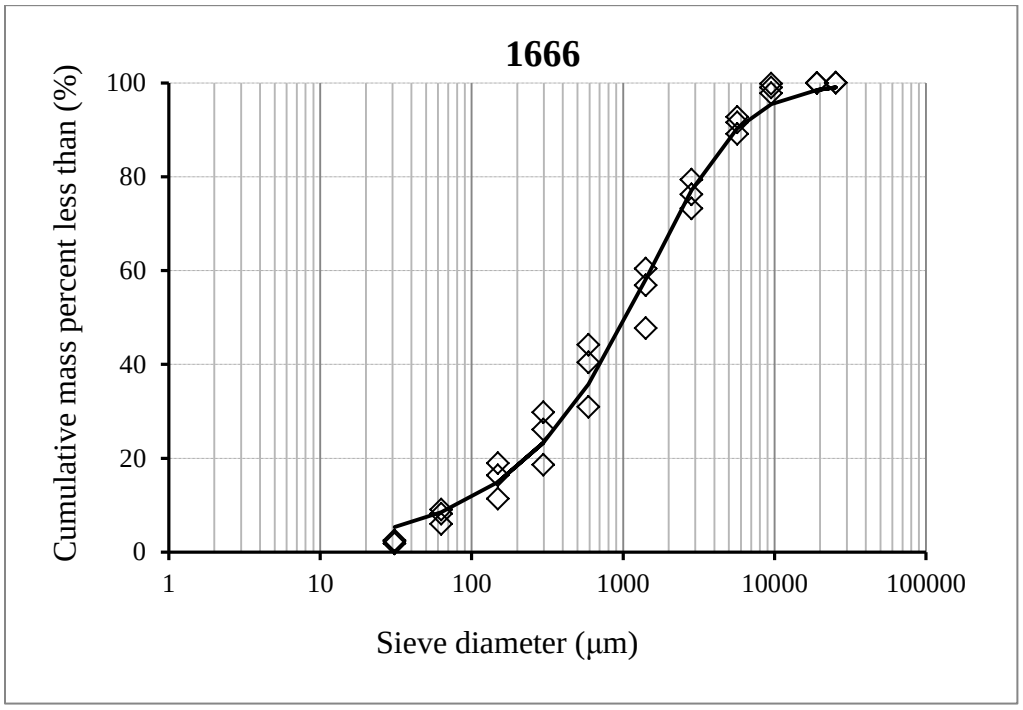
1666
Cumulative mass percent less than (%)
100
80
60
40
20
0
1
10
100
1000
10000
100000
Sieve diameter (μm)

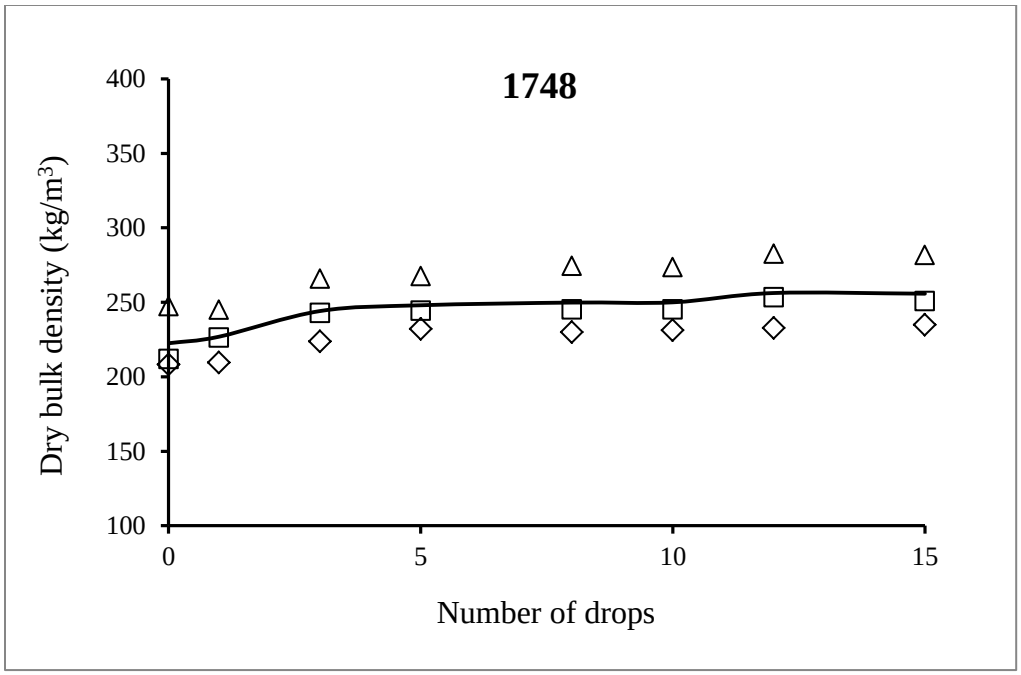
1748
Dry bulk density (kg/m3)
400
350
300
250
200
150
100
0
5
10
15
Number of drops

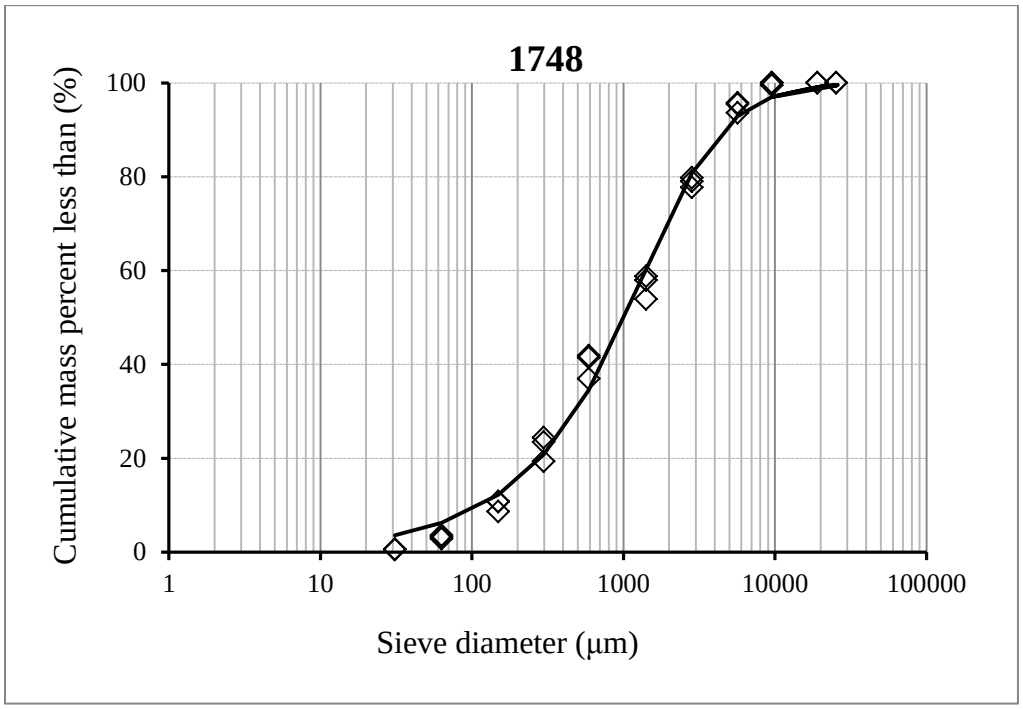
1748
Cumulative mass percent less than (%)
100
80
60
40
20
0
1
10
100
1000
10000
100000
Sieve diameter (μm)

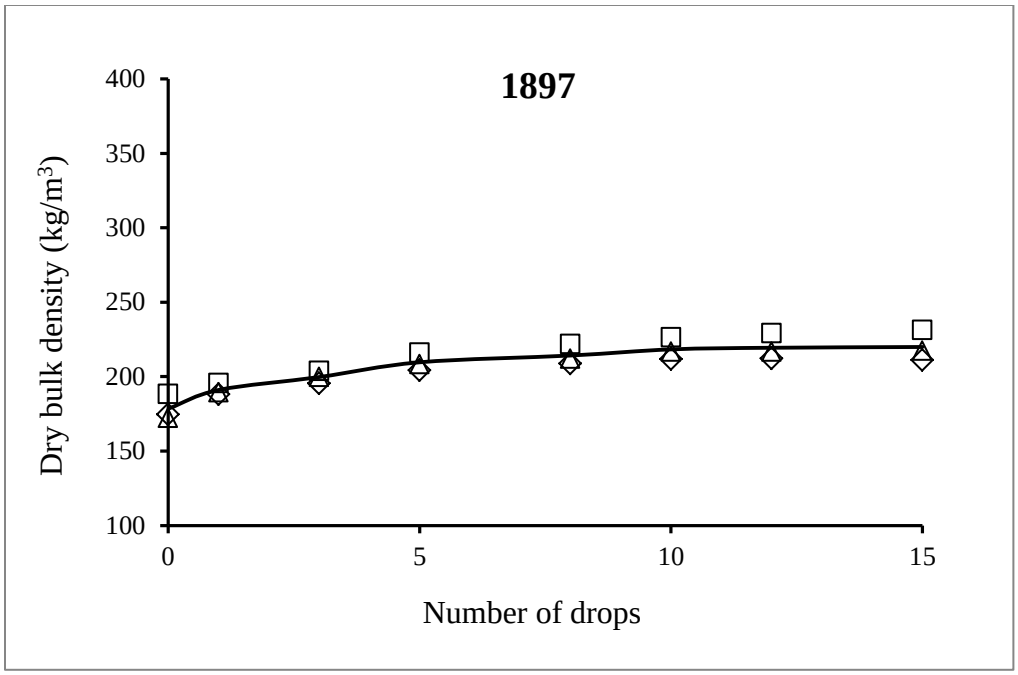
1897
Dry bulk density (kg/m3)
400
350
300
250
200
150
100
0
5
10
15
Number of drops

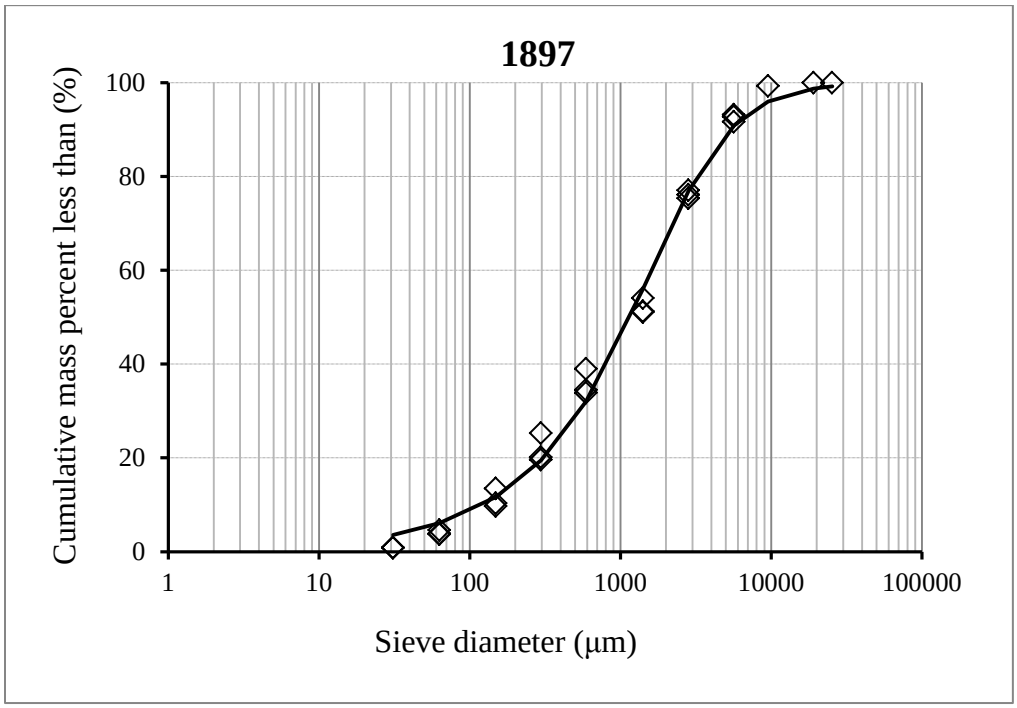
1897
Cumulative mass percent less than (%)
100
80
60
40
20
0
1
10
100
1000
10000
100000
Sieve diameter (μm)

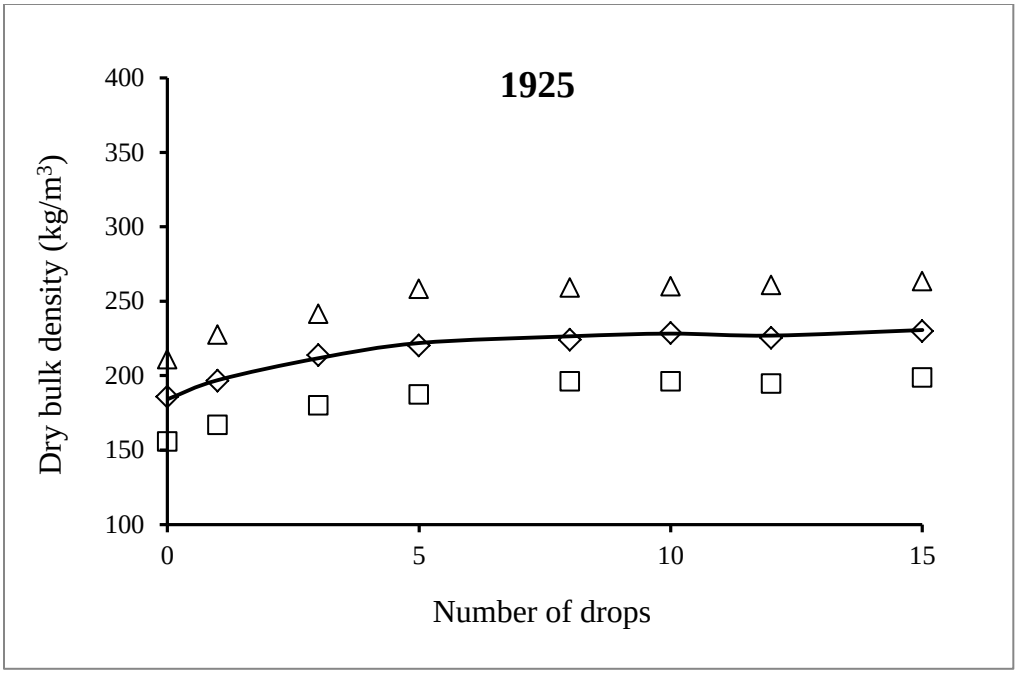
1925
Dry bulk density (kg/m³)
400
350
300
250
200
150
100
0
5
10
15
Number of drops

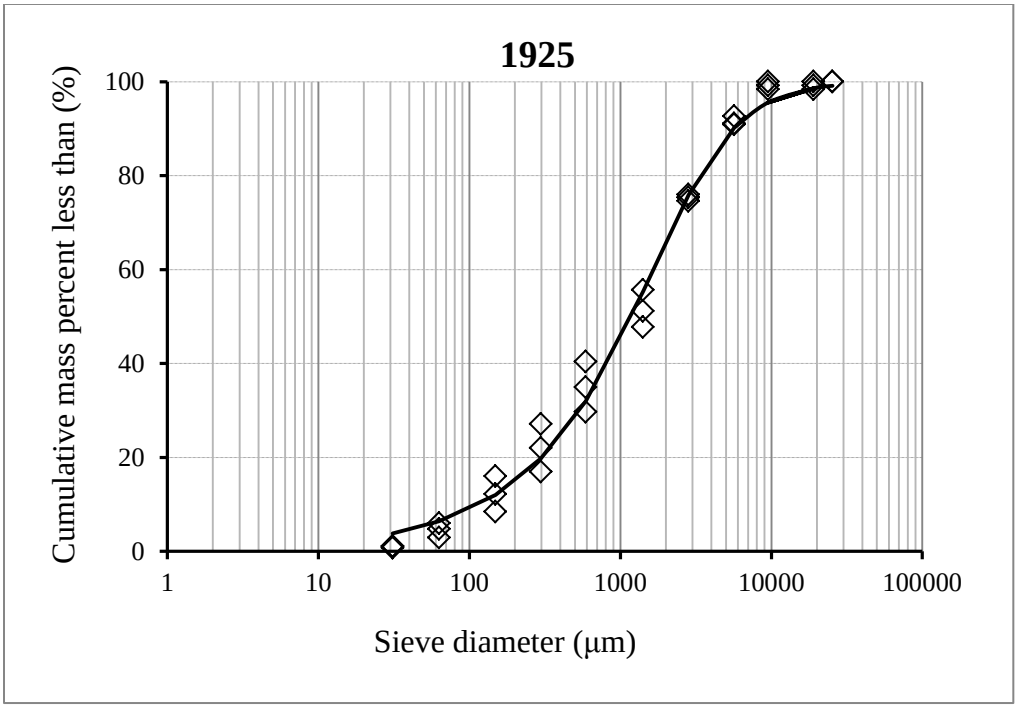
1925
Cumulative mass percent less than (%)
100
80
60
40
20
0
1
10
100
1000
10000
100000
Sieve diameter (μm)

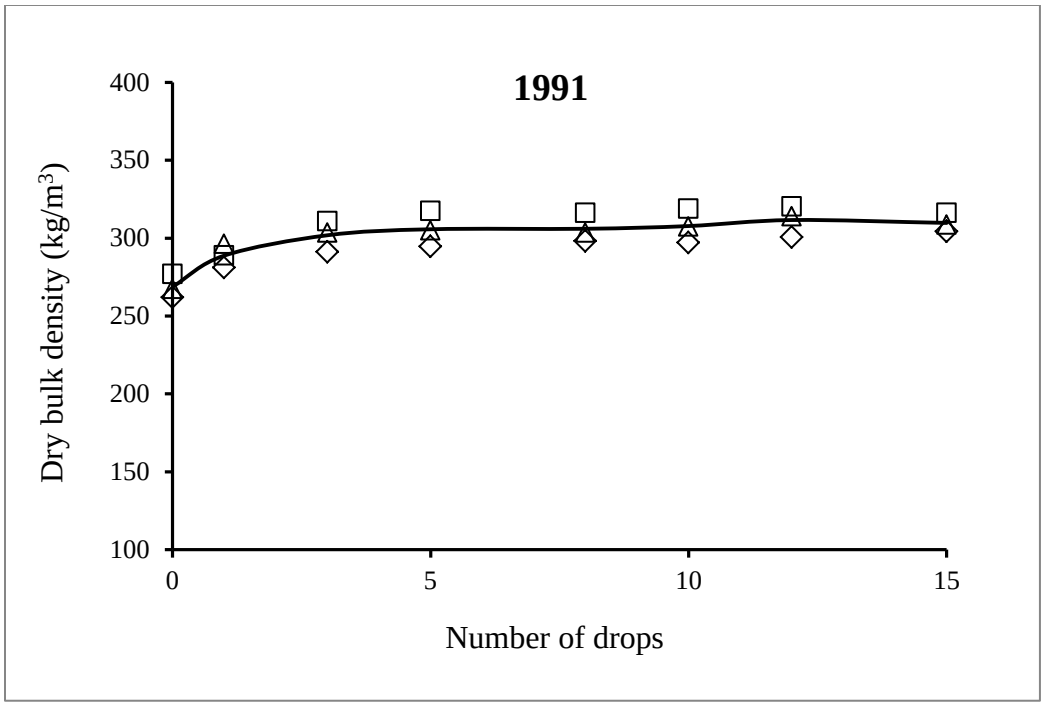
1991
Dry bulk density (kg/m3)
400
350
300
250
200
150
100
0
5
10
15
Number of drops

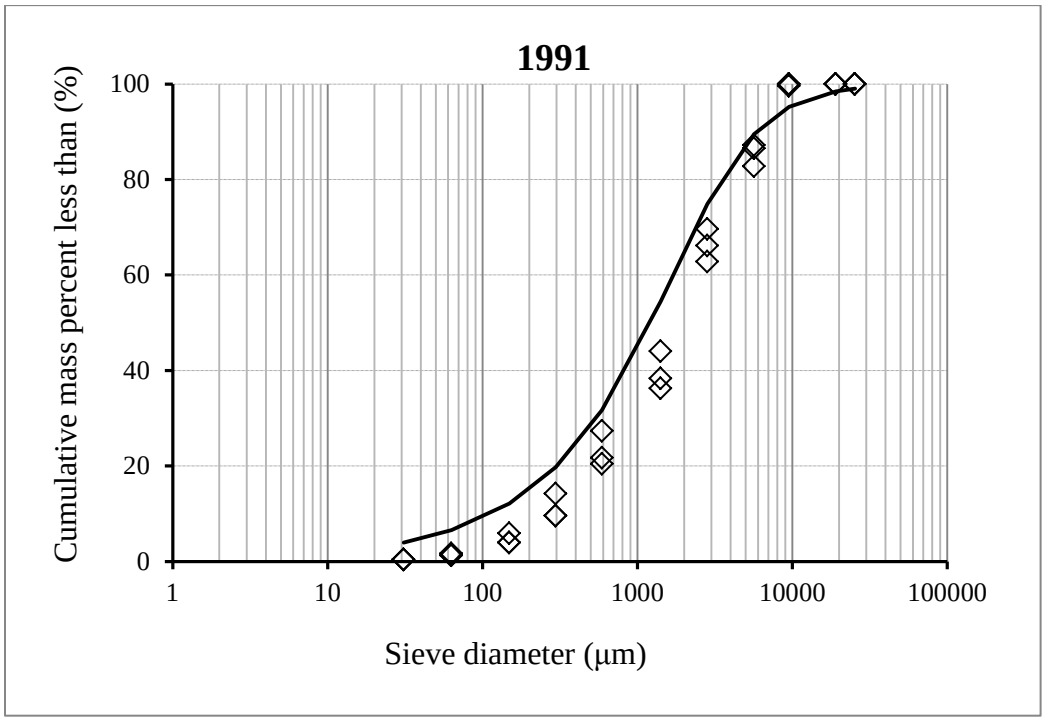
1991
Cumulative mass percent less than (%)
100
80
60
40
20
0
1
10
100
1000
10000
100000
Sieve diameter (μm)

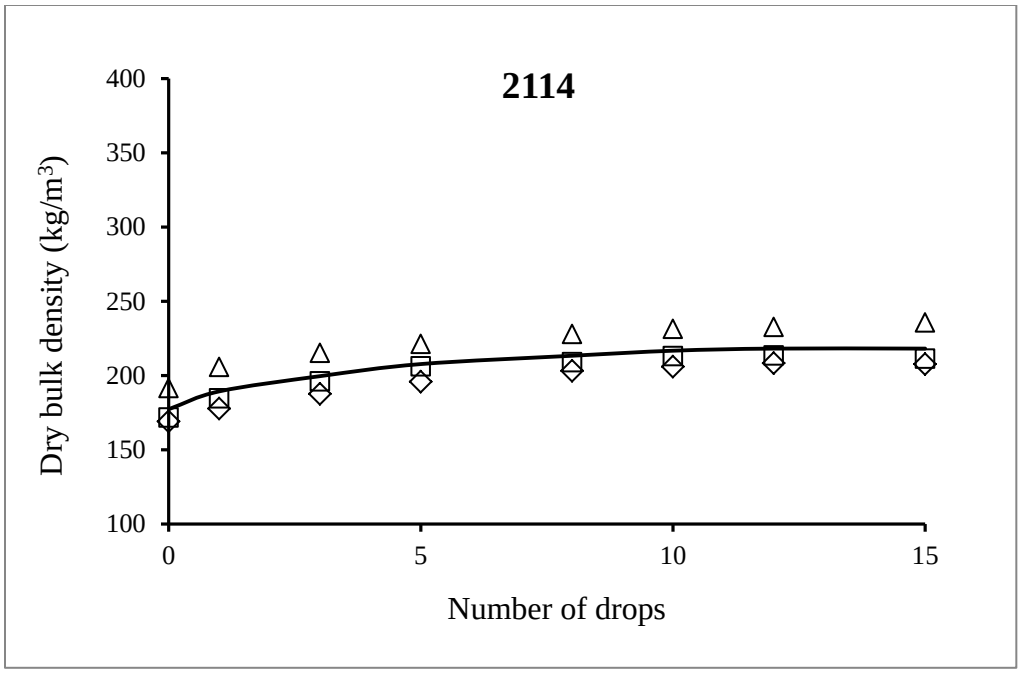
2114
Dry bulk density (kg/m³)
400
350
300
250
200
150
100
0
5
10
15
Number of drops

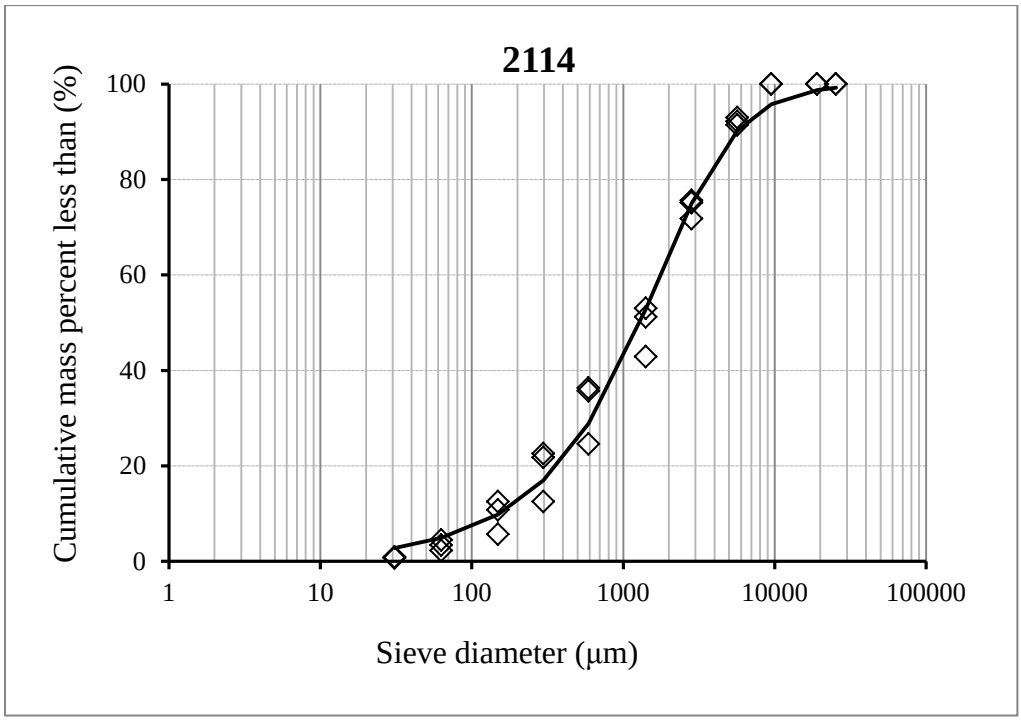
2114
Cumulative mass percent less than (%)
100
80
60
40
20
0
1
10
100
1000
10000
100000
Sieve diameter (μm)

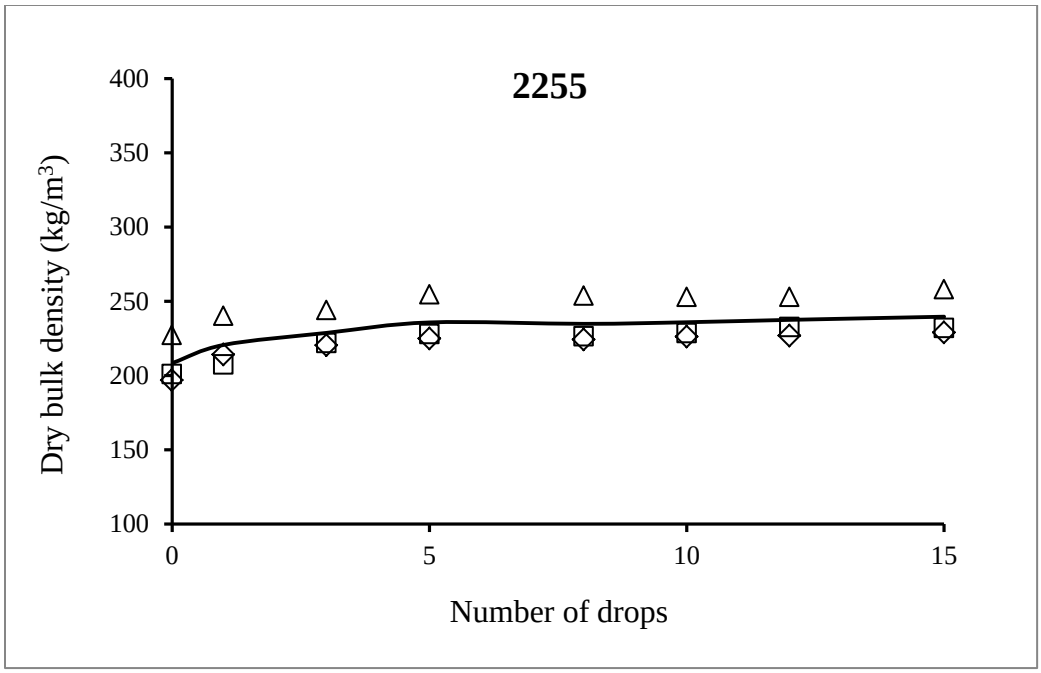
2255
Dry bulk density (kg/m3)
400
350
300
250
200
150
100
0
5
10
15
Number of drops

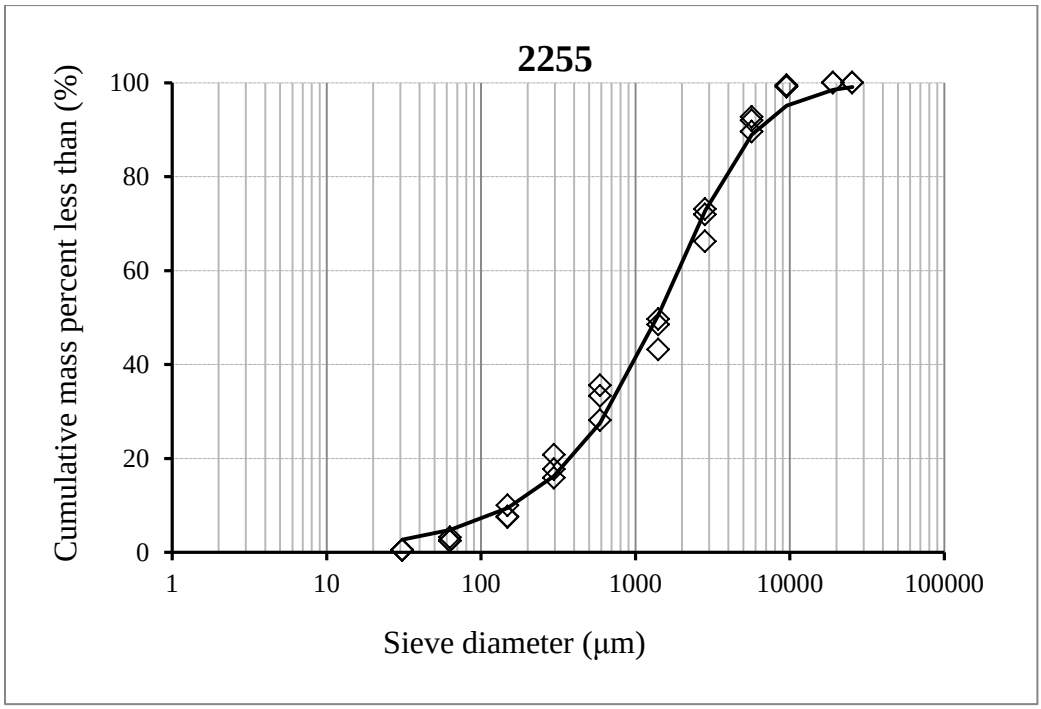
2255
Cumulative mass percent less than (%)
100
80
60
40
20
0
1
10
100
1000
10000
100000
Sieve diameter (μm)

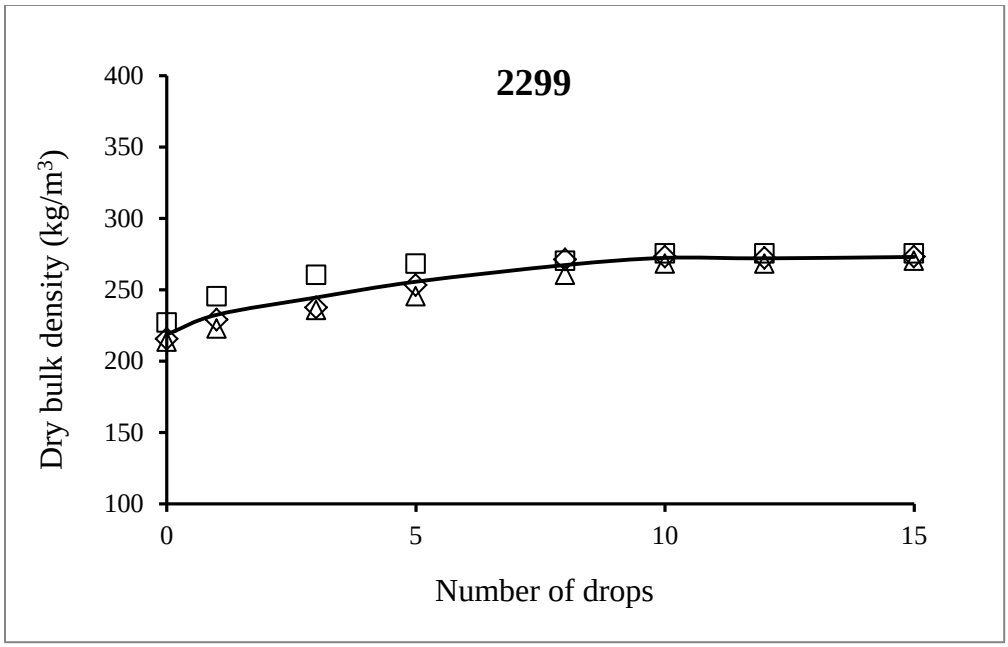
2299
Dry bulk density (kg/m3)
400
350
300
250
200
150
100
0
5
10
15
Number of drops

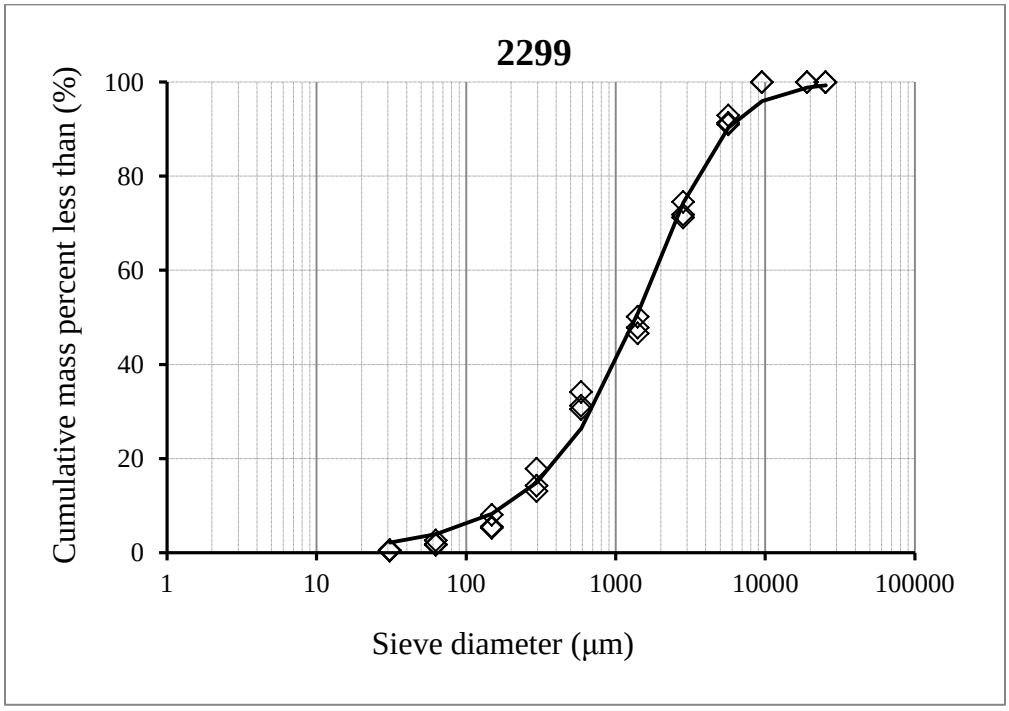
2299
Cumulative mass percent less than (%)
100
80
60
40
20
0
1
10
100
1000
10000
100000
Sieve diameter (μm)

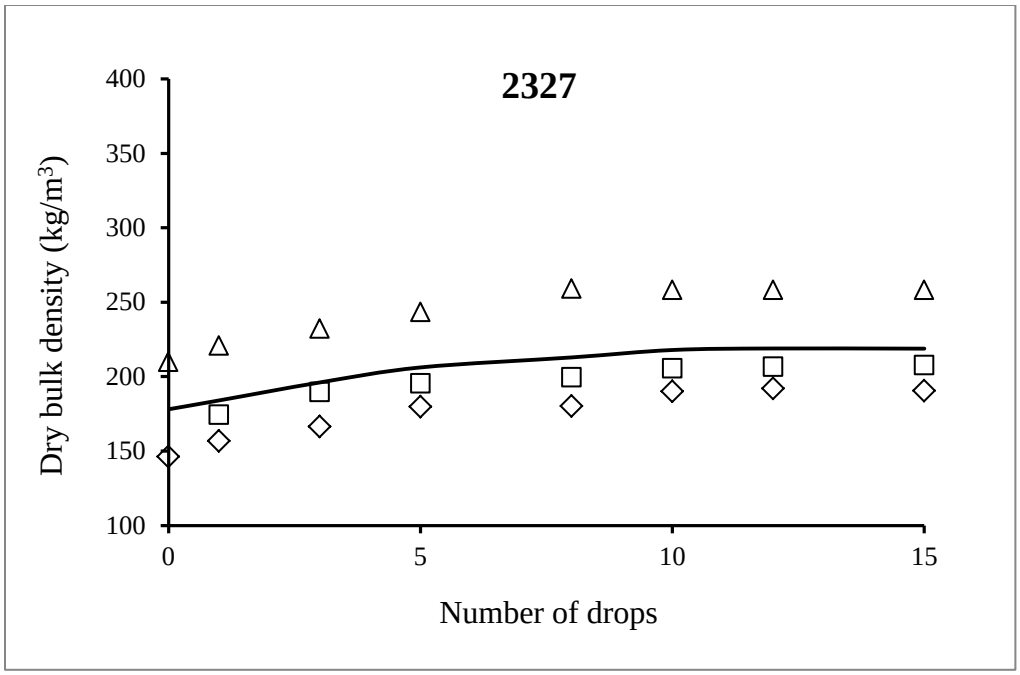
2327
Dry bulk density (kg/m3)
400
350
300
250
200
150
100
0
5
10
15
Number of drops

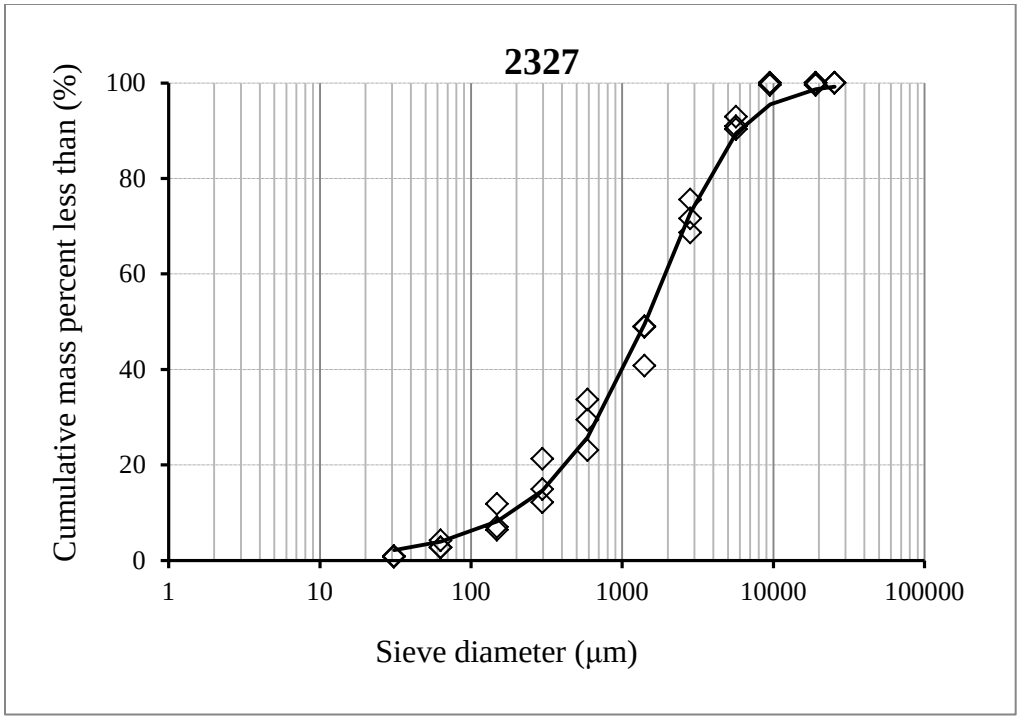
2327
Cumulative mass percent less than (%)
100
80
60
40
20
0
1
10
100
1000
10000
100000
Sieve diameter (μm)

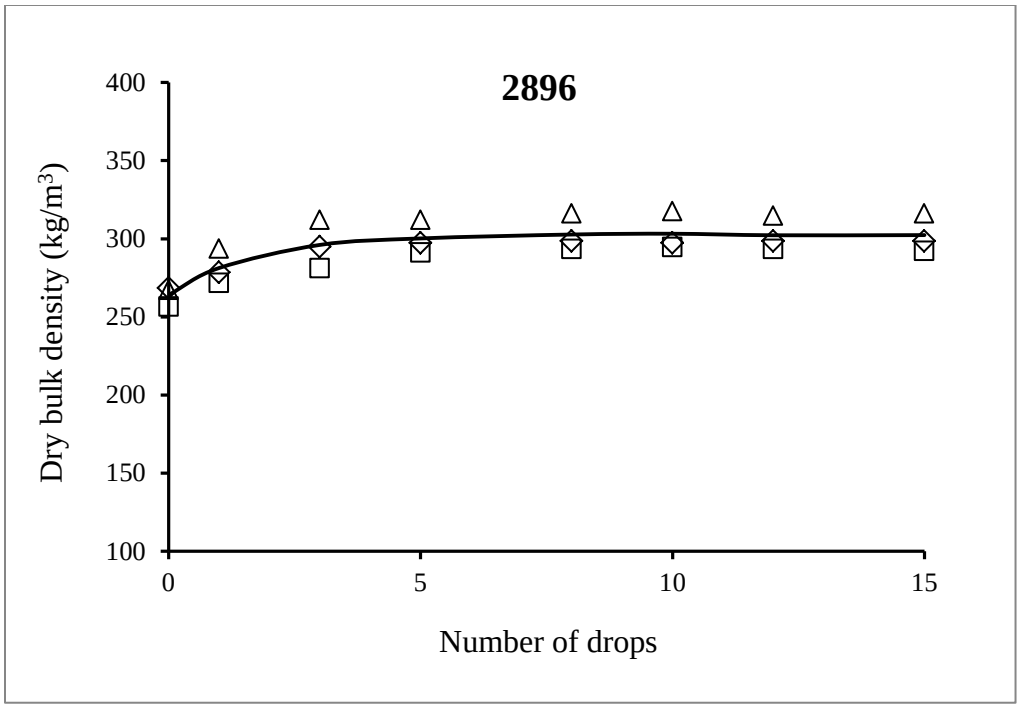
2896
Dry bulk density (kg/m3)
400
350
300
250
200
150
100
0
5
10
15
Number of drops

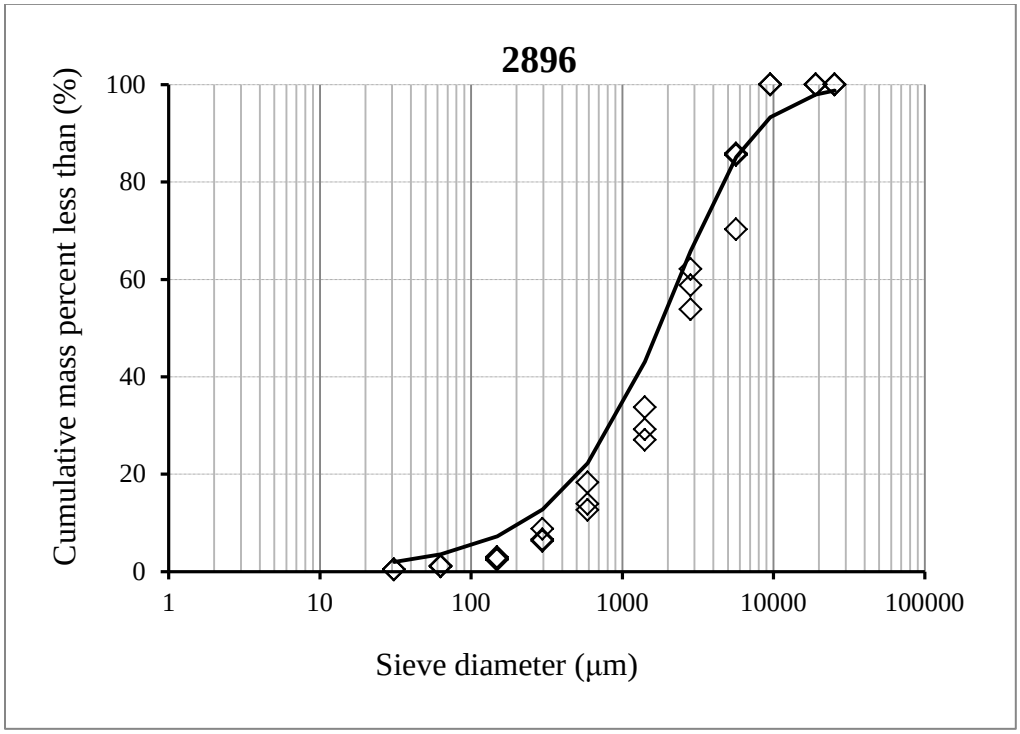
2896
Cumulative mass percent less than (%)
100
80
60
40
20
0
1
10
100
1000
10000
100000
Sieve diameter (μm)

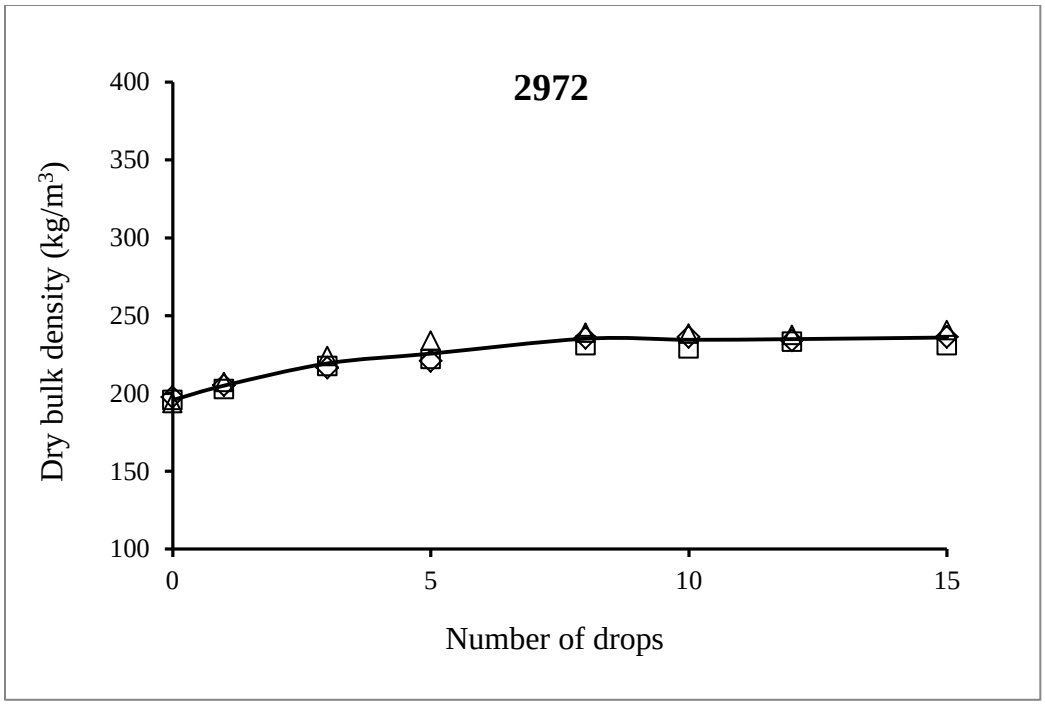
2972
Dry bulk density (kg/m3)
400
350
300
250
200
150
100
0
5
10
15
Number of drops

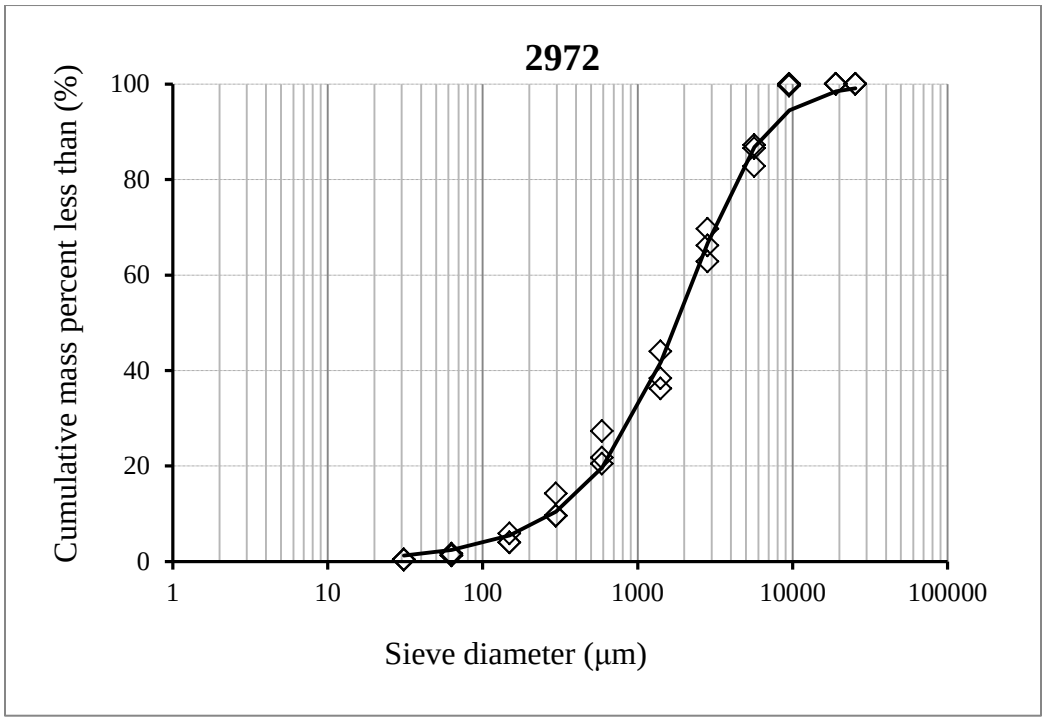
2972
Cumulative mass percent less than (%)
100
80
60
40
20
0
1
10
100
1000
10000
100000
Sieve diameter (μm)

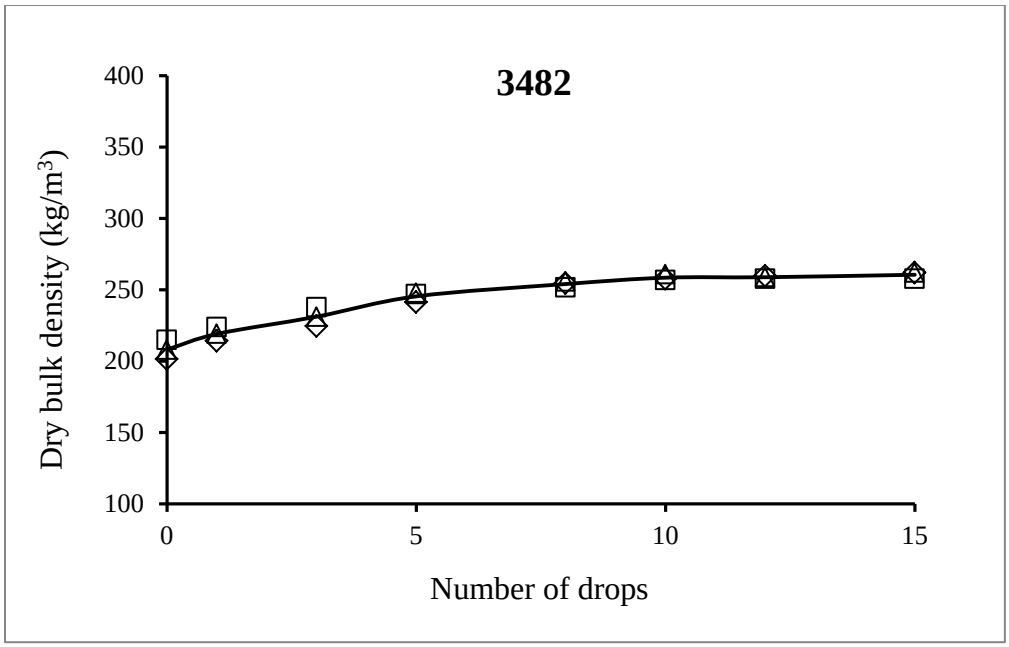
3482
Dry bulk density (kg/m3)
400
350
300
250
200
150
100
0
5
10
15
Number of drops

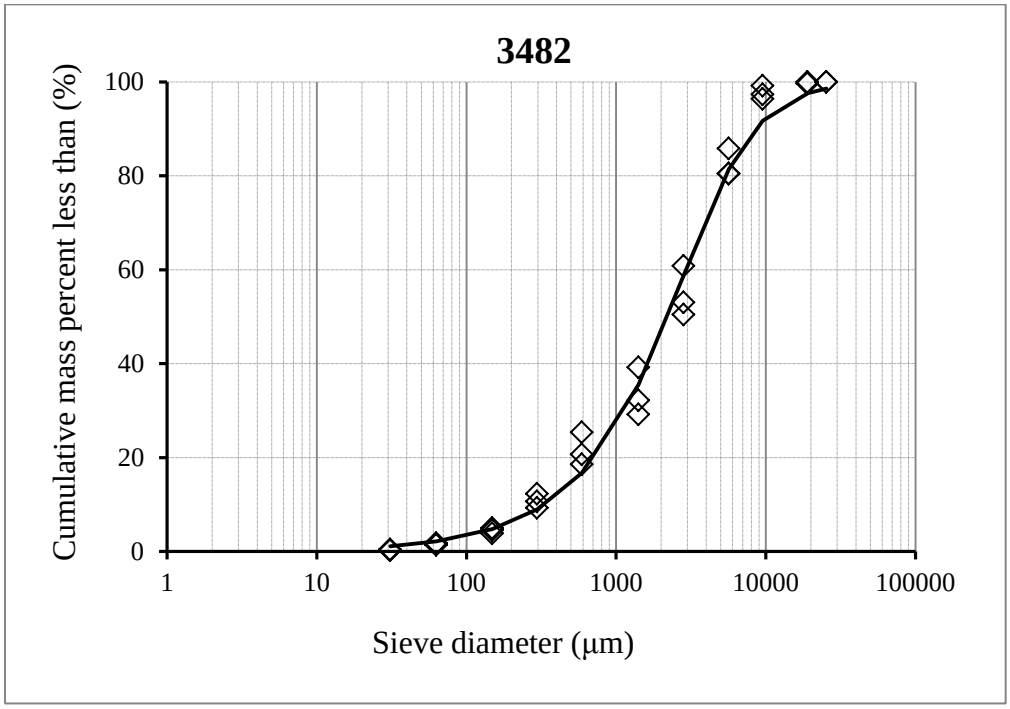
3482
Cumulative mass percent less than (%)
100
80
60
40
20
0
1
10
100
1000
10000
100000
Sieve diameter (μm)

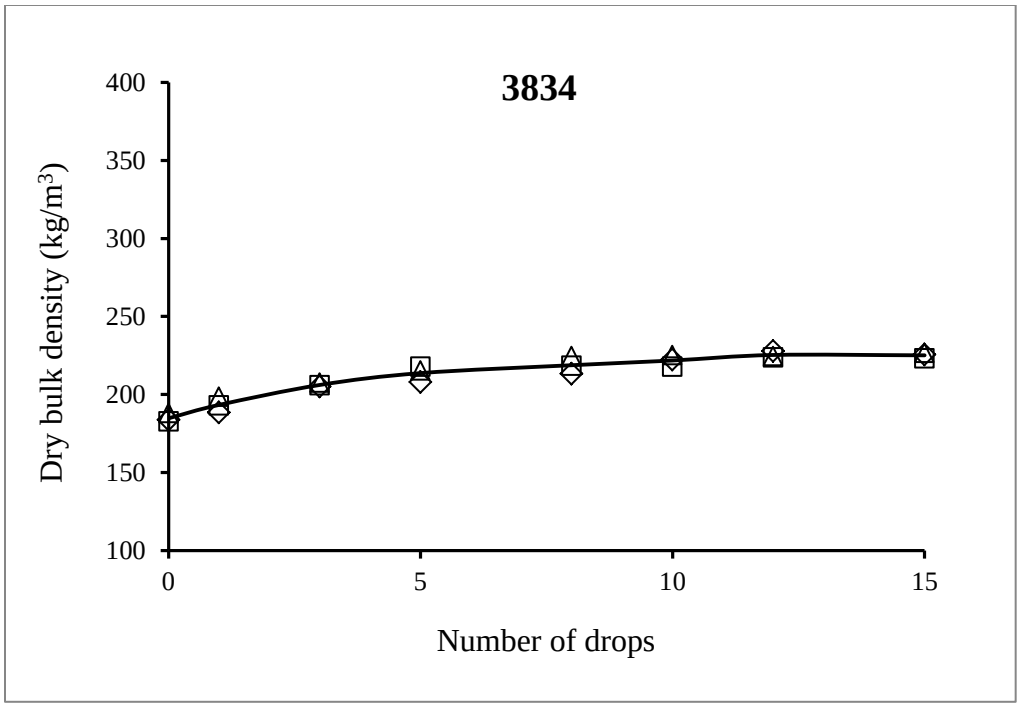
3834
Dry bulk density (kg/m3)
400
350
300
250
200
150
100
0
5
10
15
Number of drops

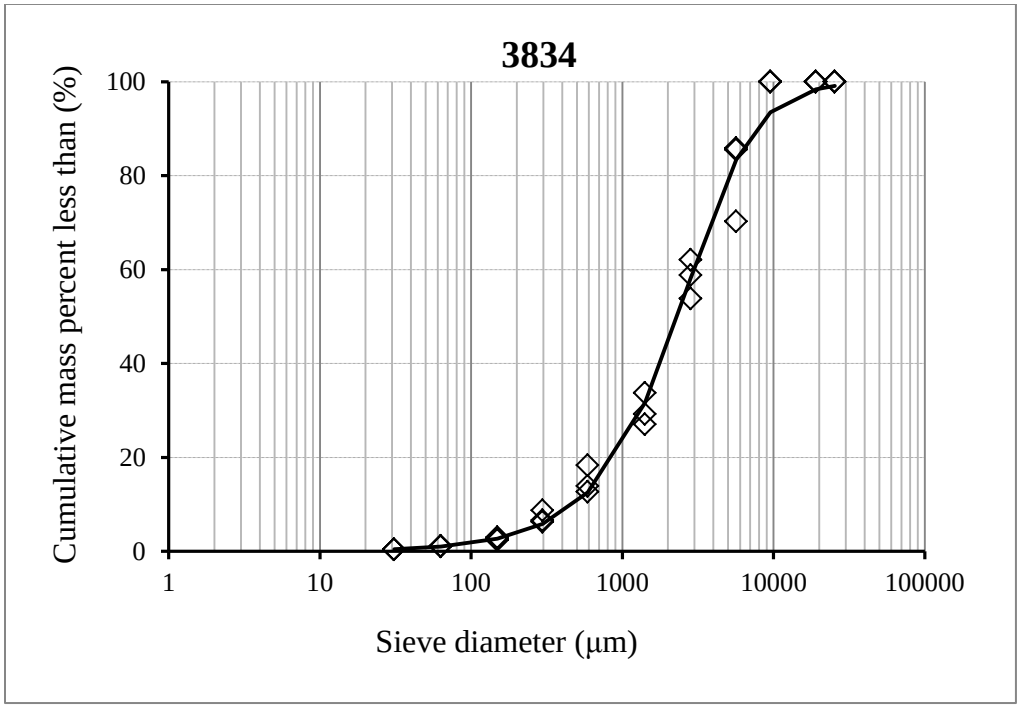
3834
Cumulative mass percent less than (%)
100
80
60
40
20
0
1
10
100
1000
10000
100000
Sieve diameter (μm)

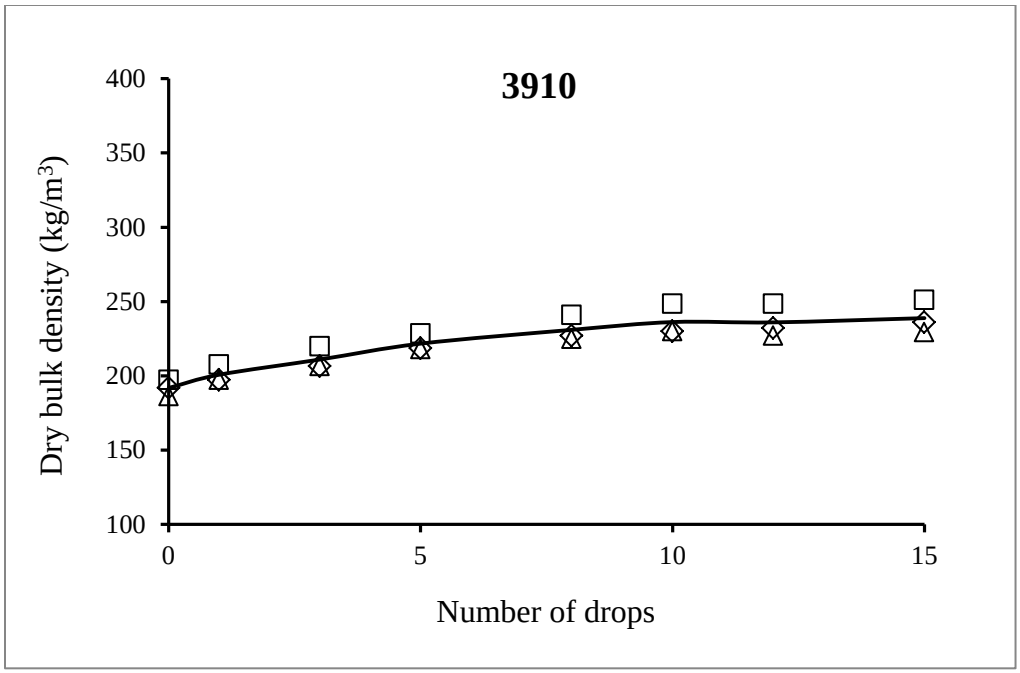
3910
Dry bulk density (kg/m3)
400
350
300
250
200
150
100
0
5
10
15
Number of drops

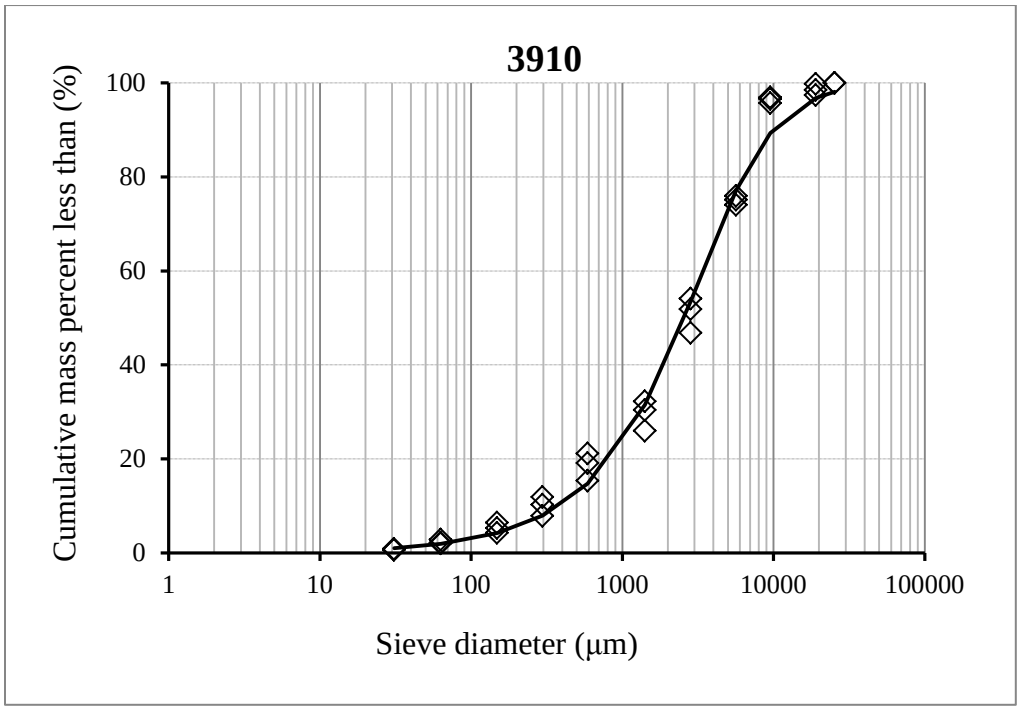
3910
Cumulative mass percent less than (%)
100
80
60
40
20
0
1
10
100
1000
10000
100000
Sieve diameter (μm)

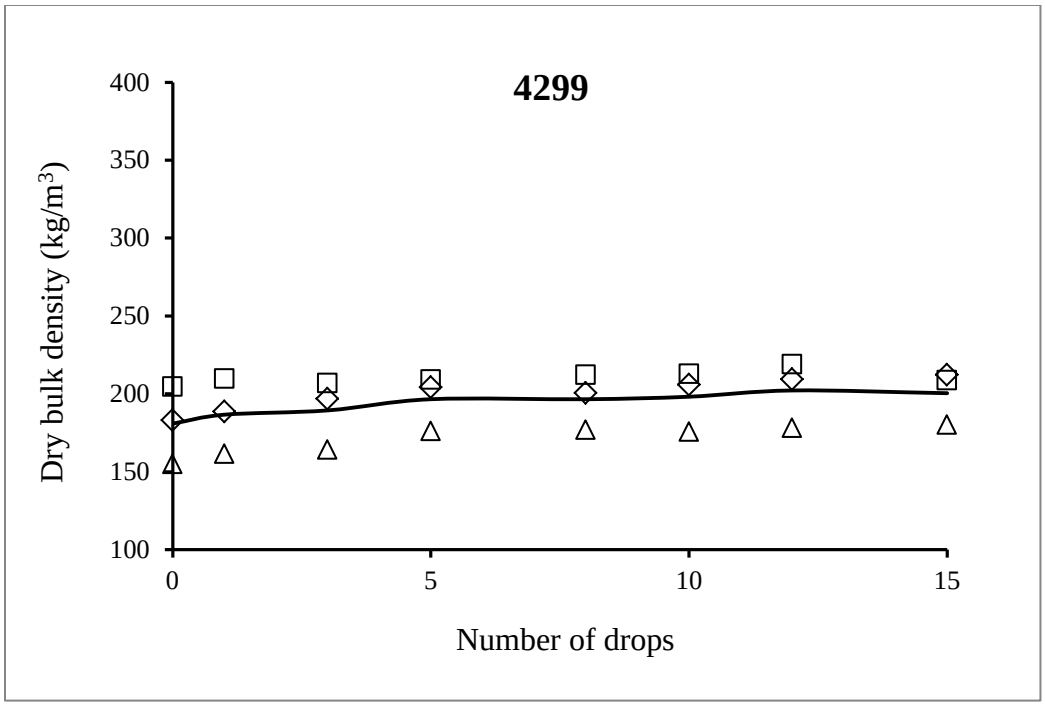
4299
Dry bulk density (kg/m3)
400
350
300
250
200
150
100
0
5
10
15
Number of drops

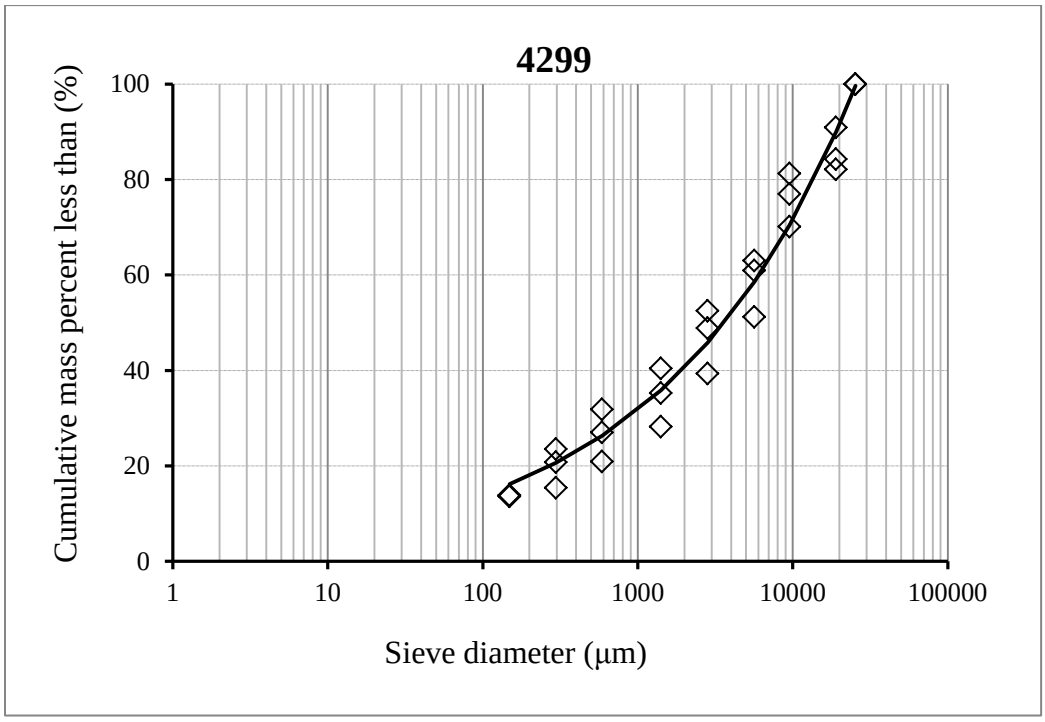
4299
Cumulative mass percent less than (%)
100
80
60
40
20
0
1
10
100
1000
10000
100000
Sieve diameter (μm)

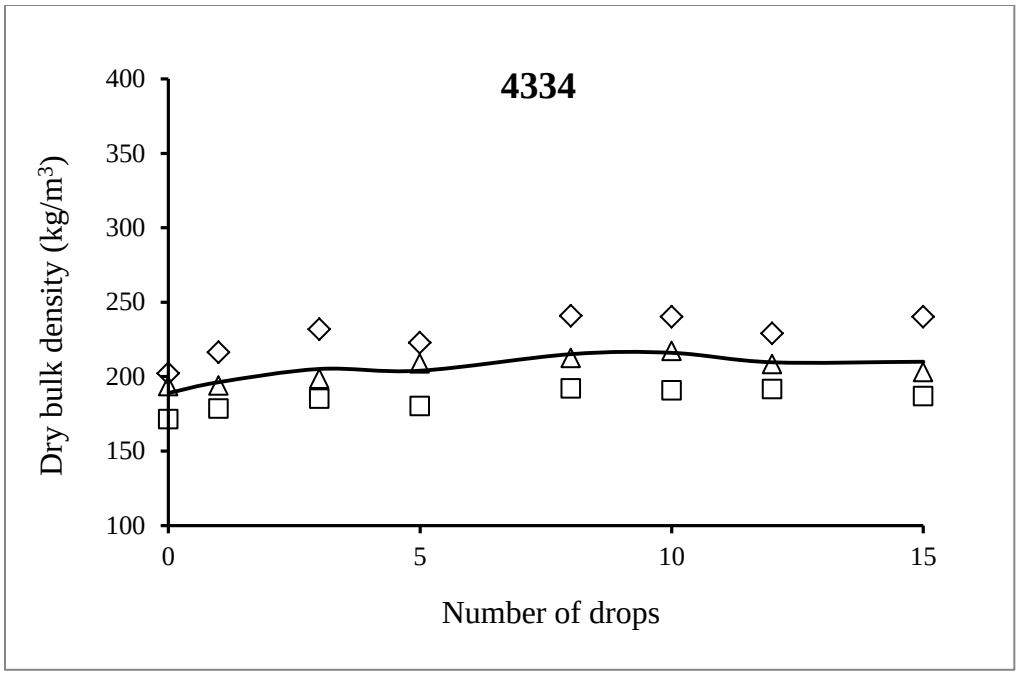
4334
Dry bulk density (kg/m3)
400
350
300
250
200
150
100
0
5
10
15
Number of drops

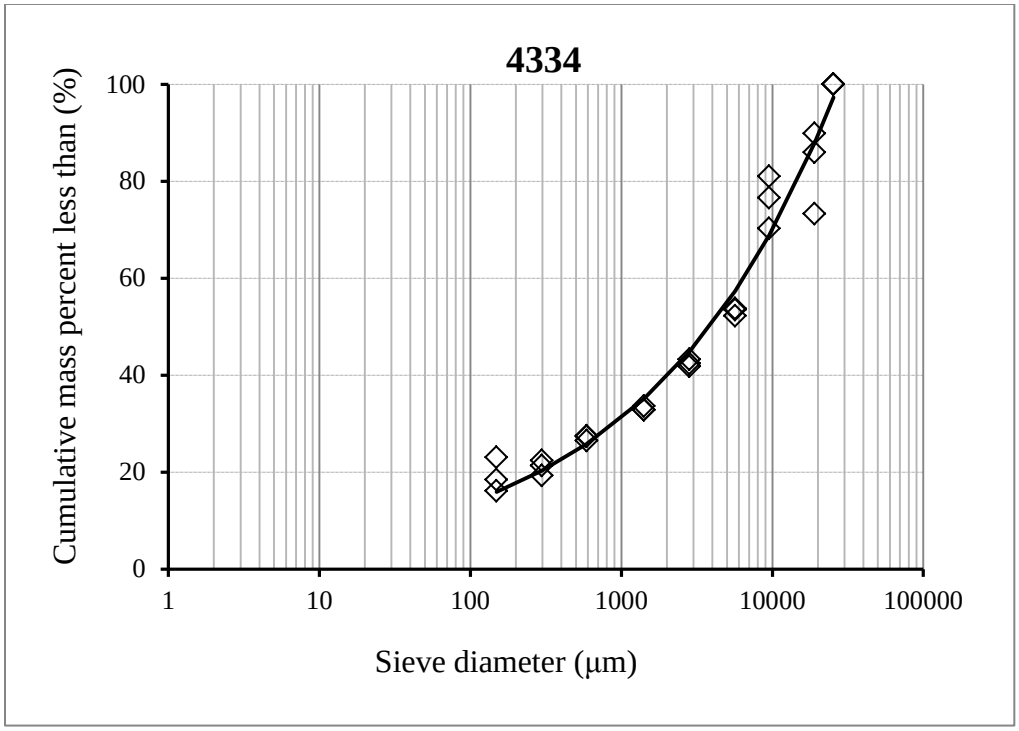
4334
Cumulative mass percent less than (%)
100
80
60
40
20
0
1
10
100
1000
10000
100000
Sieve diameter (μm)

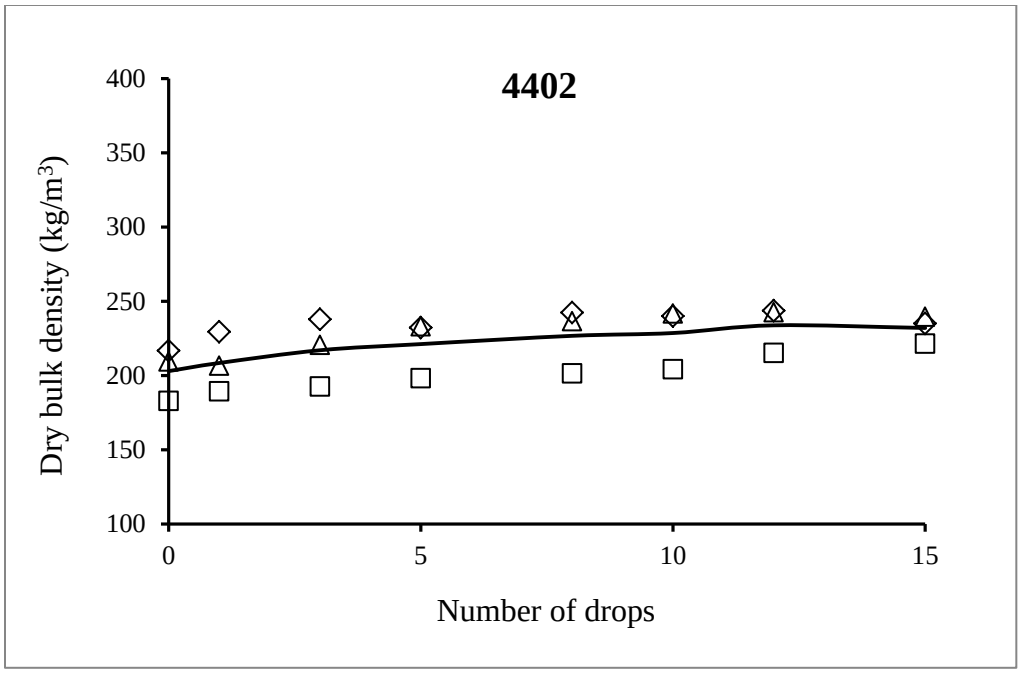
4402
Dry bulk density (kg/m3)
400
350
300
250
200
150
100
0
5
10
15
Number of drops

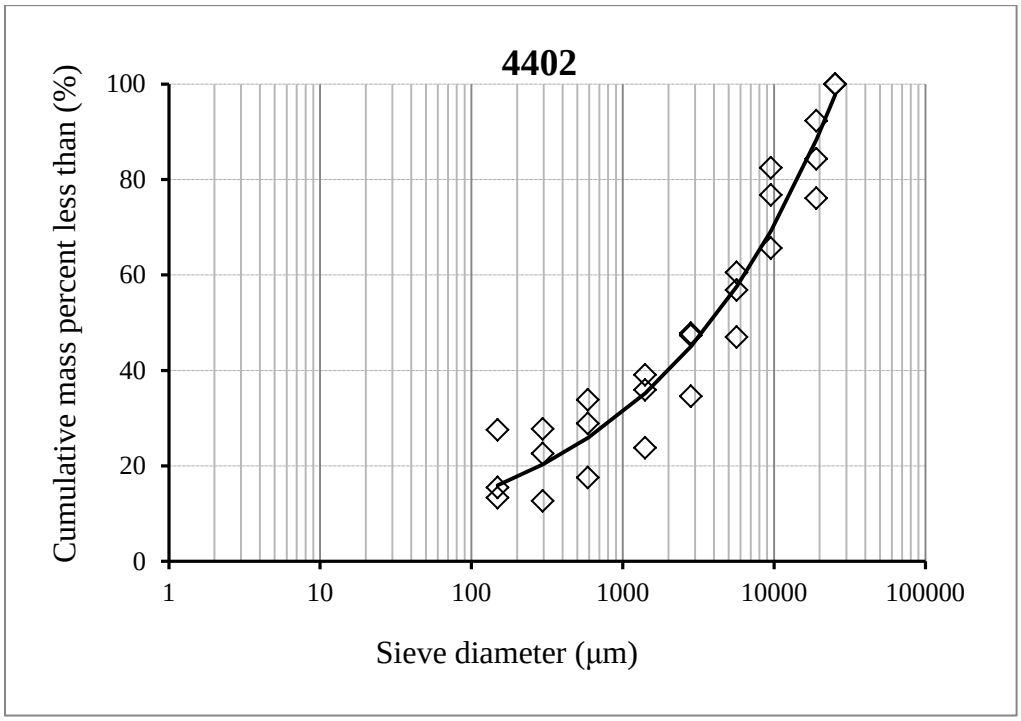
4402
Cumulative mass percent less than (%)
100
80
60
40
20
0
1
10
100
1000
10000
100000
Sieve diameter (μm)

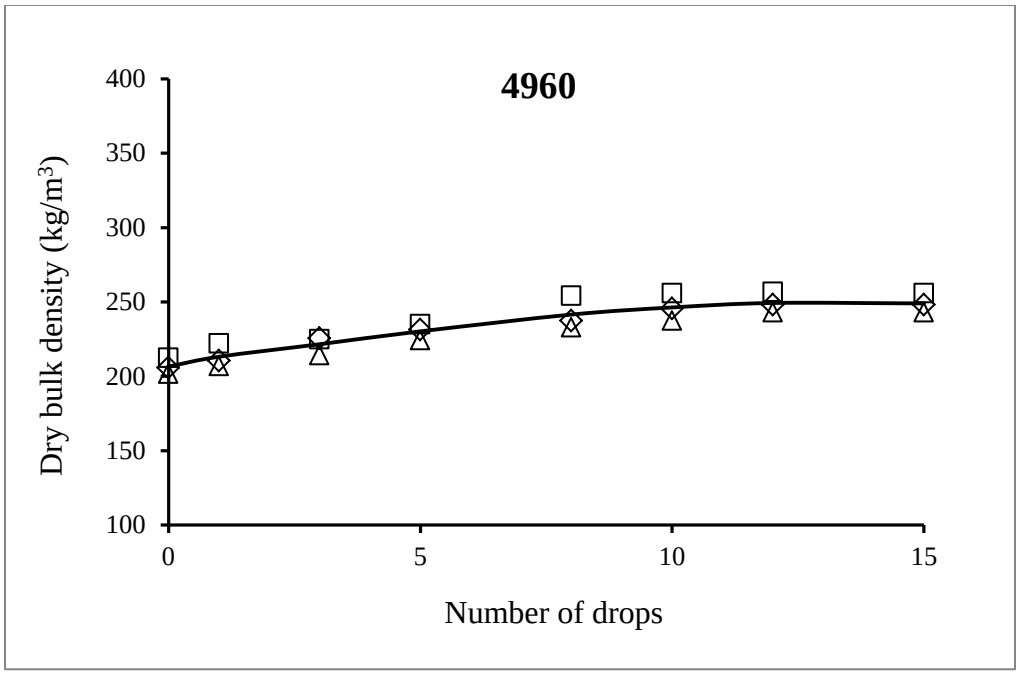
4960
Dry bulk density (kg/m3)
400
350
300
250
200
150
100
0
5
10
15
Number of drops

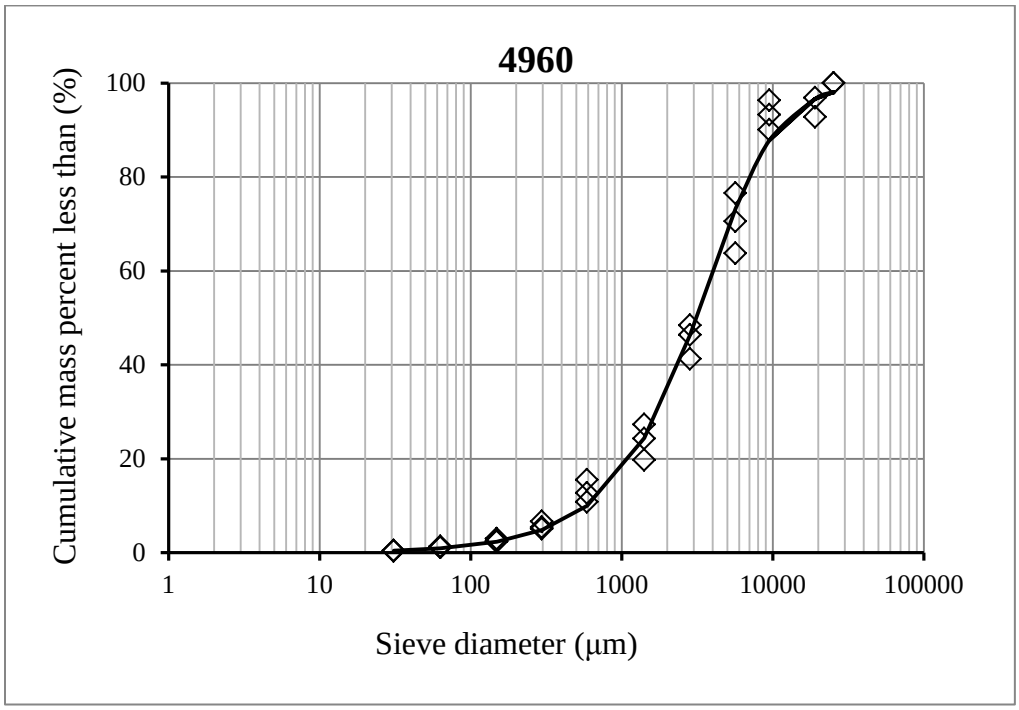
4960
Cumulative mass percent less than (%)
100
80
60
40
20
0
1
10
100
1000
10000
100000
Sieve diameter (μm)

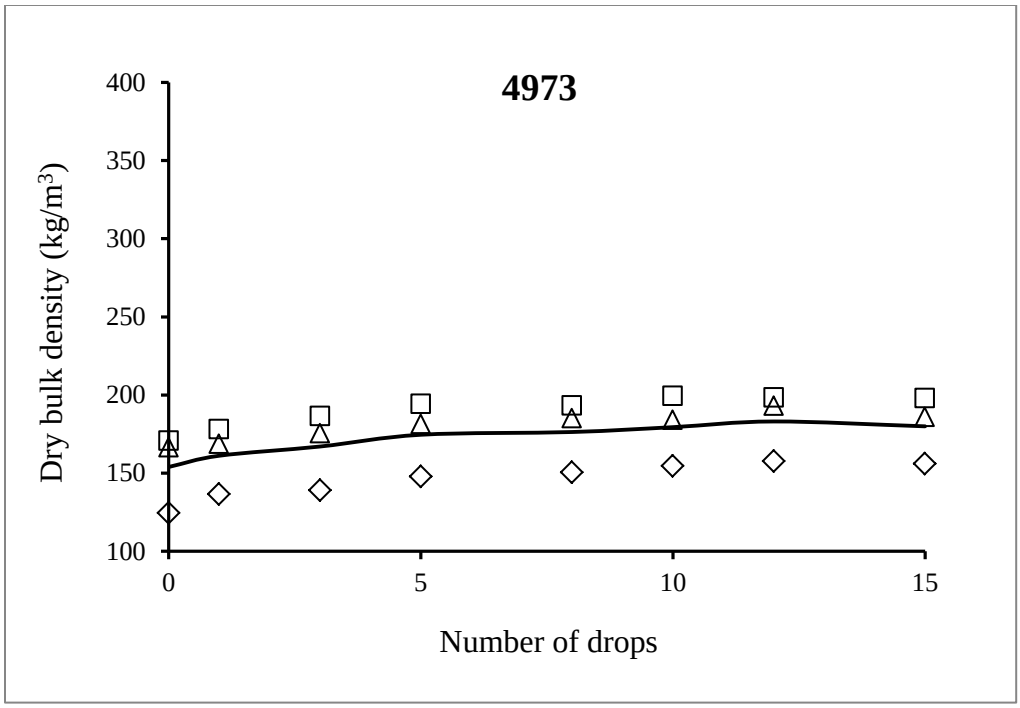
4973
Dry bulk density (kg/m3)
400
350
300
250
200
150
100
0
5
10
15
Number of drops

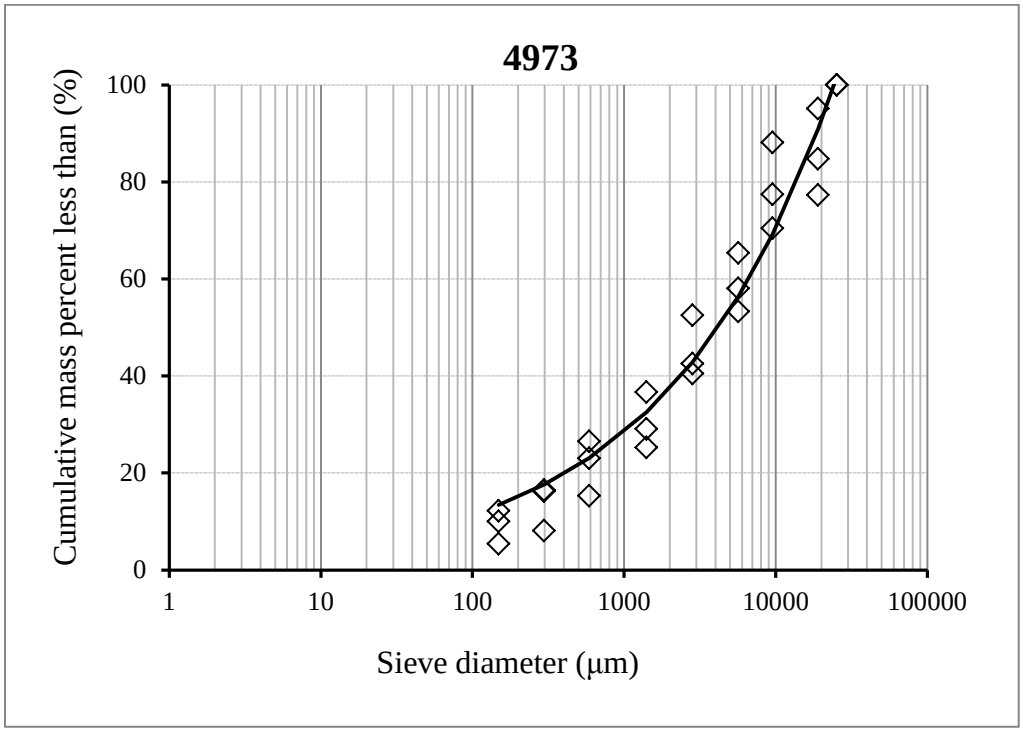
4973
Cumulative mass percent less than (%)
100
80
60
40
20
0
1
10
100
1000
10000
100000
Sieve diameter (μm)

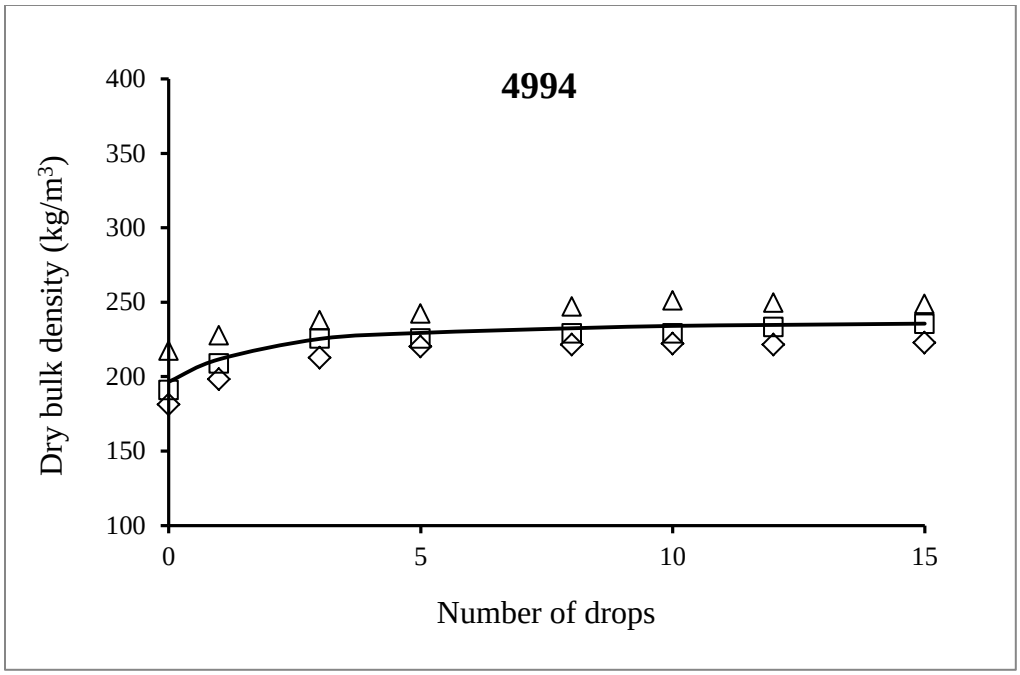
4994
Dry bulk density (kg/m³)
400
350
300
250
200
150
100
0
5
10
15
Number of drops

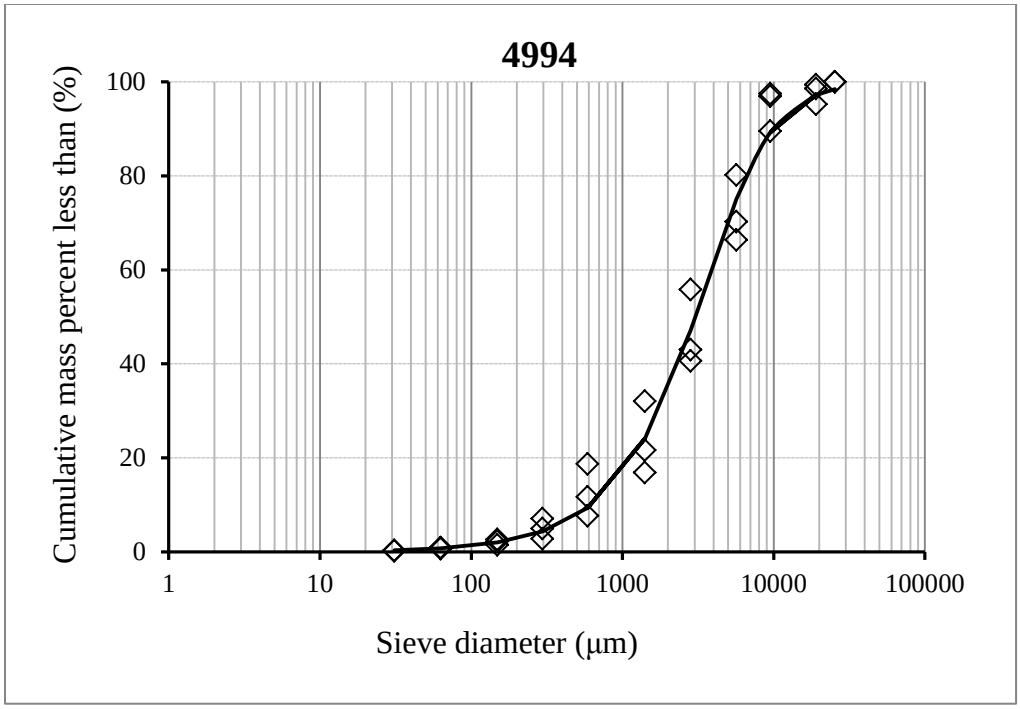
4994
Cumulative mass percent less than (%)
100
80
60
40
20
0
1
10
100
1000
10000
100000
Sieve diameter (μm)

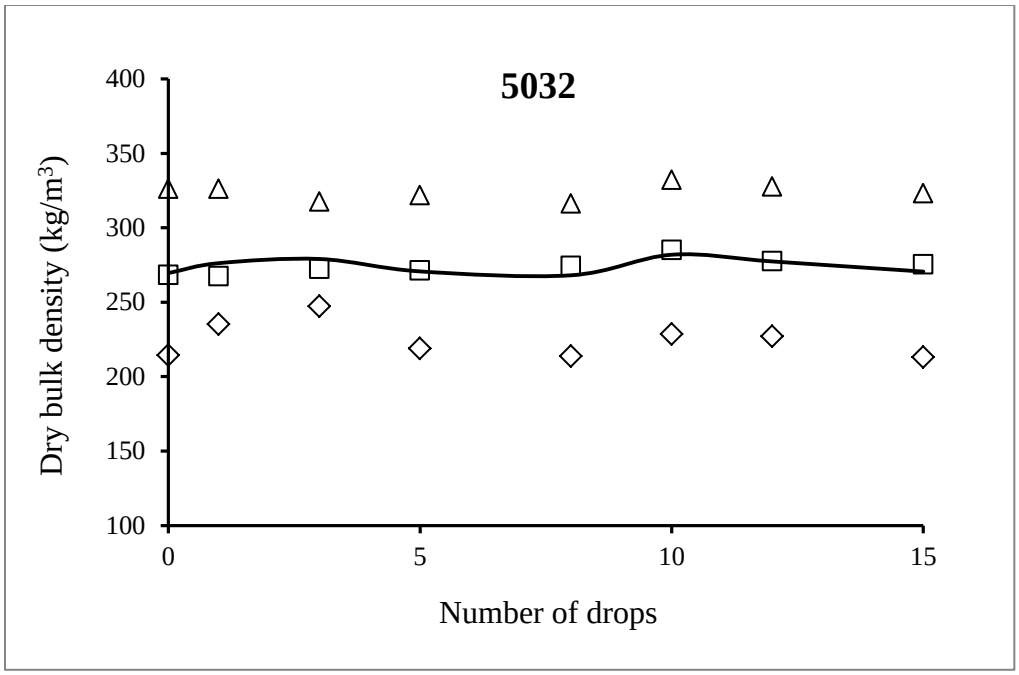
5032
Dry bulk density (kg/m³)
400
350
300
250
200
150
100
0
5
10
15
Number of drops

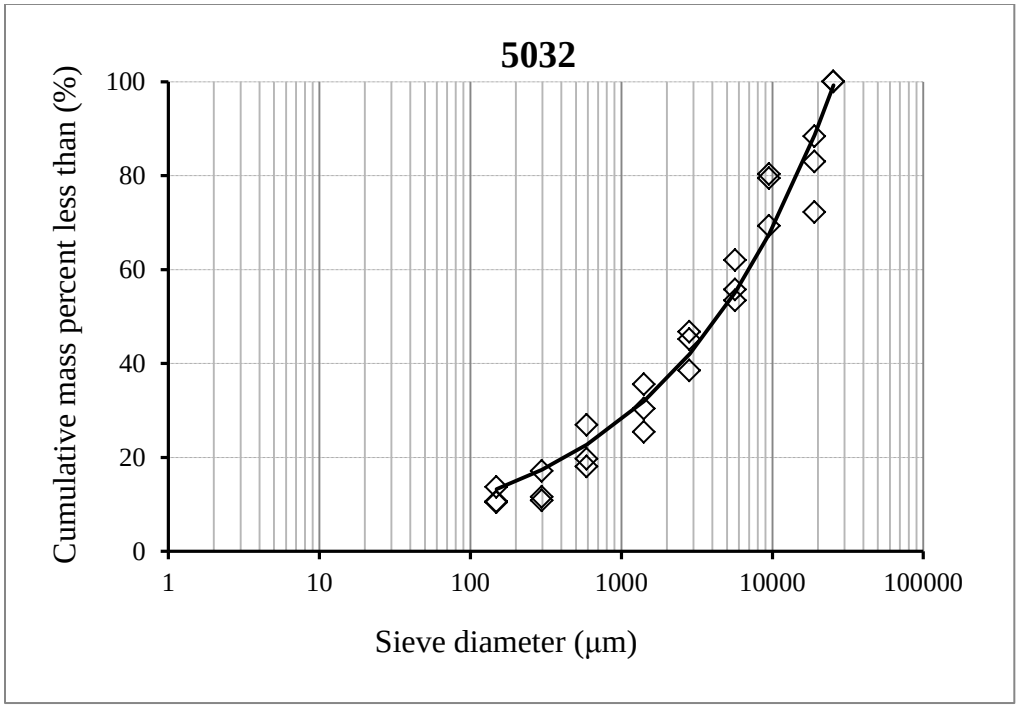
5032
Cumulative mass percent less than (%)
100
80
60
40
20
0
1
10
100
1000
10000
100000
Sieve diameter (μm)

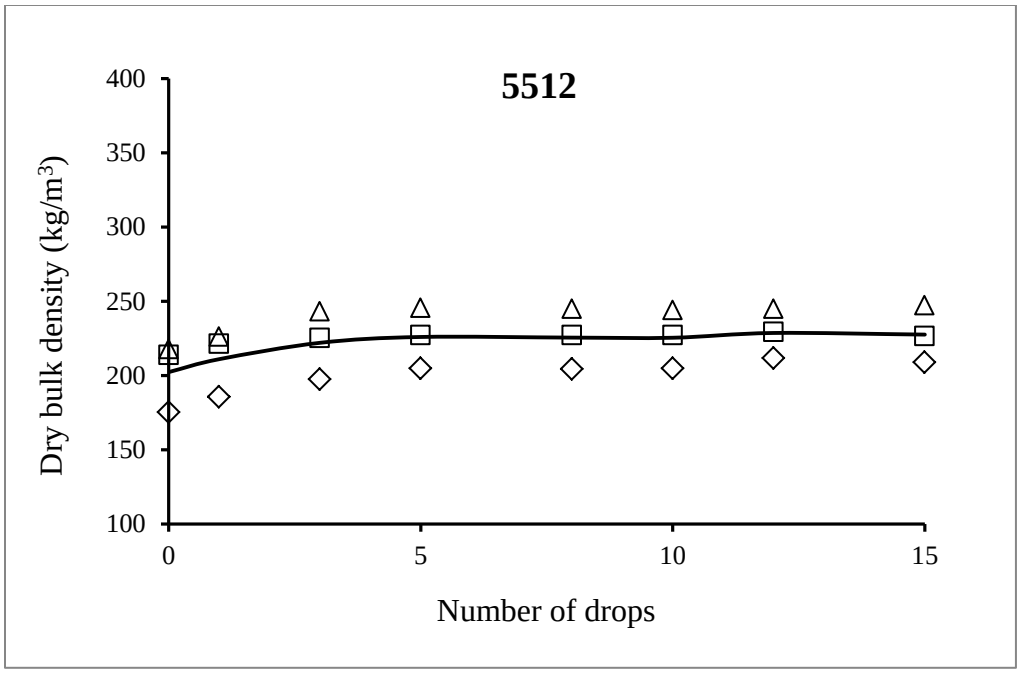
5512
Dry bulk density (kg/m3)
400
350
300
250
200
150
100
0
5
10
15
Number of drops

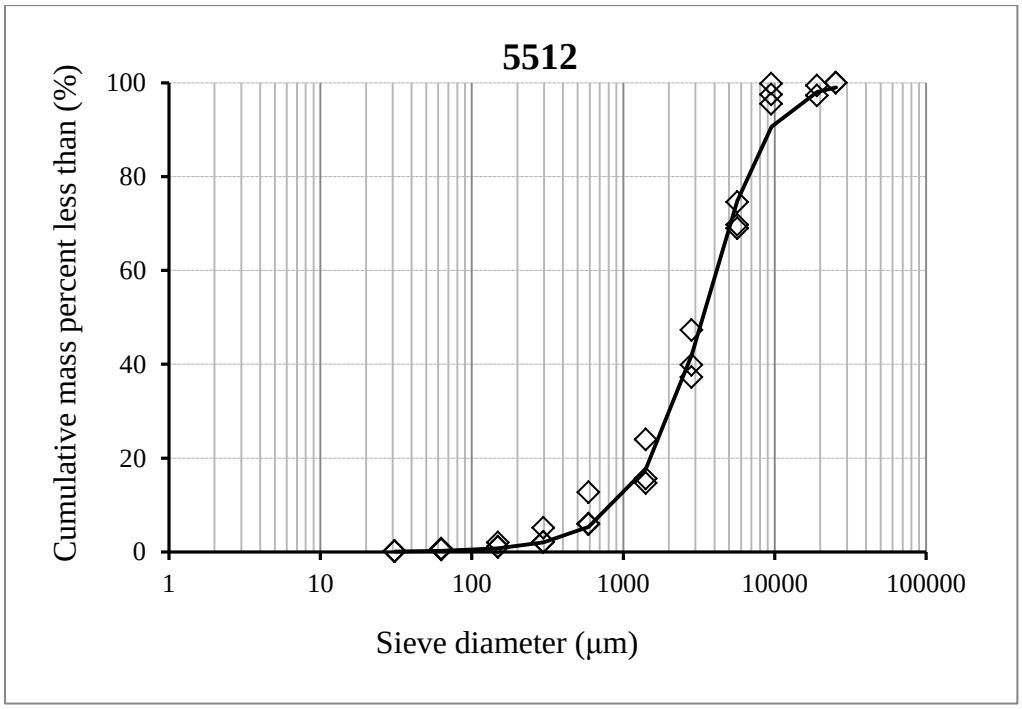
5512
Cumulative mass percent less than (%)
100
80
60
40
20
0
1
10
100
1000
10000
100000
Sieve diameter (μm)

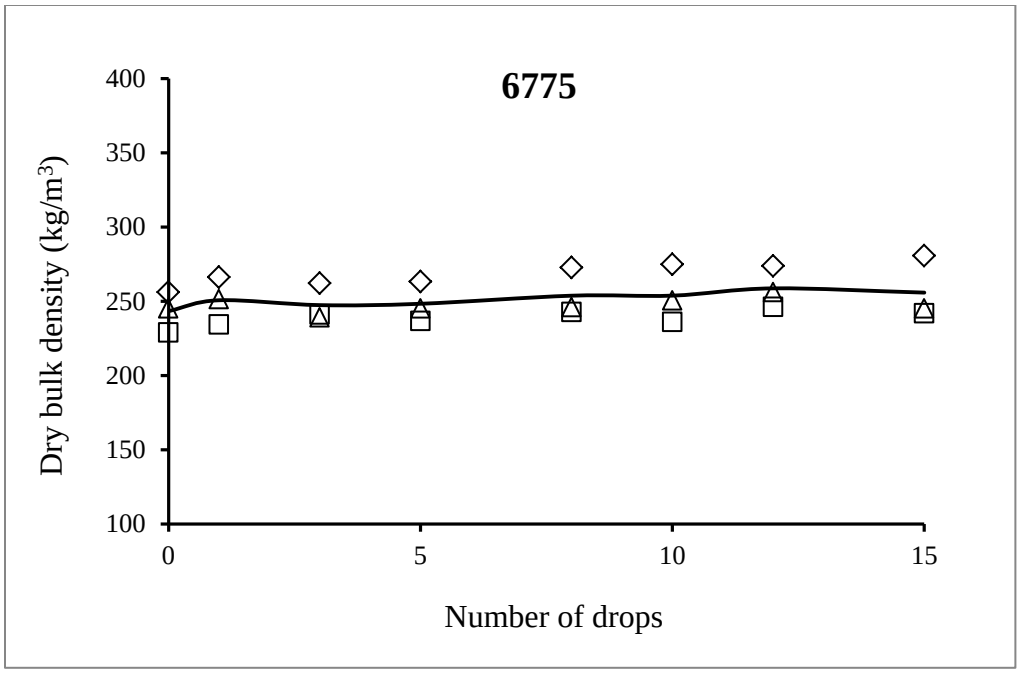
6775
Dry bulk density (kg/m3)
400
350
300
250
200
150
100
0
5
10
15
Number of drops

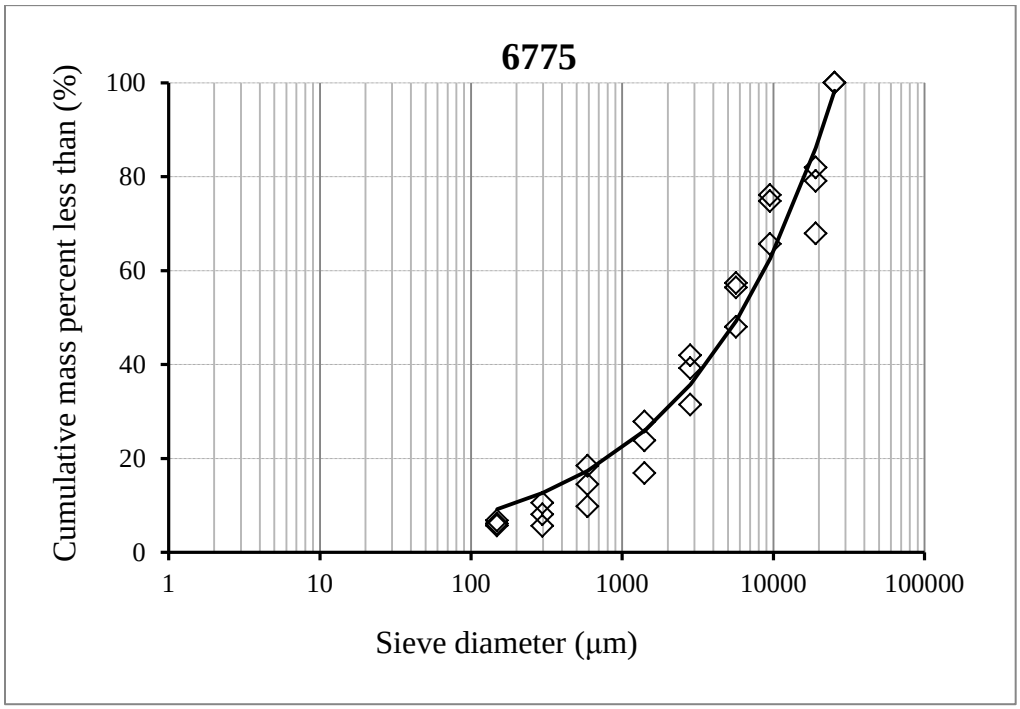
6775
Cumulative mass percent less than (%)
100
80
60
40
20
0
1
10
100
1000
10000
100000
Sieve diameter (μm)

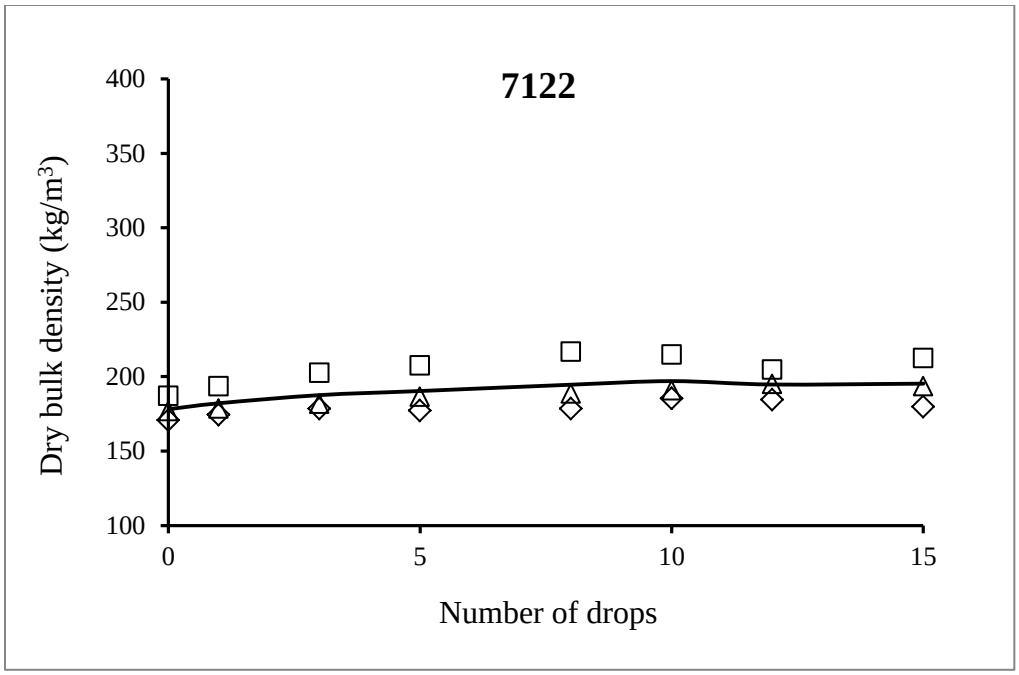
7122
Dry bulk density (kg/m3)
400
350
300
250
200
150
100
0
5
10
15
Number of drops

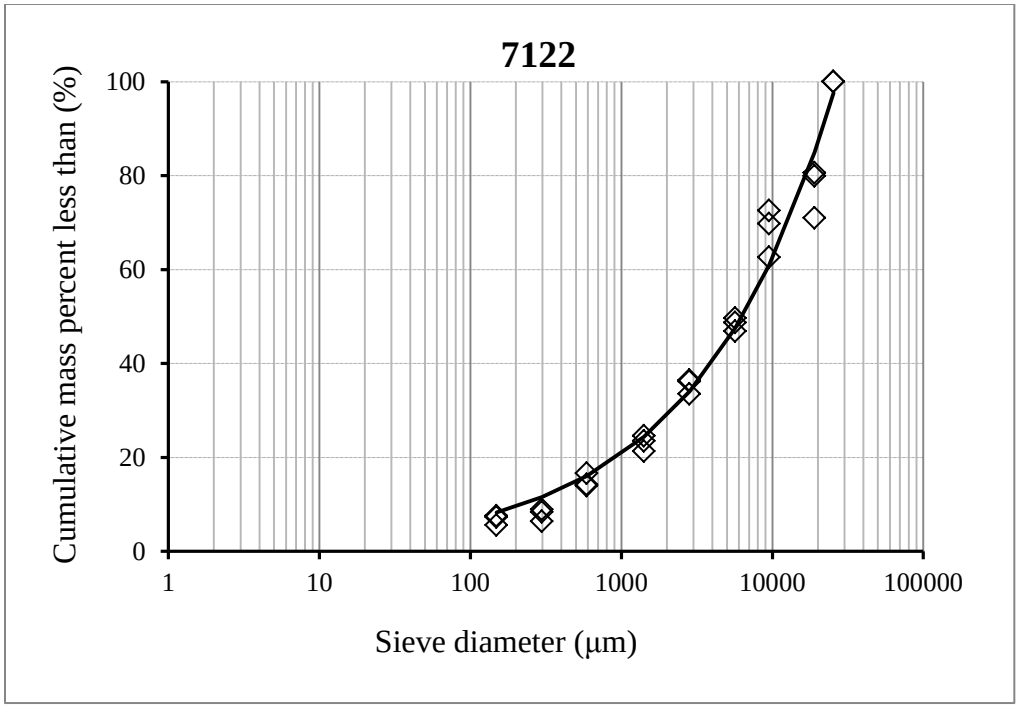
7122
Cumulative mass percent less than (%)
100
80
60
40
20
0
1
10
100
1000
10000
100000
Sieve diameter (μm)

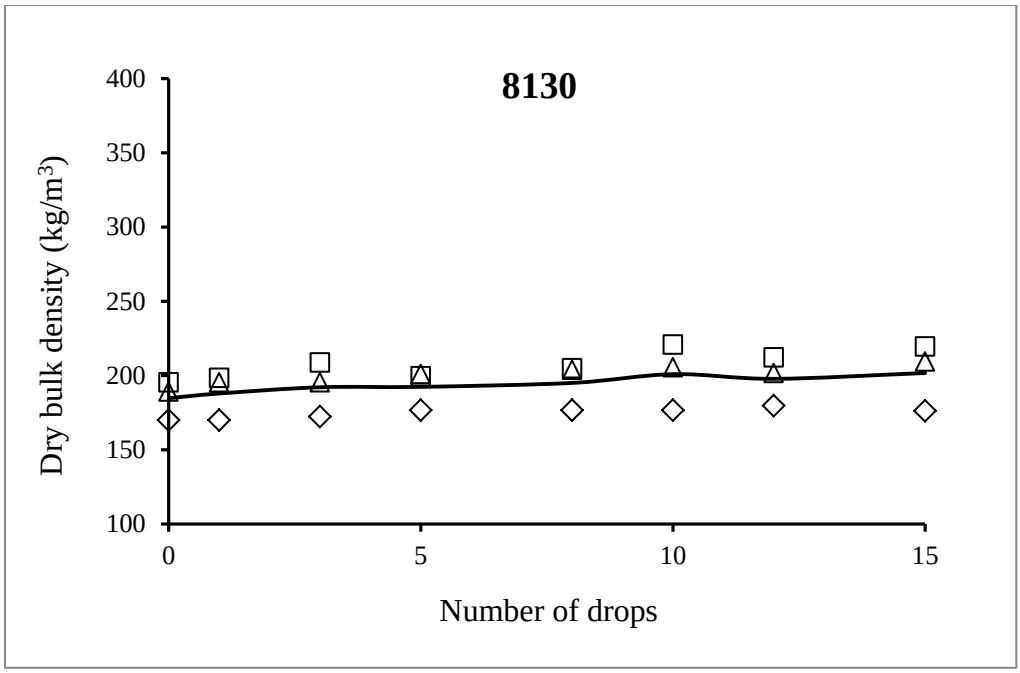
8130
Dry bulk density (kg/m3)
400
350
300
250
200
150
100
0
5
10
15
Number of drops

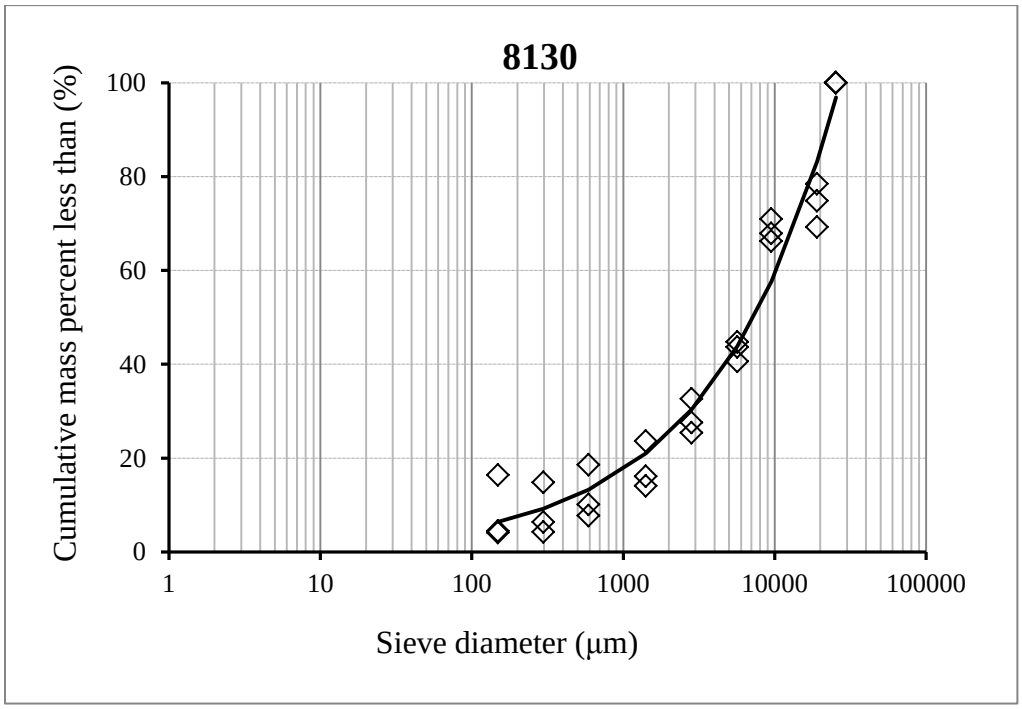
8130
Cumulative mass percent less than (%)
100
80
60
40
20
0
1
10
100
1000
10000
100000
Sieve diameter (μm)

Appendix II. Measured (symbols) and predicted (lines) cumulative outflow and pressure potential of the six samples selected for hydraulic characterization. Samples are labeled by their geometric mean diameter, d_g (in µm). Sample replicate numbers are given within parentheses.

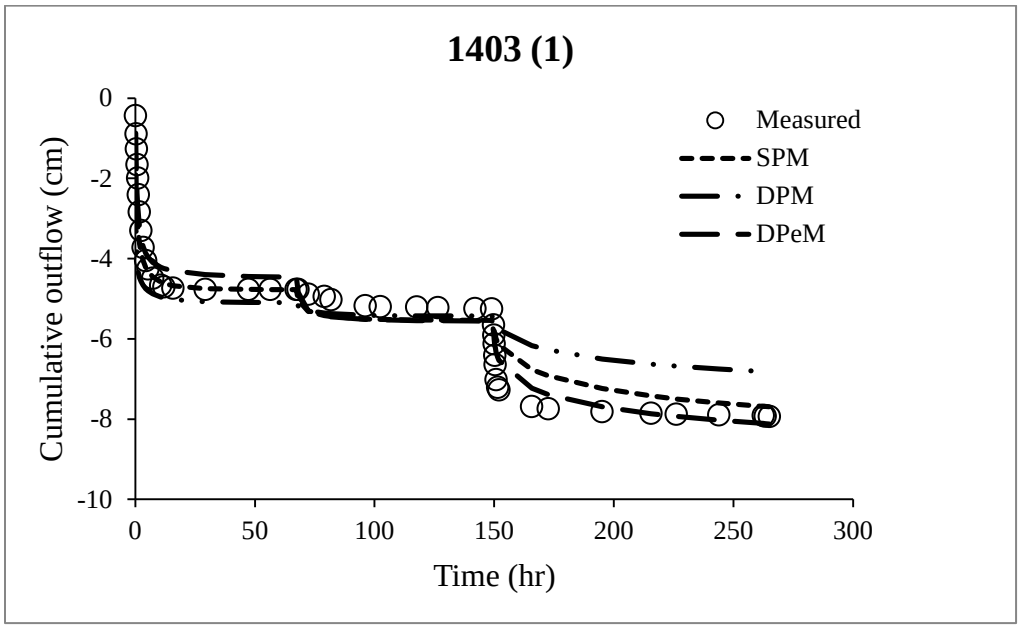

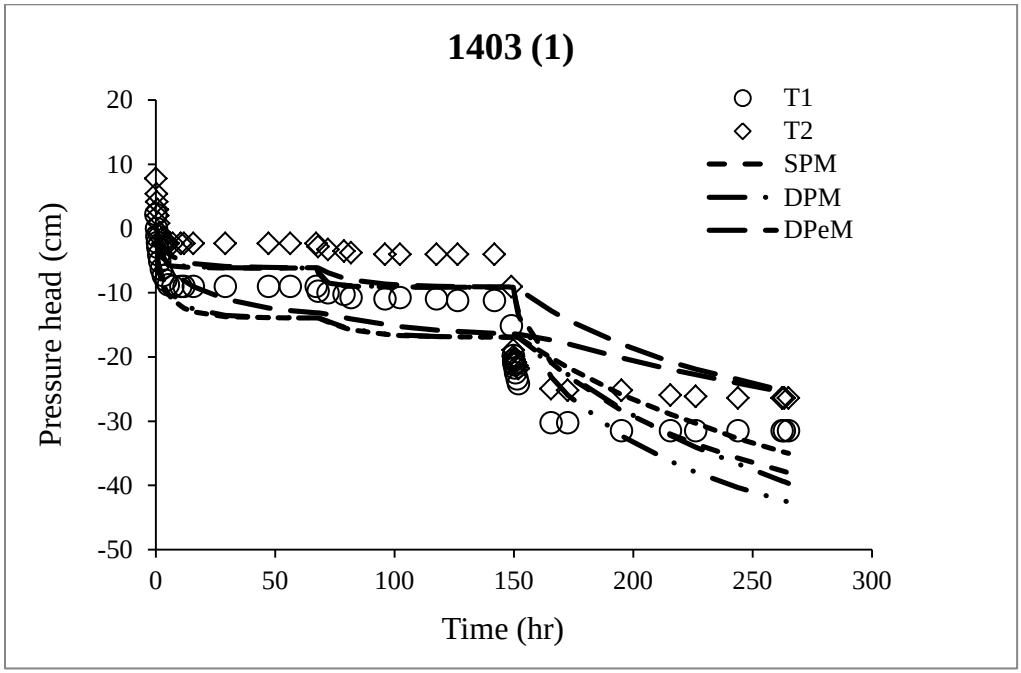

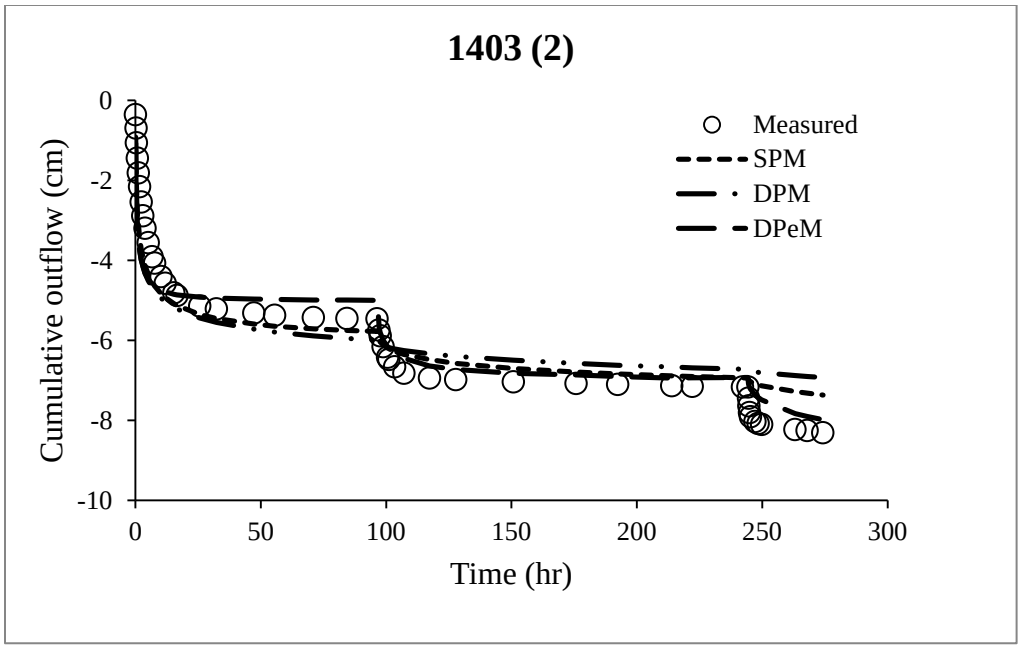
1403 (2)
Cumulative outflow (cm)
0
-2
-4
-6
-8
-10
0
50
100
150
200
250
300
Time (hr)
Measured
SPM
DPM
DPeM

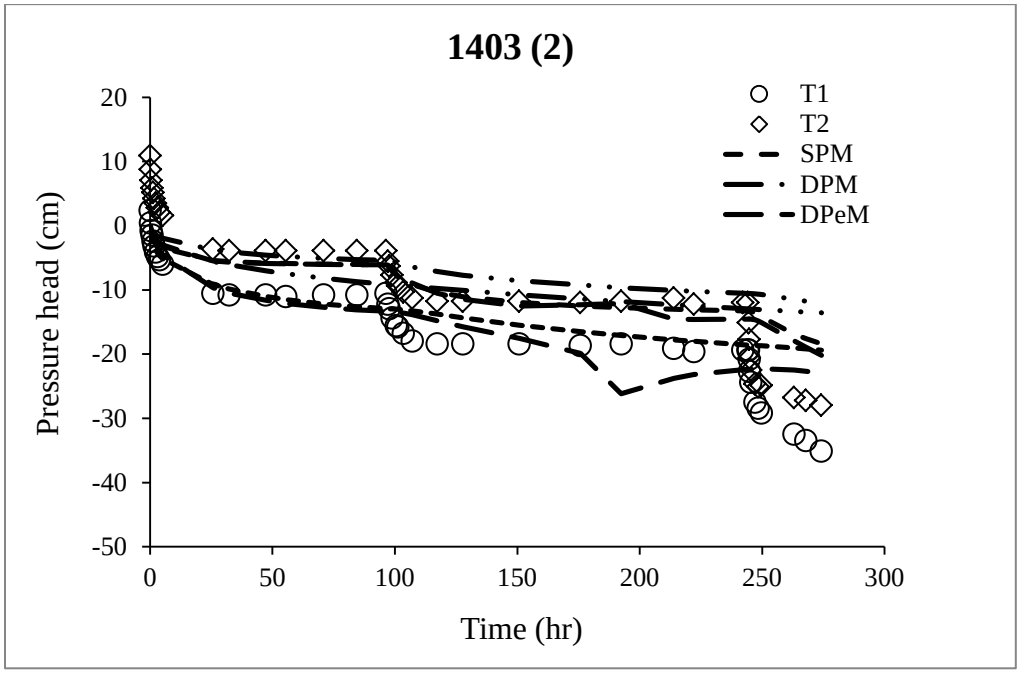
1403 (2)
Pressure head (cm)
20
10
0
-10
-20
-30
-40
-50
0
50
100
150
200
250
300
Time (hr)
T1
T2
SPM
DPM
DPeM

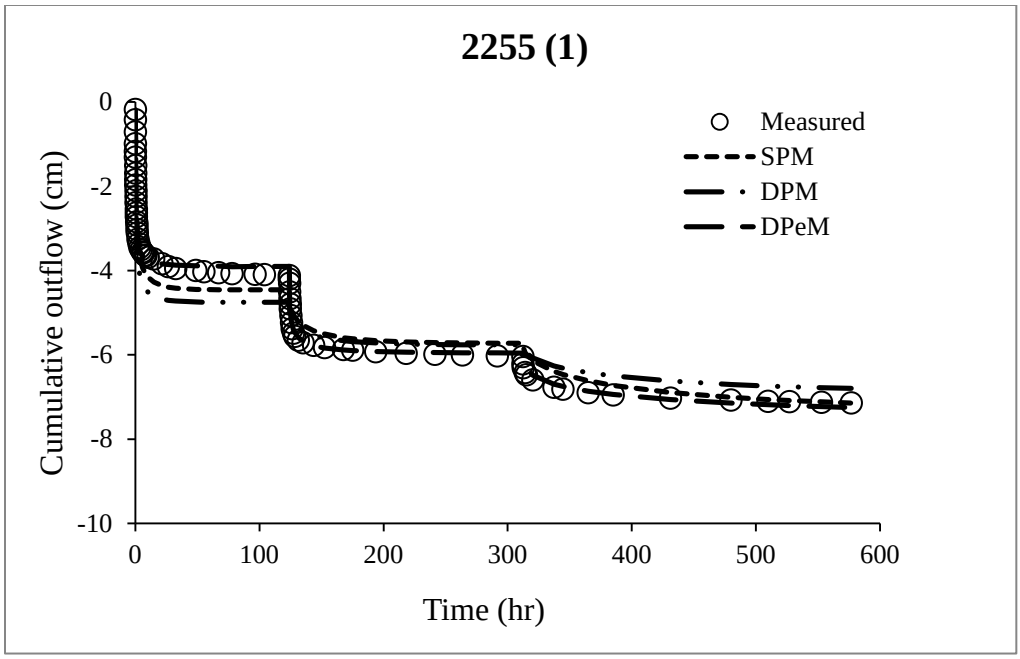
2255 (1)
Measured
SPM
DPM
DPeM
Cumulative outflow (cm)
0
-2
-4
-6
-8
-10
0
100
200
300
400
500
600
Time (hr)

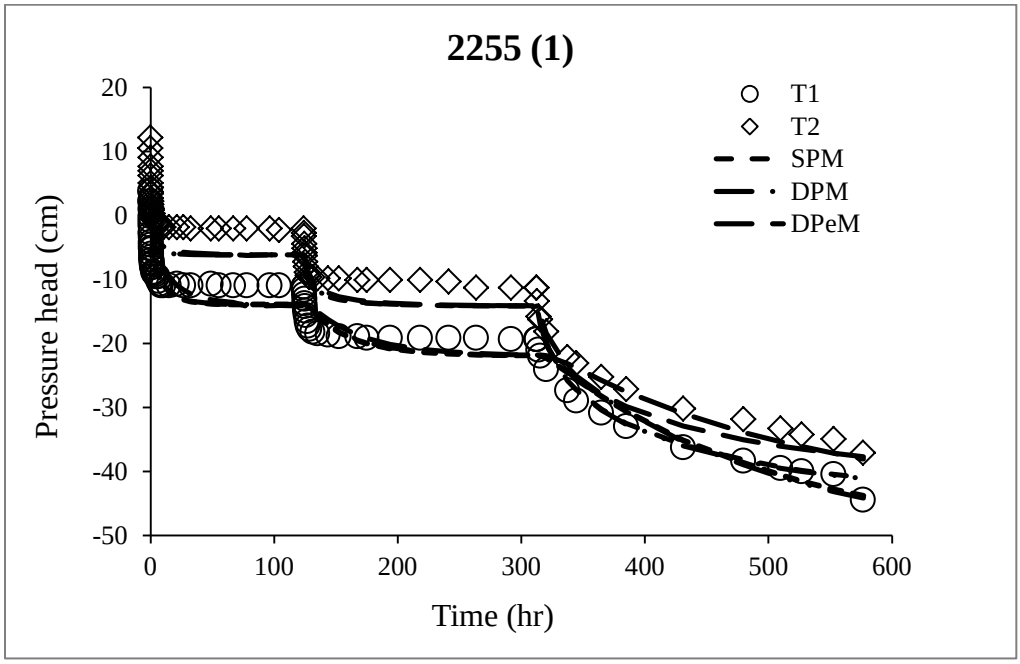
2255 (1)
T1
T2
SPM
DPM
DPeM
Pressure head (cm)
20
10
0
-10
-20
-30
-40
-50
0
100
200
300
400
500
600
Time (hr)

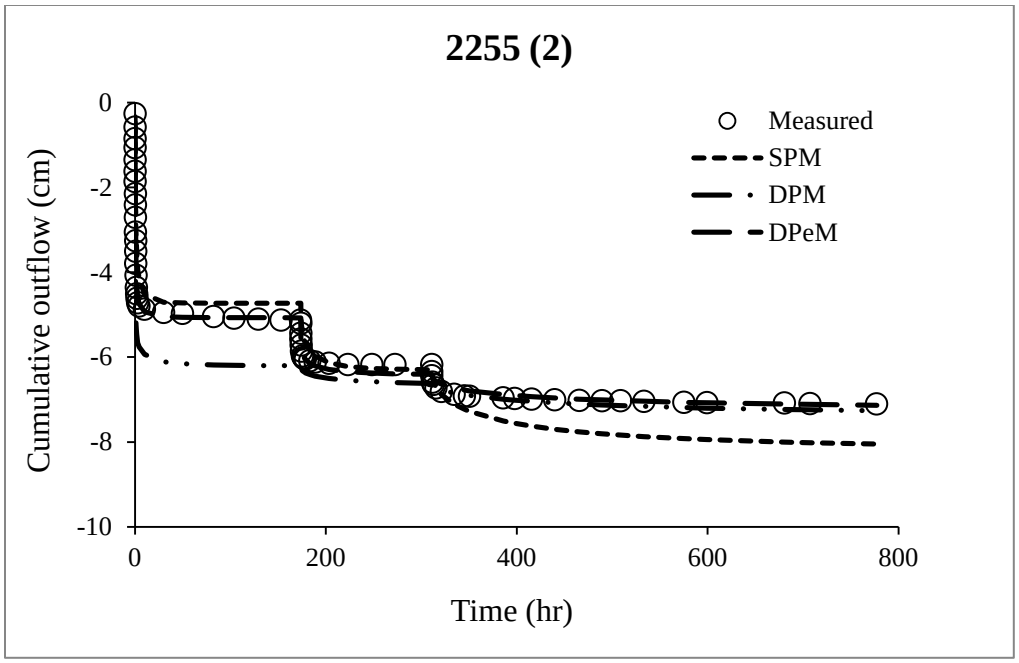
2255 (2)
Cumulative outflow (cm)
0
-2
-4
-6
-8
-10
0
200
400
600
800
Time (hr)
Measured
SPM
DPM
DPeM

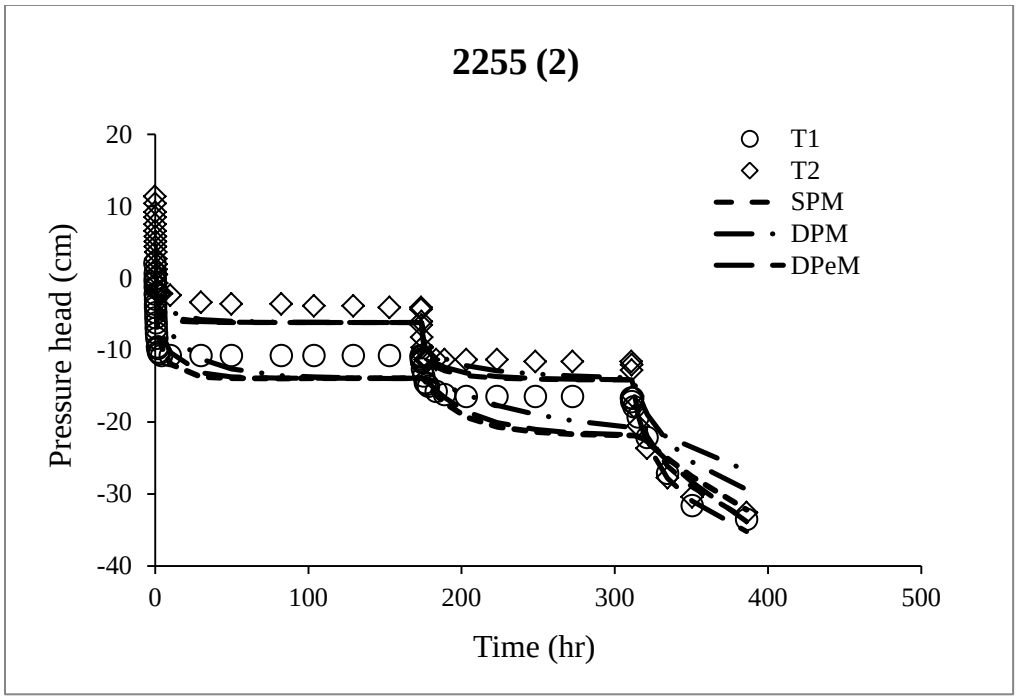
2255 (2)
Pressure head (cm)
20
10
0
-10
-20
-30
-40
0
100
200
300
400
500
Time (hr)
T1
T2
SPM
DPM
DPeM

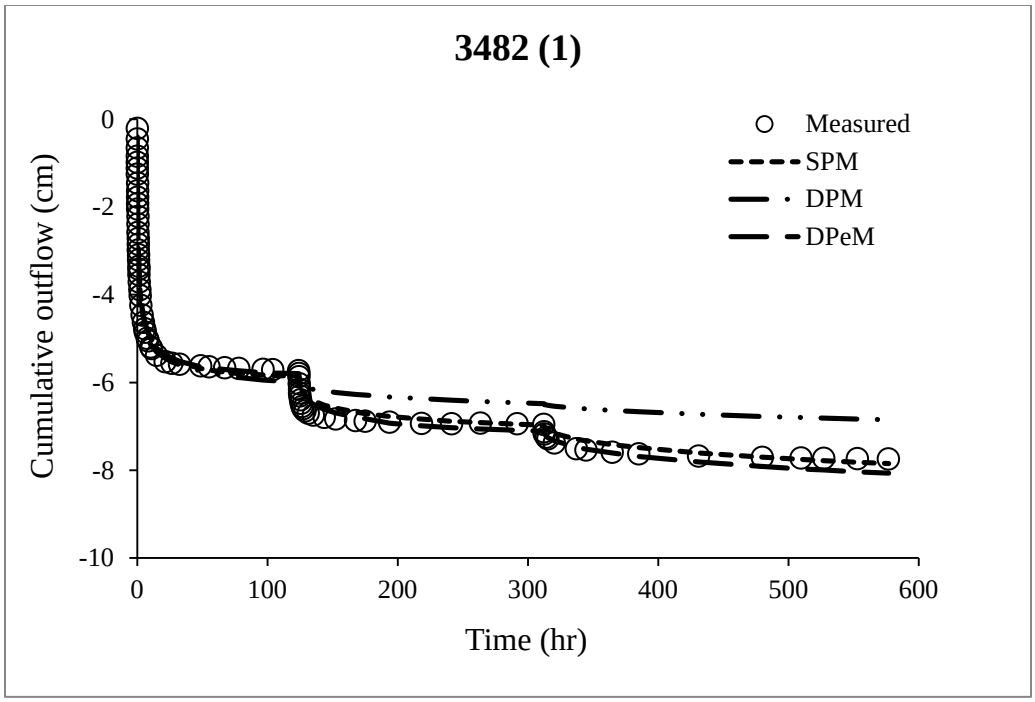
3482 (1)
Measured
SPM
DPM
DPeM
Cumulative outflow (cm)
0
-2
-4
-6
-8
-10
0
100
200
300
400
500
600
Time (hr)

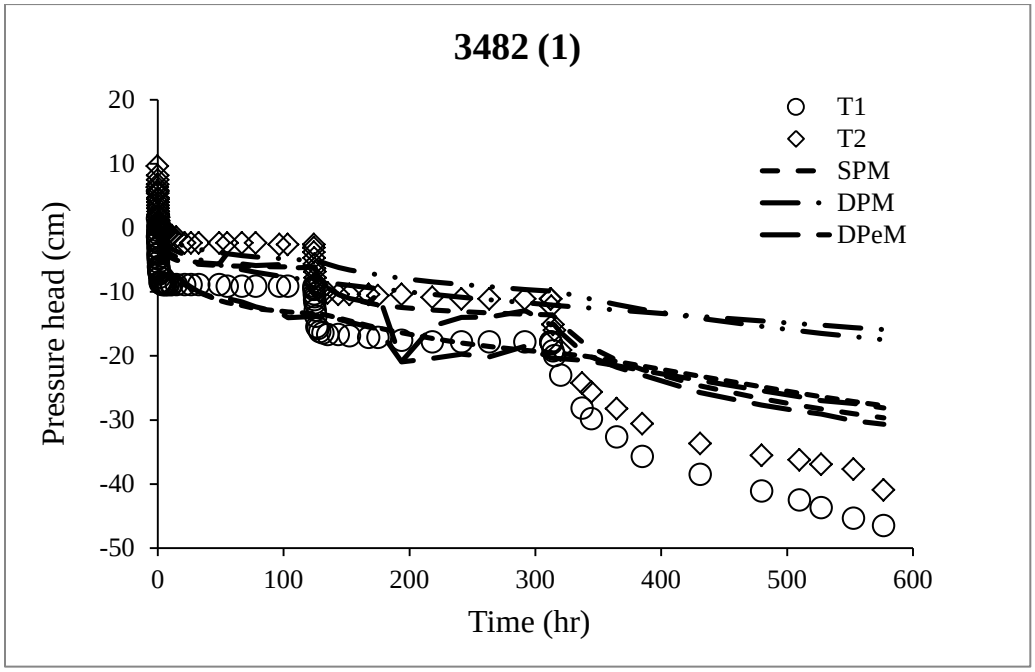
3482 (1)
T1
T2
SPM
DPM
DPeM
Pressure head (cm)
20
10
0
-10
-20
-30
-40
-50
0
100
200
300
400
500
600
Time (hr)

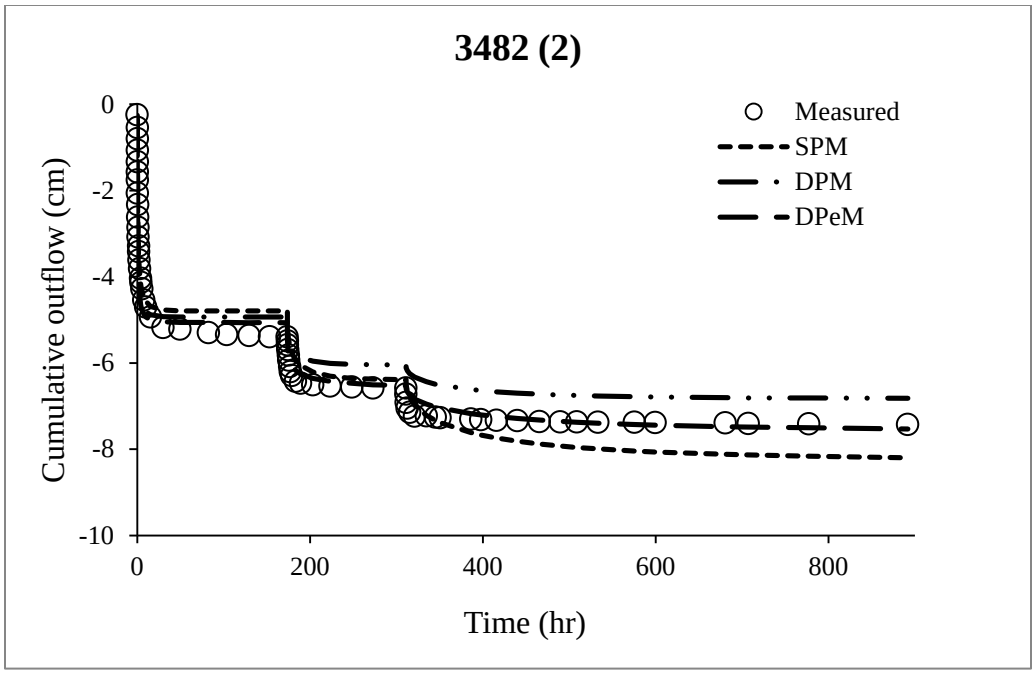
3482 (2)
Measured
SPM
DPM
DPeM
Cumulative outflow (cm)
0
-2
-4
-6
-8
-10
0
200
400
600
800
Time (hr)

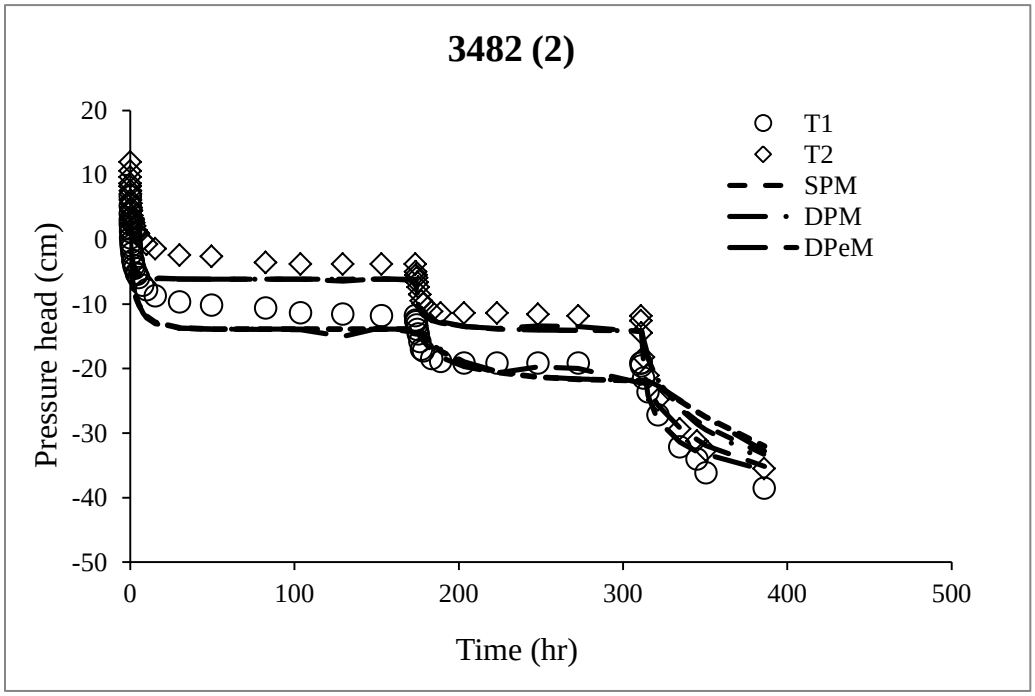
3482 (2)
T1
T2
SPM
DPM
DPeM
Pressure head (cm)
20
10
0
-10
-20
-30
-40
-50
0
100
200
300
400
500
Time (hr)

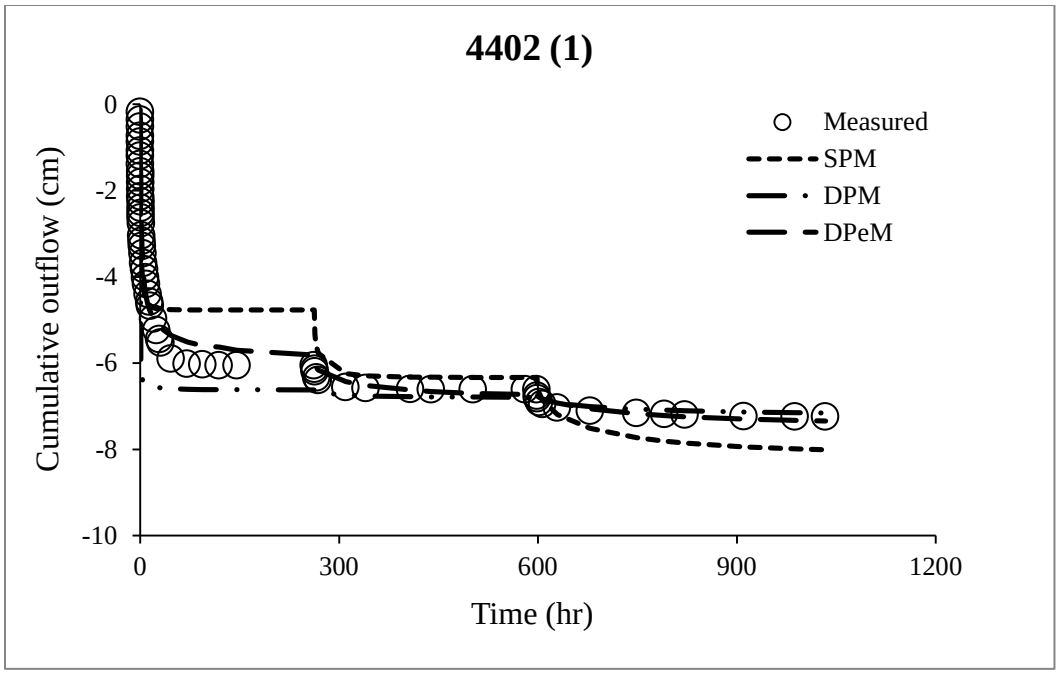
4402 (1)
Cumulative outflow (cm)
0
-2
-4
-6
-8
-10
0
300
600
900
1200
Time (hr)
Measured
SPM
DPM
DPeM

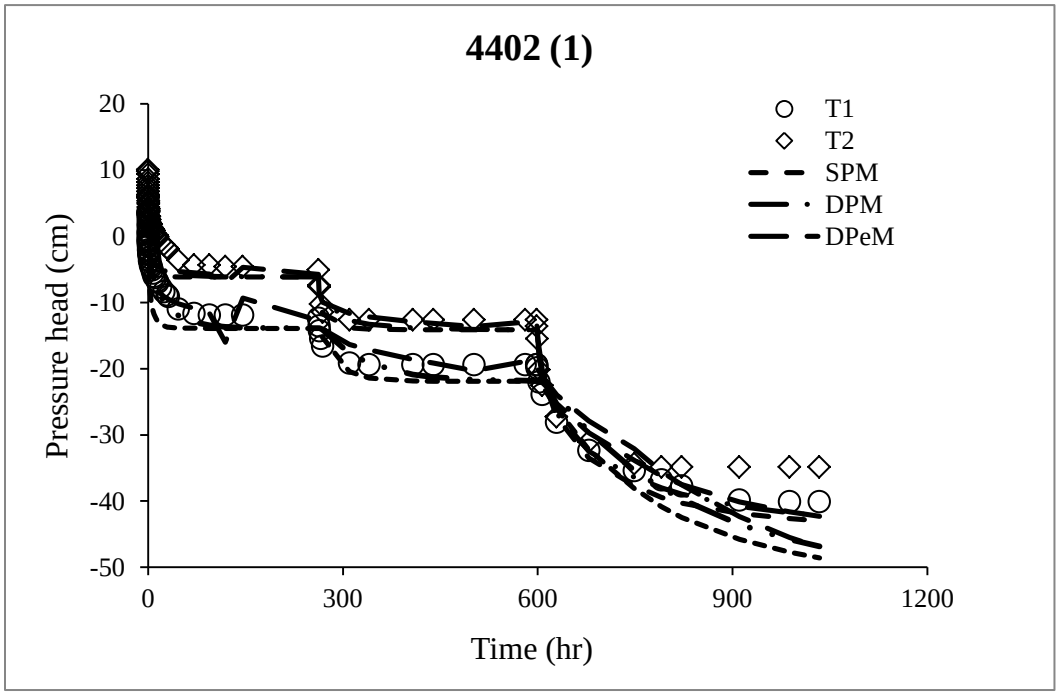
4402 (1)
Pressure head (cm)
20
10
0
-10
-20
-30
-40
-50
0
300
600
900
1200
Time (hr)
T1
T2
SPM
DPM
DPeM

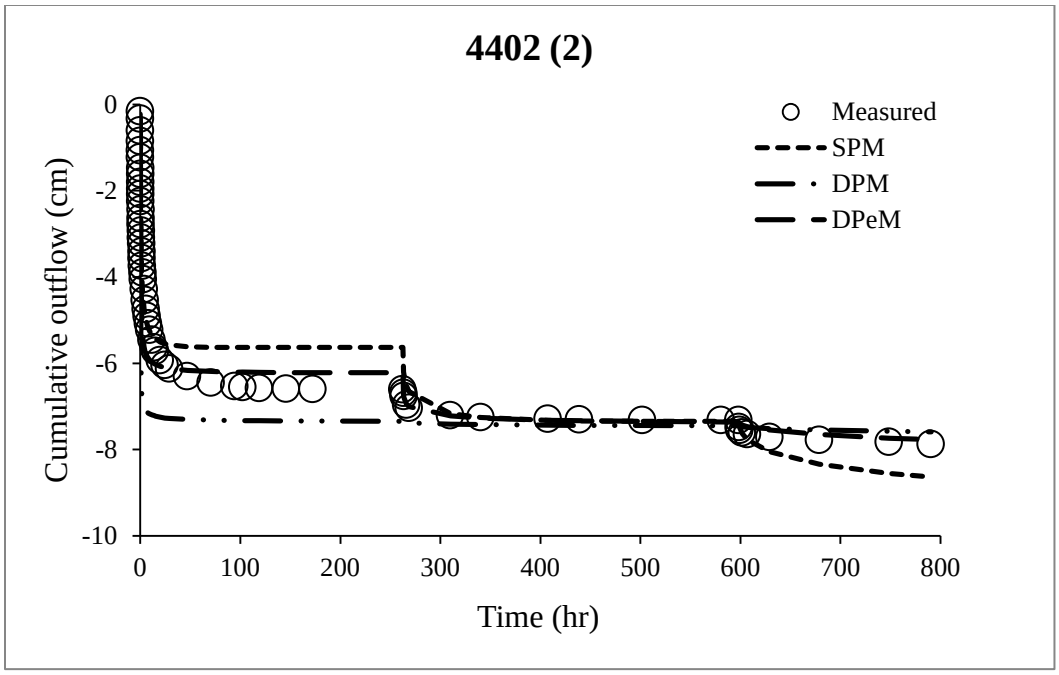
4402 (2)
Measured
SPM
DPM
DPeM
Cumulative outflow (cm)
0
-2
-4
-6
-8
-10
0
100
200
300
400
500
600
700
800
Time (hr)

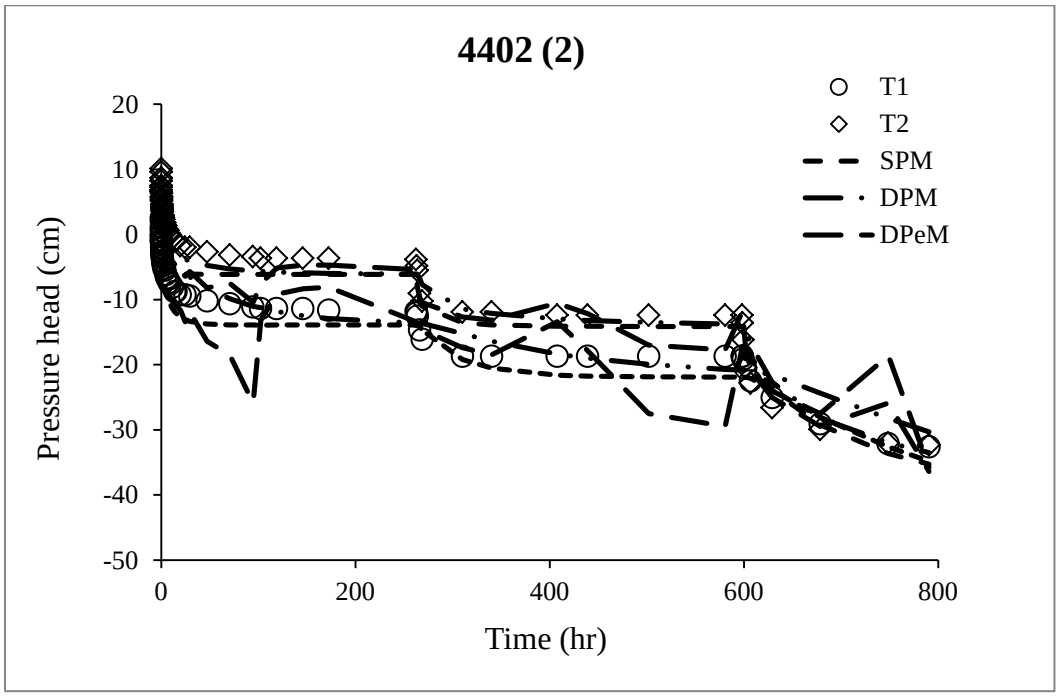
4402 (2)
T1
T2
SPM
DPM
DPeM
Pressure head (cm)
20
10
0
-10
-20
-30
-40
-50
0
200
400
600
800
Time (hr)

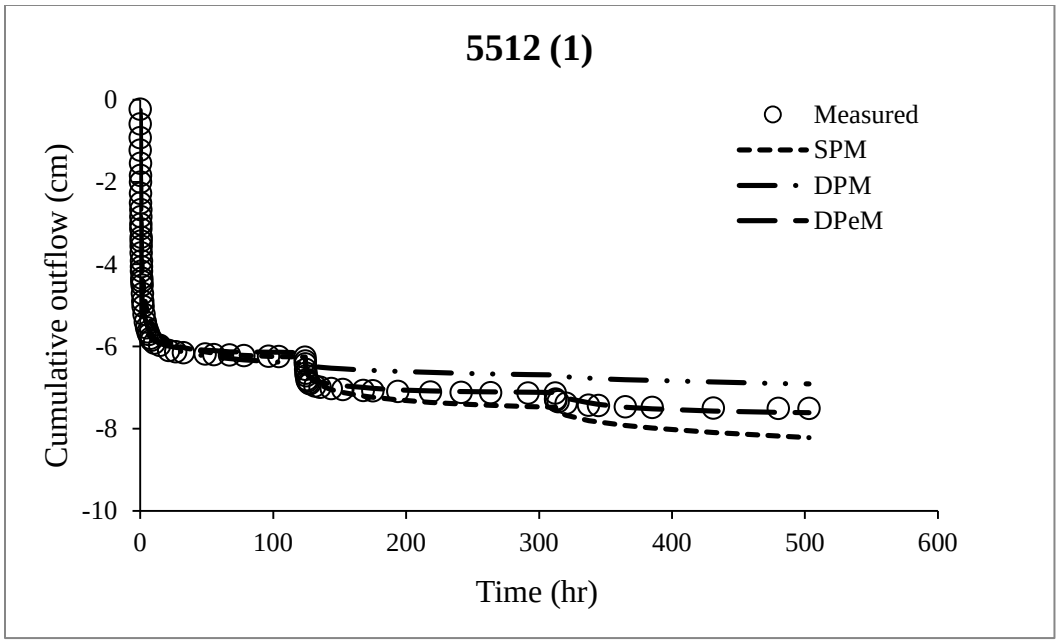
5512 (1)
Measured
SPM
DPM
DPeM
Cumulative outflow (cm)
0
-2
-4
-6
-8
-10
0
100
200
300
400
500
600
Time (hr)

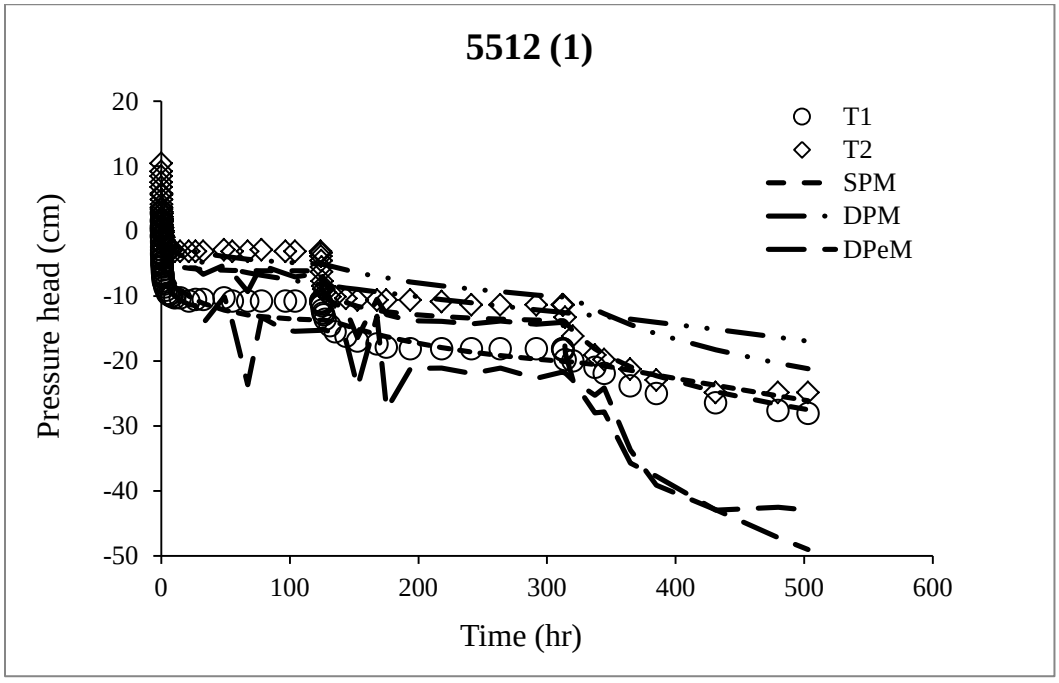
5512 (1)
T1
T2
SPM
DPM
DPeM
Pressure head (cm)
20
10
0
-10
-20
-30
-40
-50
0
100
200
300
400
500
600
Time (hr)

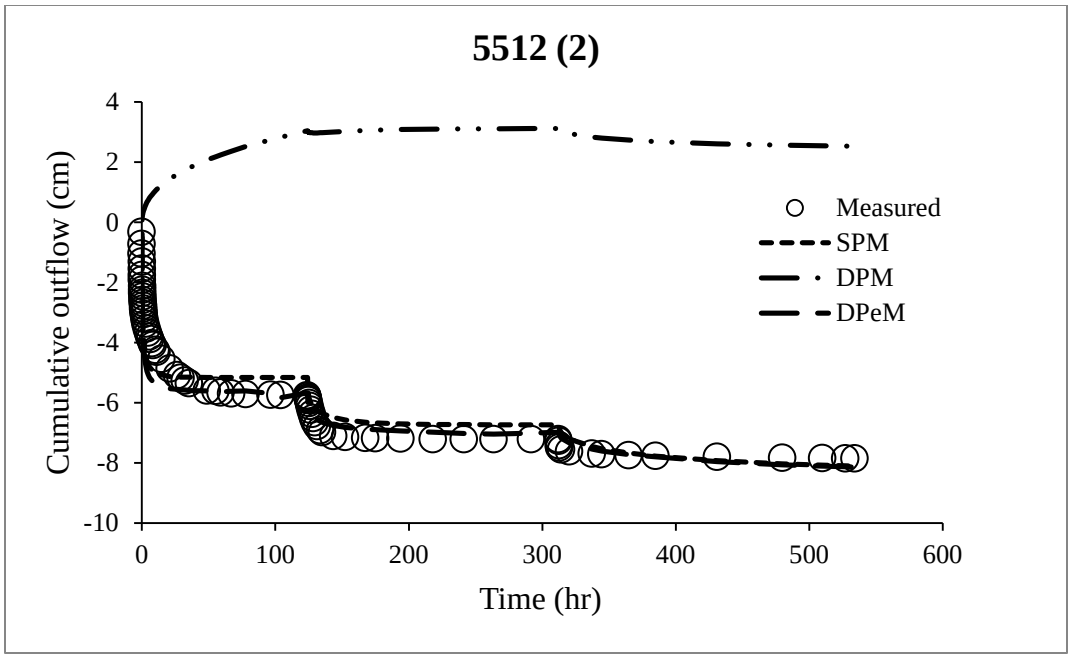
5512 (2)
Cumulative outflow (cm)
Time (hr)
Measured
SPM
DPM
DPeM
4
2
0
-2
-4
-6
-8
-10
0
100
200
300
400
500
600

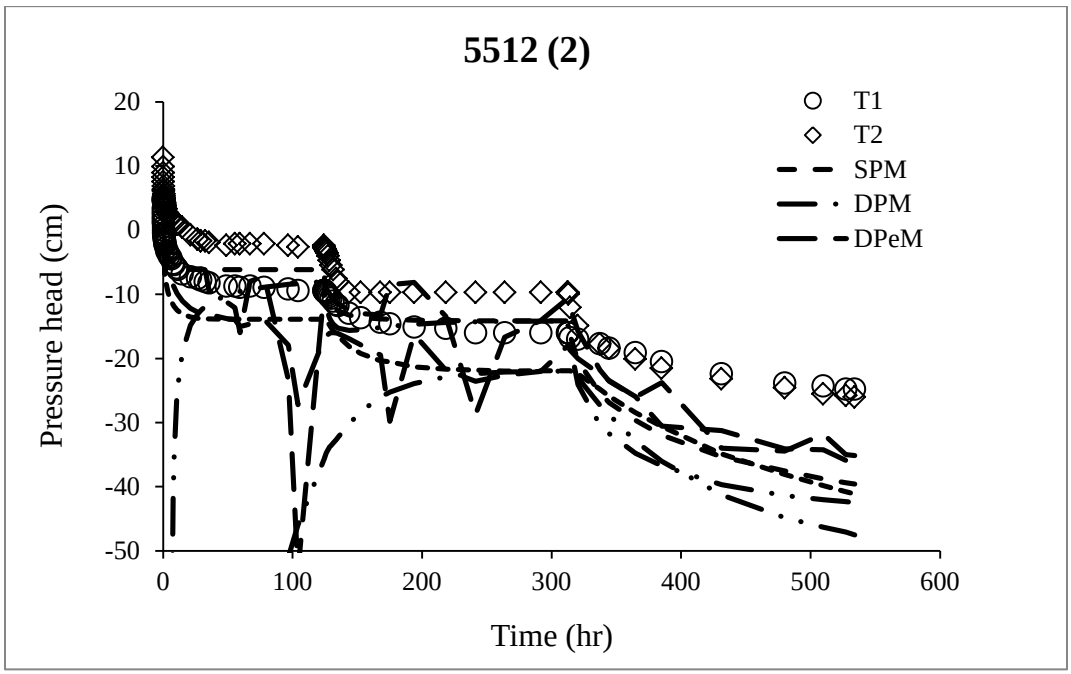
5512 (2)
Pressure head (cm)
Time (hr)
T1
T2
SPM
DPM
DPeM
20
10
0
-10
-20
-30
-40
-50
0
100
200
300
400
500
600

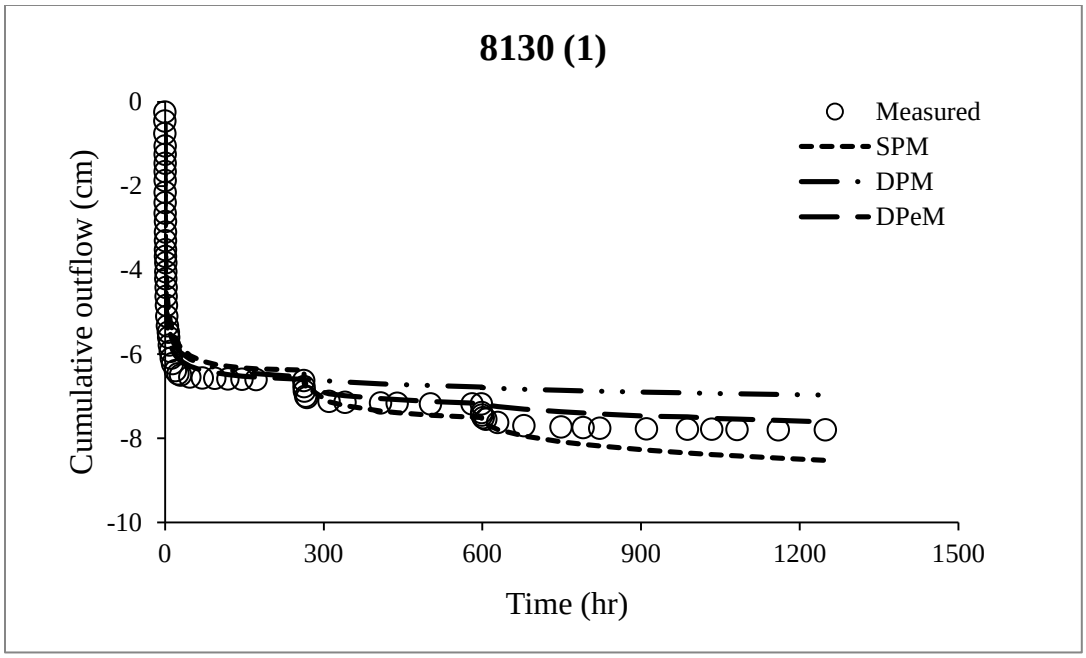
8130 (1)
Measured
SPM
DPM
DPeM
Cumulative outflow (cm)
0
-2
-4
-6
-8
-10
0
300
600
900
1200
1500
Time (hr)

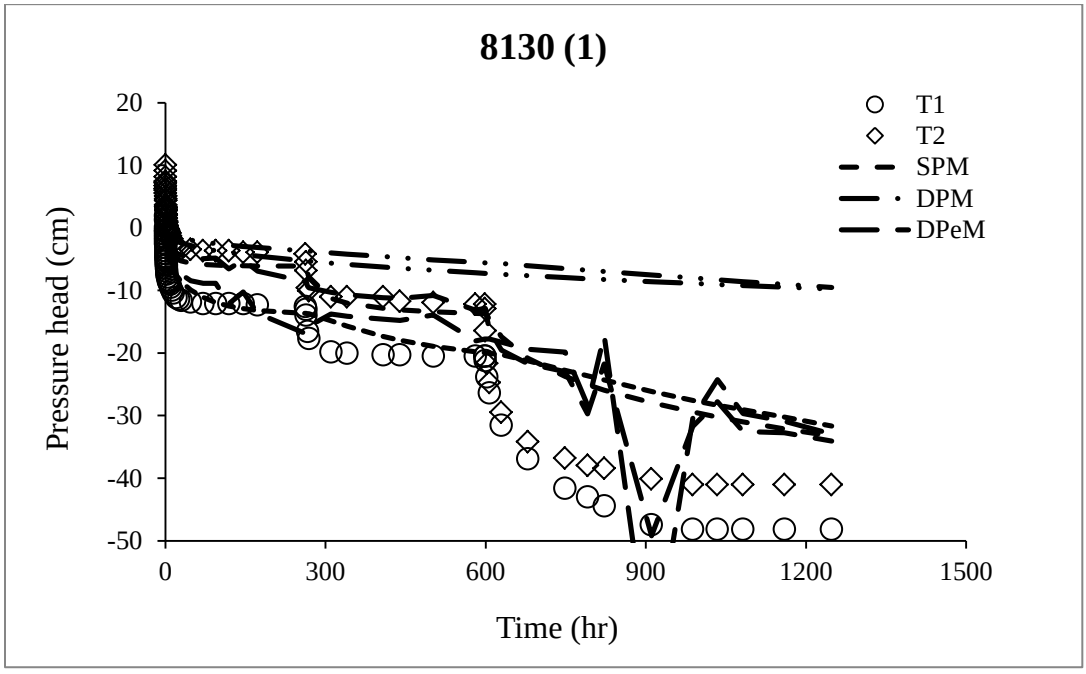
8130 (1)
T1
T2
SPM
DPM
DPeM
Pressure head (cm)
20
10
0
-10
-20
-30
-40
-50
0
300
600
900
1200
1500
Time (hr)

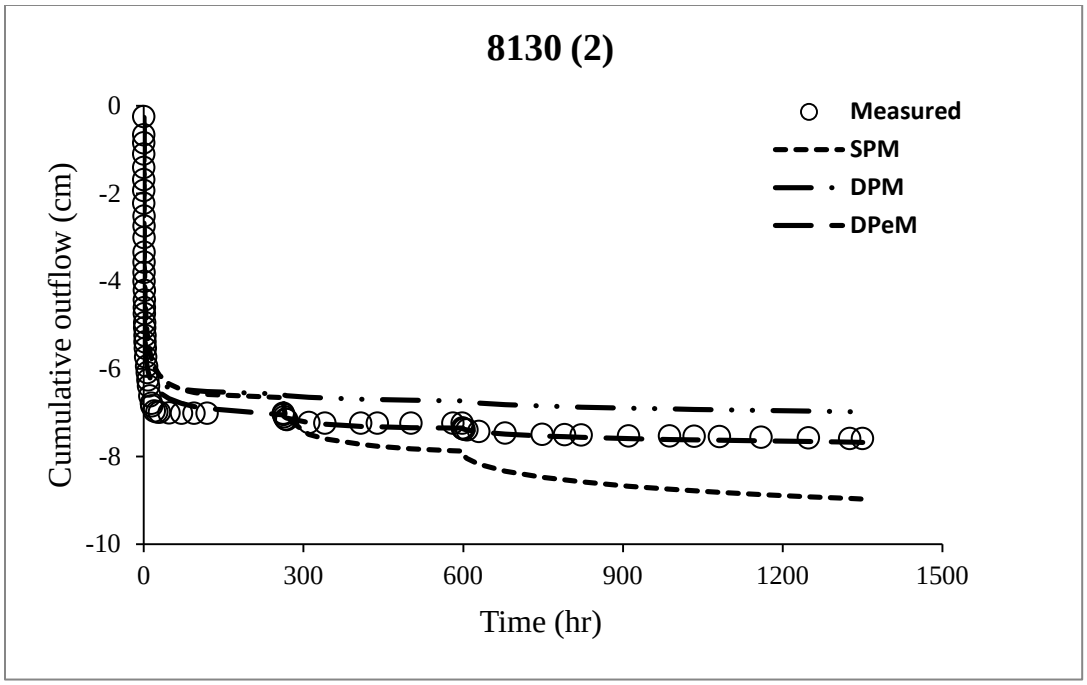
8130 (2)
Measured
SPM
DPM
DPeM
Cumulative outflow (cm)
0
-2
-4
-6
-8
-10
0
300
600
900
1200
1500
Time (hr)

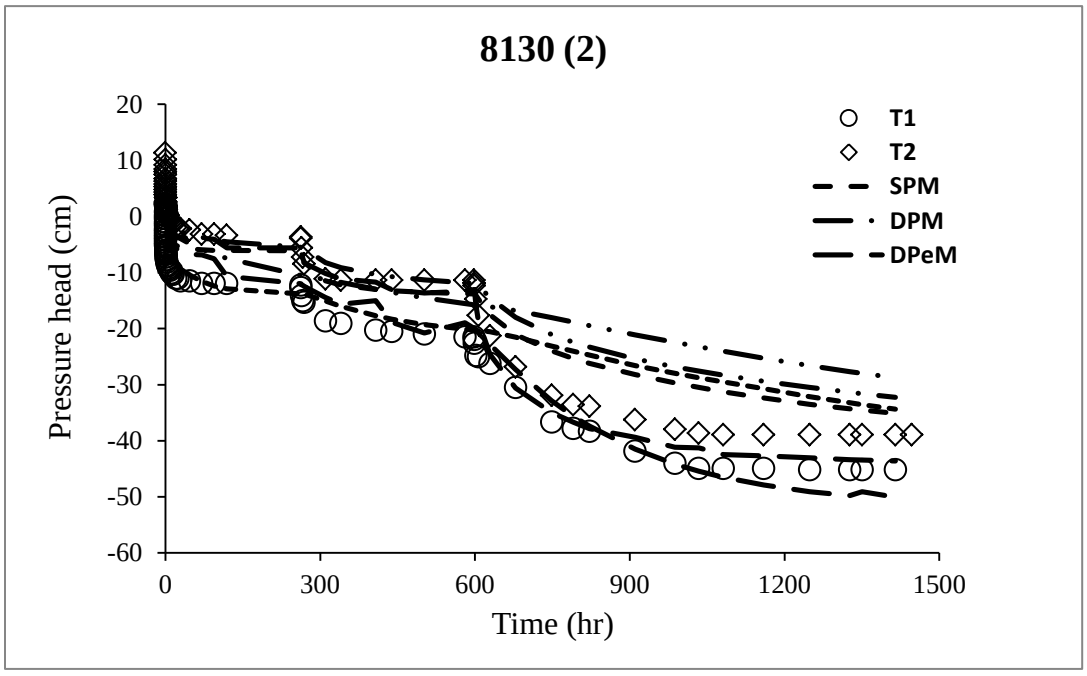
8130 (2)
T1
T2
SPM
DPM
DPeM
Pressure head (cm)
20
10
0
-10
-20
-30
-40
-50
-60
0
300
600
900
1200
1500
Time (hr)

Appendix III. Measured (symbols) and predicted (lines) water retention and unsaturated hydraulic conductivity of the six samples selected for hydraulic characterization. Samples are labeled by their geometric mean diameter, d_g (in µm). Sample replicate numbers are given within parentheses. The measured saturated hydraulic conductivities (K_s) are indicated in the log-scale of the K(h) charts at h= -0.1 cm instead of h=0 cm.

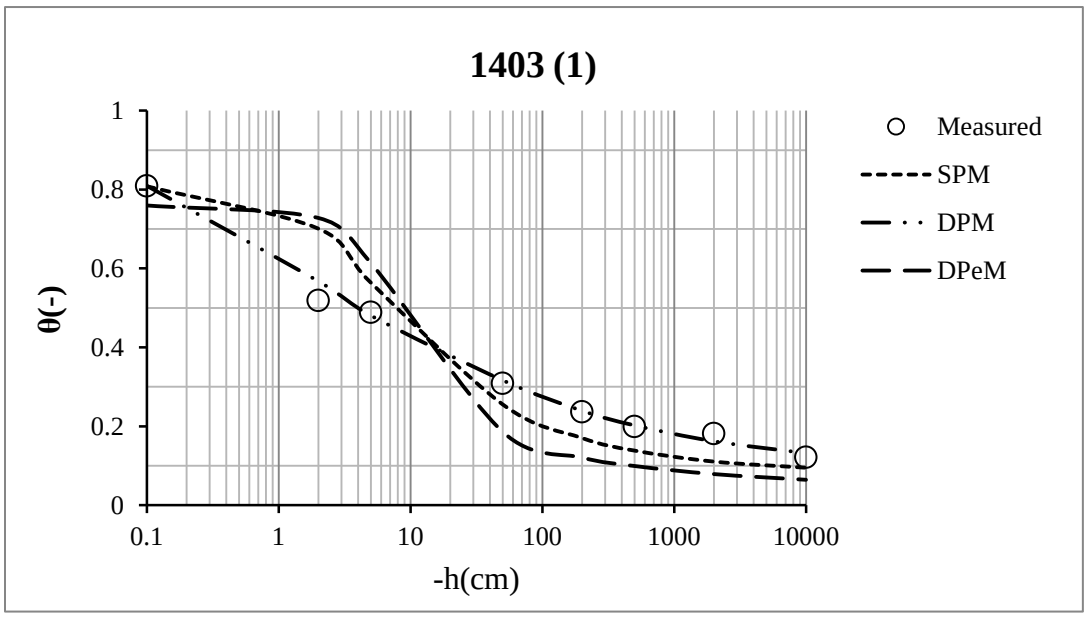

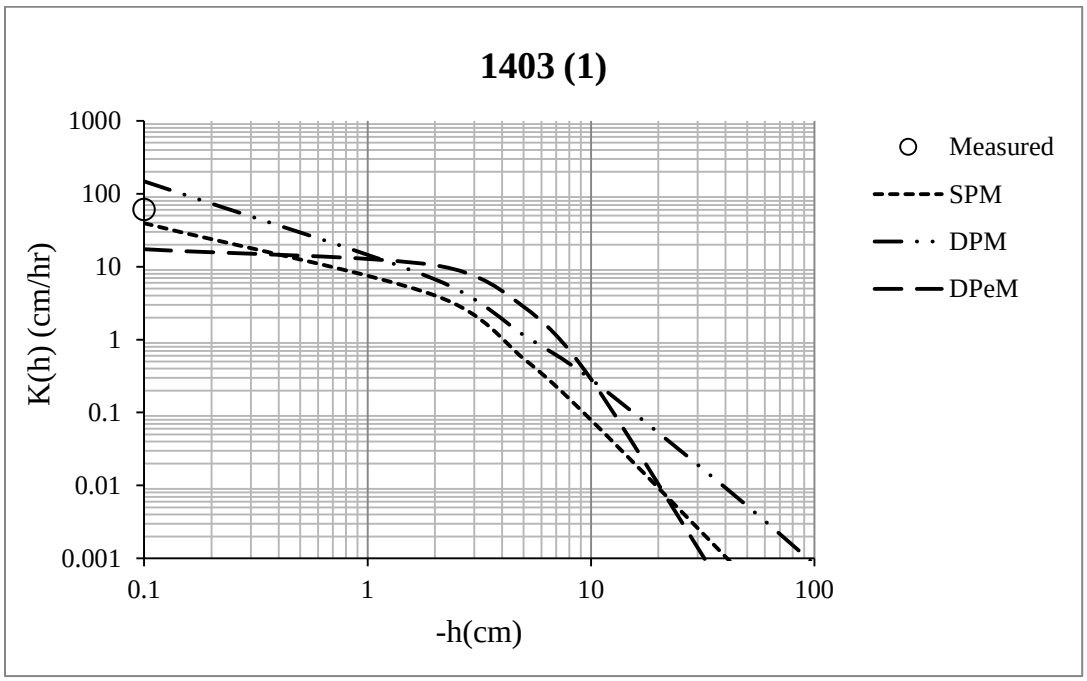

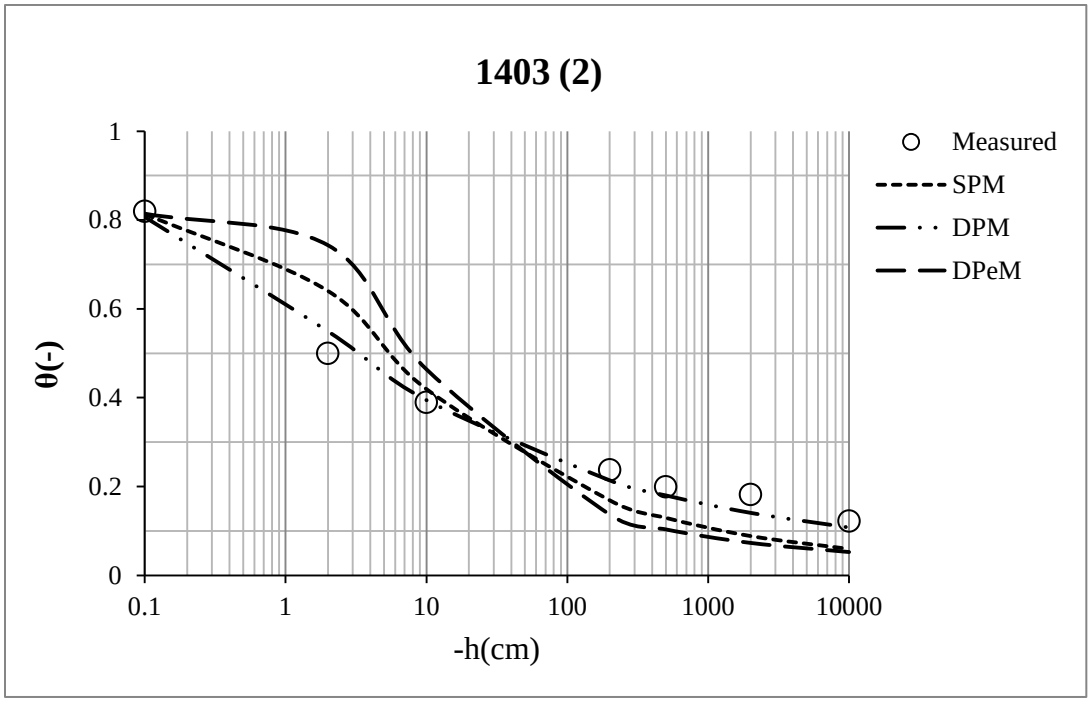
1403 (2)
θ(-)
-h(cm)
Measured
SPM
DPM
DPeM
1
0.8
0.6
0.4
0.2
0
0.1
1
10
100
1000
10000

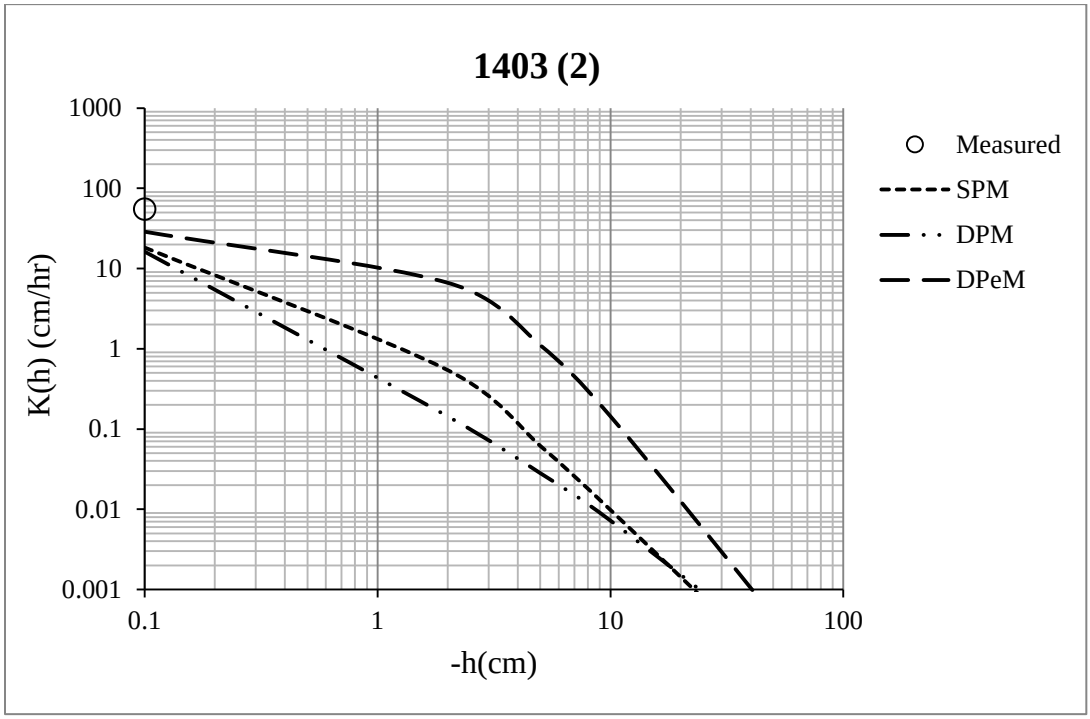
1403 (2)
K(h) (cm/hr)
-h(cm)
Measured
SPM
DPM
DPeM
1000
100
10
1
0.1
0.01
0.001
0.1
1
10
100

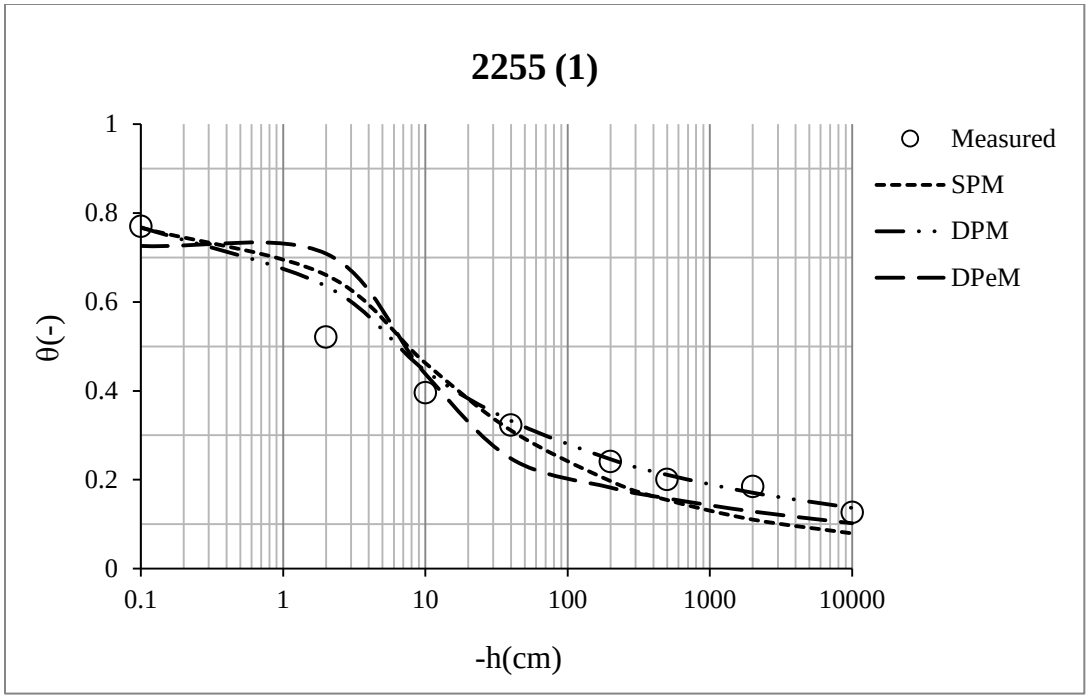
2255 (1)
θ(-)
1
0.8
0.6
0.4
0.2
0
0.1
1
10
100
1000
10000
-h(cm)
Measured
SPM
DPM
DPeM

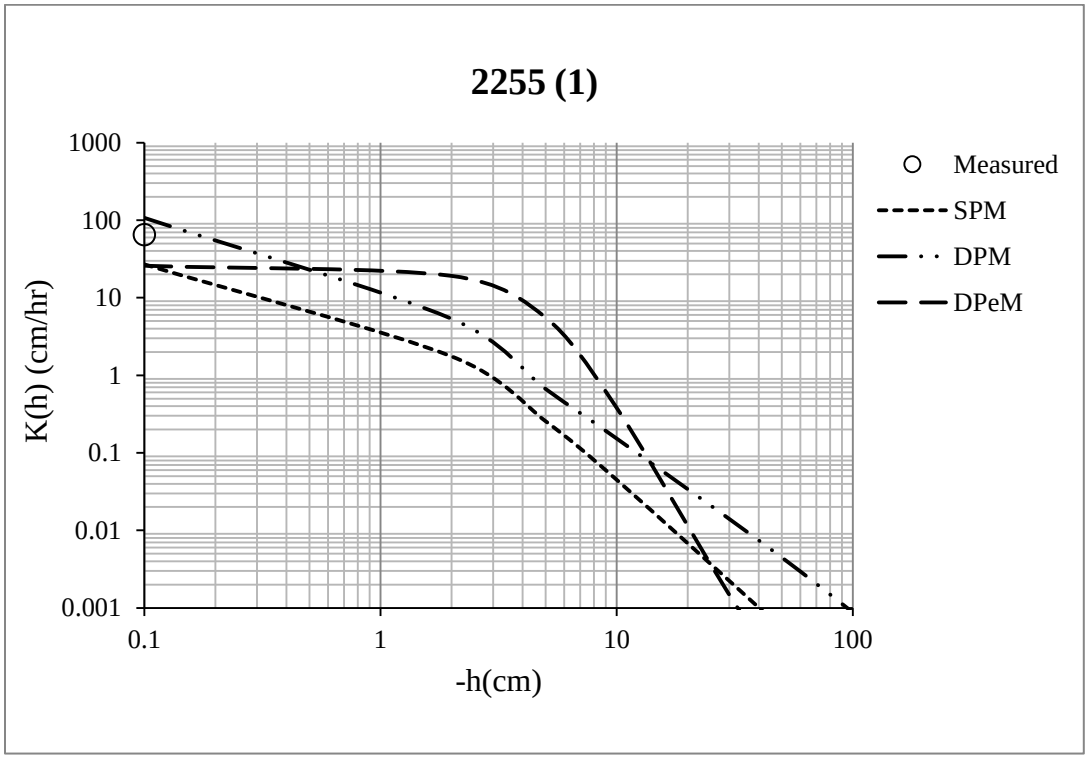
2255 (1)
K(h) (cm/hr)
1000
100
10
1
0.1
0.01
0.001
0.1
1
10
100
-h(cm)
Measured
SPM
DPM
DPeM

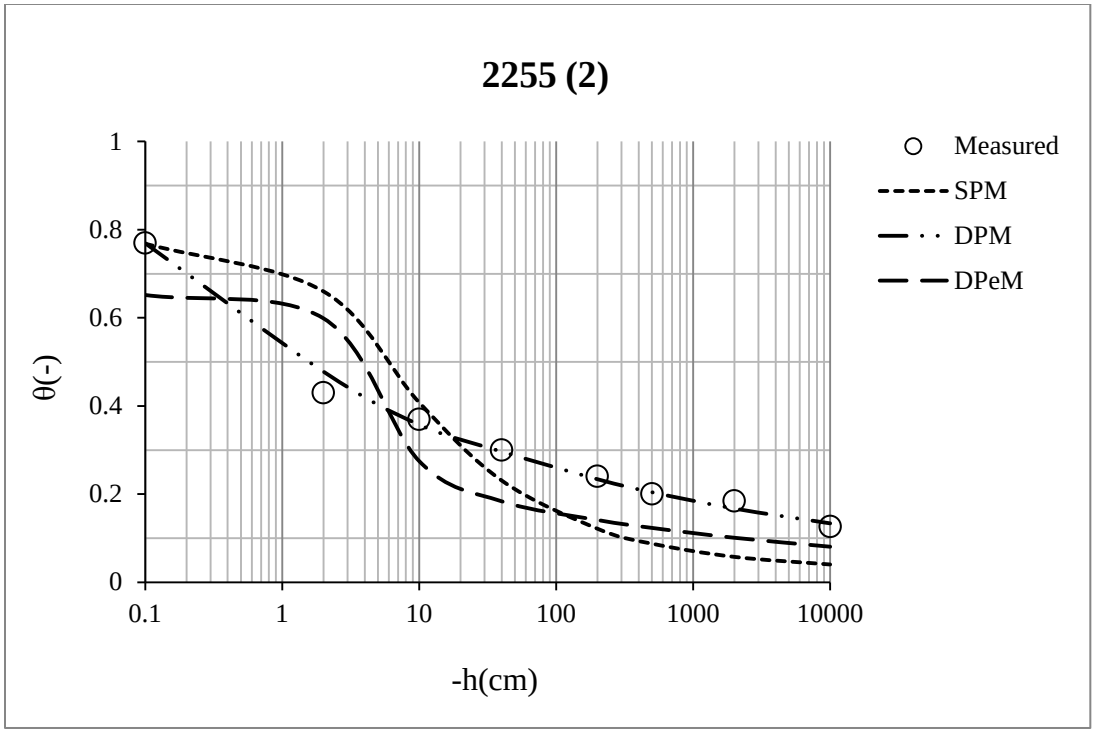
2255 (2)
θ(-)
1
0.8
0.6
0.4
0.2
0
0.1
1
10
100
1000
10000
-h(cm)
Measured
SPM
DPM
DPeM

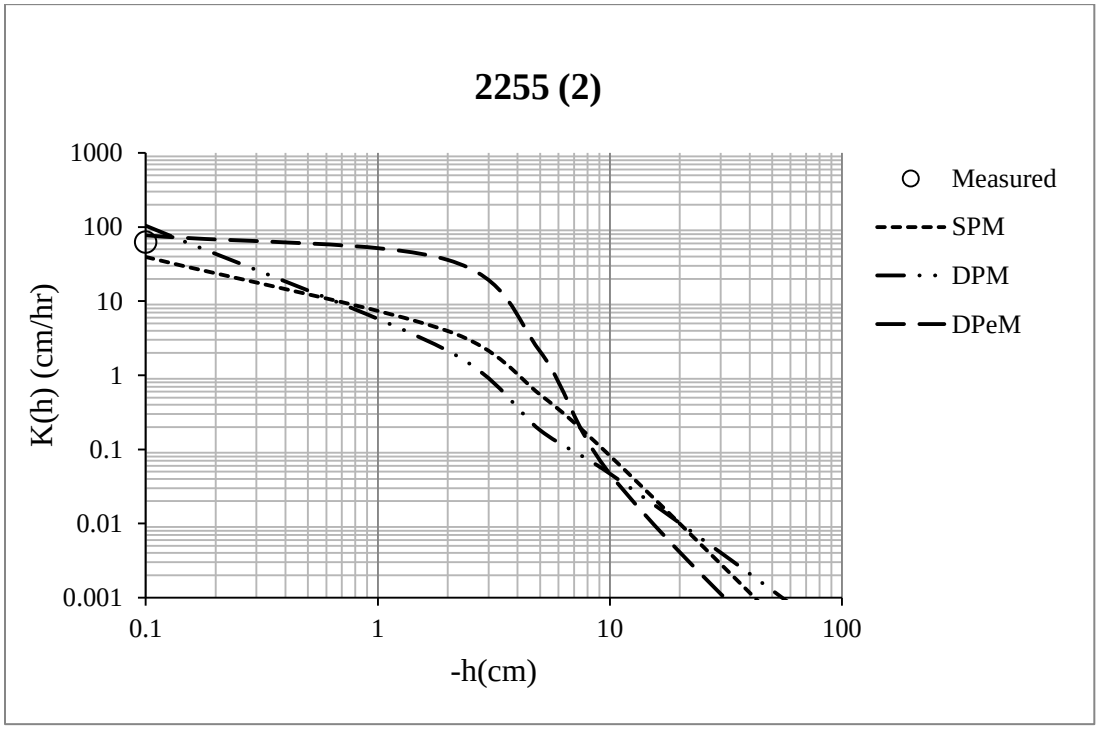
2255 (2)
K(h) (cm/hr)
1000
100
10
1
0.1
0.01
0.001
0.1
1
10
100
-h(cm)
Measured
SPM
DPM
DPeM

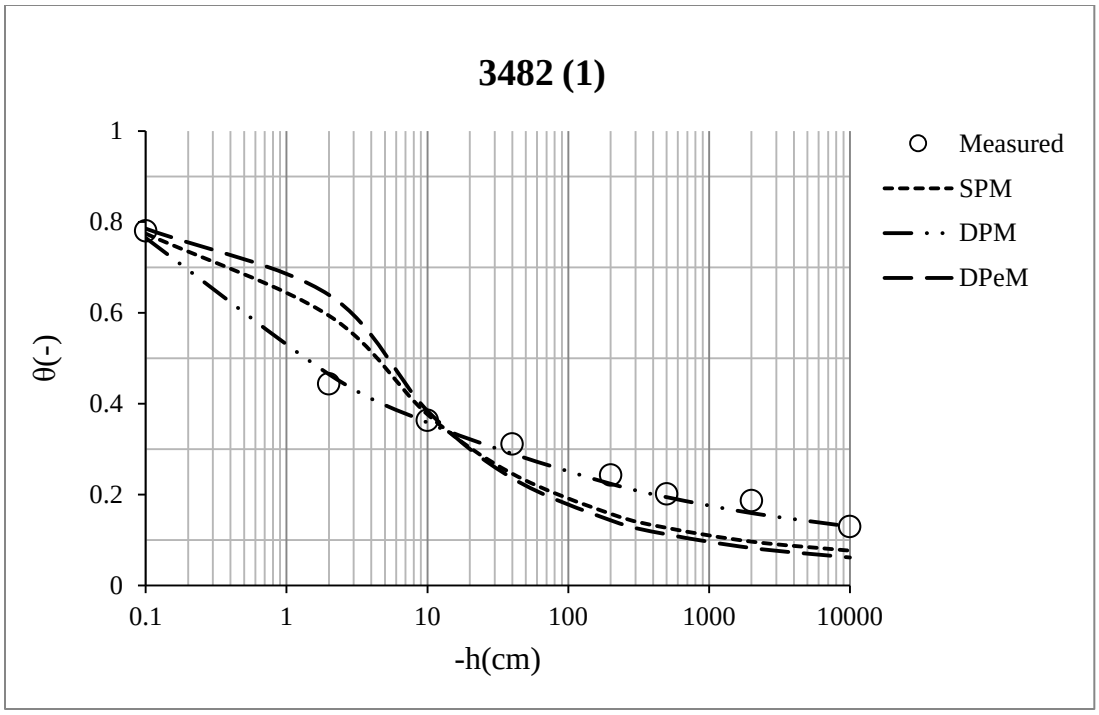
3482 (1)
θ(-)
-h(cm)
Measured
SPM
DPM
DPeM
1
0.8
0.6
0.4
0.2
0
0.1
1
10
100
1000
10000

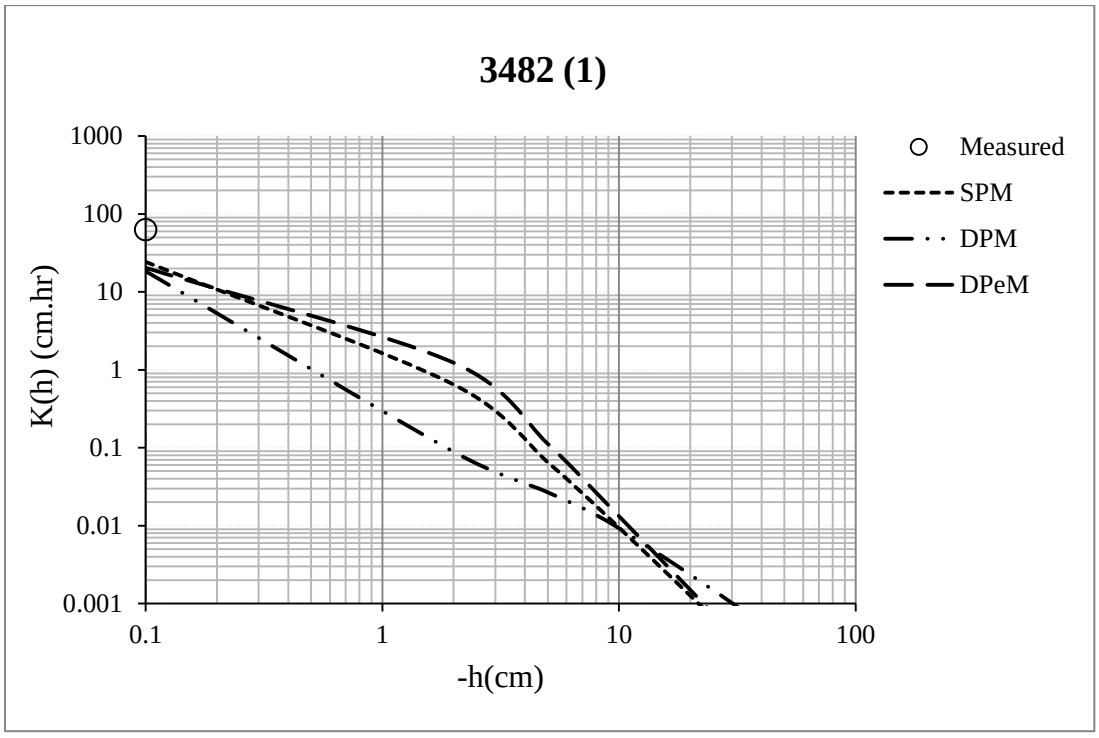
3482 (1)
K(h) (cm.hr)
-h(cm)
Measured
SPM
DPM
DPeM
1000
100
10
1
0.1
0.01
0.001
0.1
1
10
100

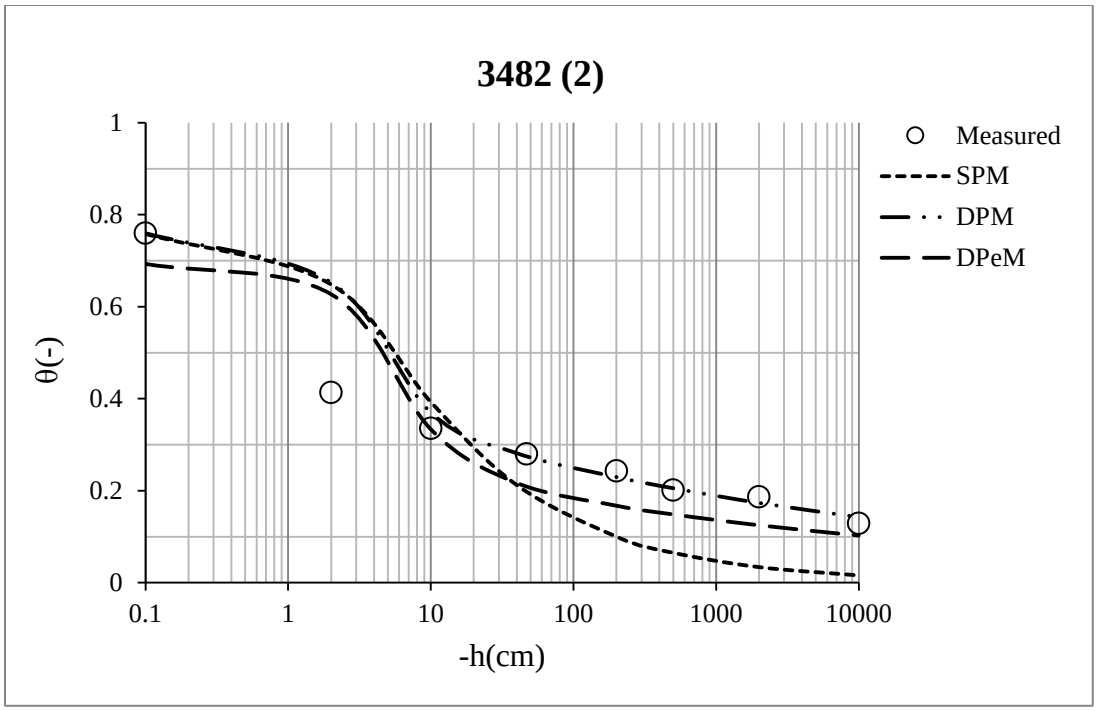
3482 (2)
θ(-)
1
0.8
0.6
0.4
0.2
0
0.1
1
10
100
1000
10000
-h(cm)
Measured
SPM
DPM
DPeM

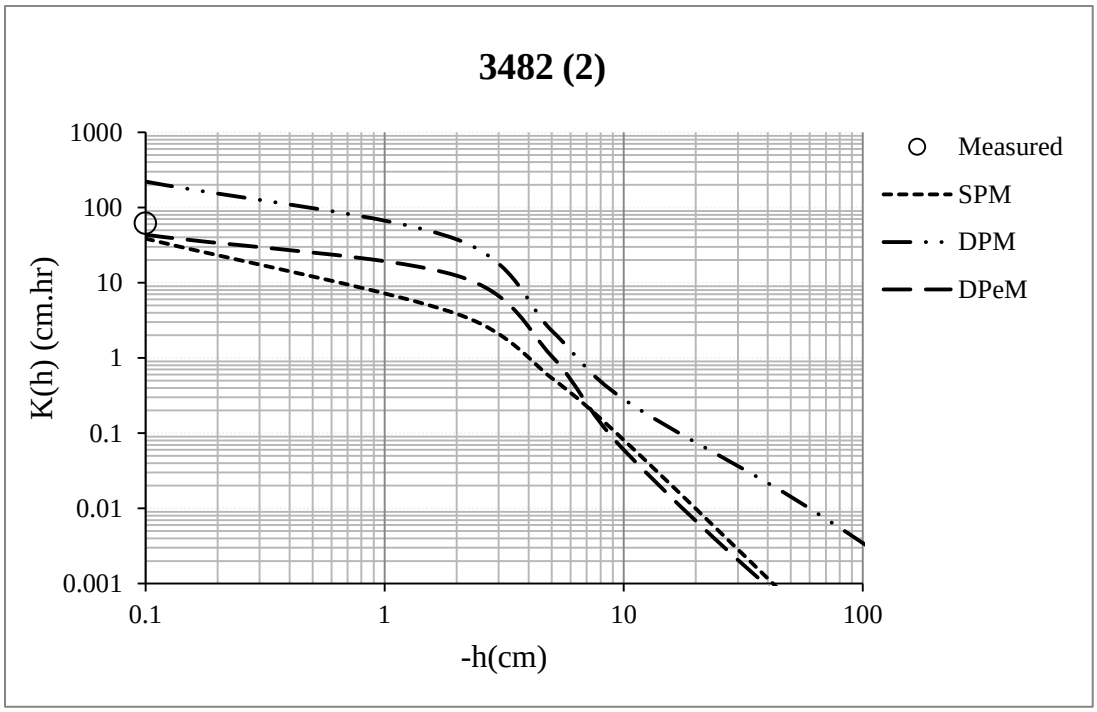
3482 (2)
K(h) (cm.hr)
1000
100
10
1
0.1
0.01
0.001
0.1
1
10
100
-h(cm)
Measured
SPM
DPM
DPeM

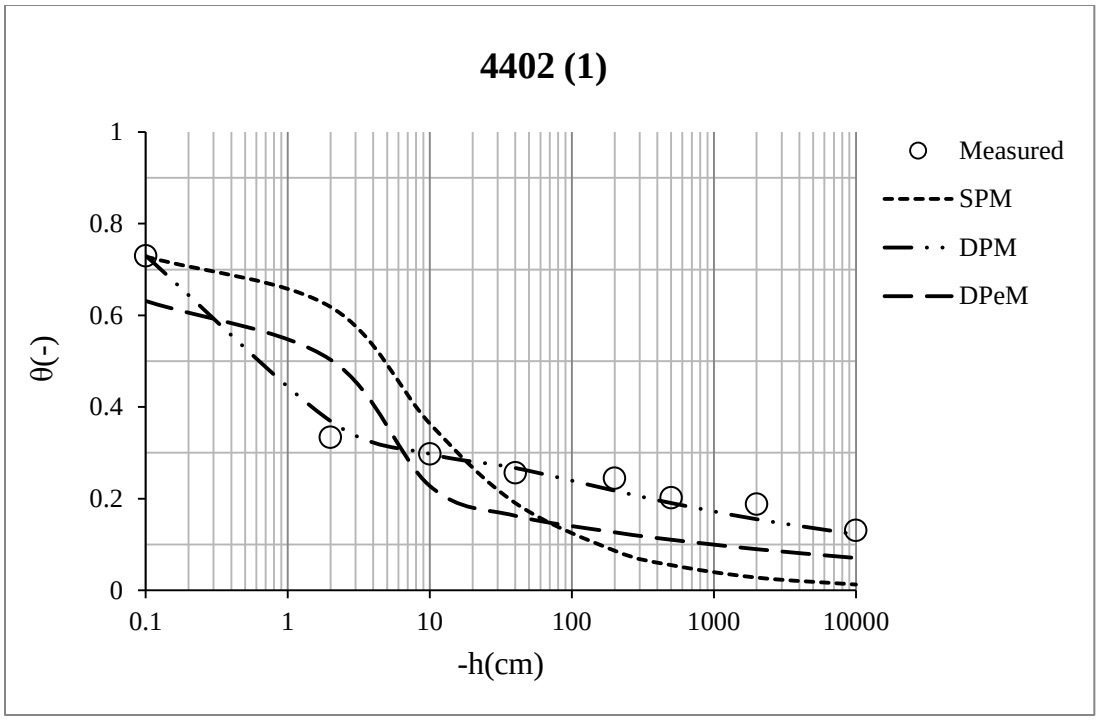
4402 (1)
θ(-)
1
0.8
0.6
0.4
0.2
0
0.1
1
10
100
1000
10000
-h(cm)
Measured
SPM
DPM
DPeM

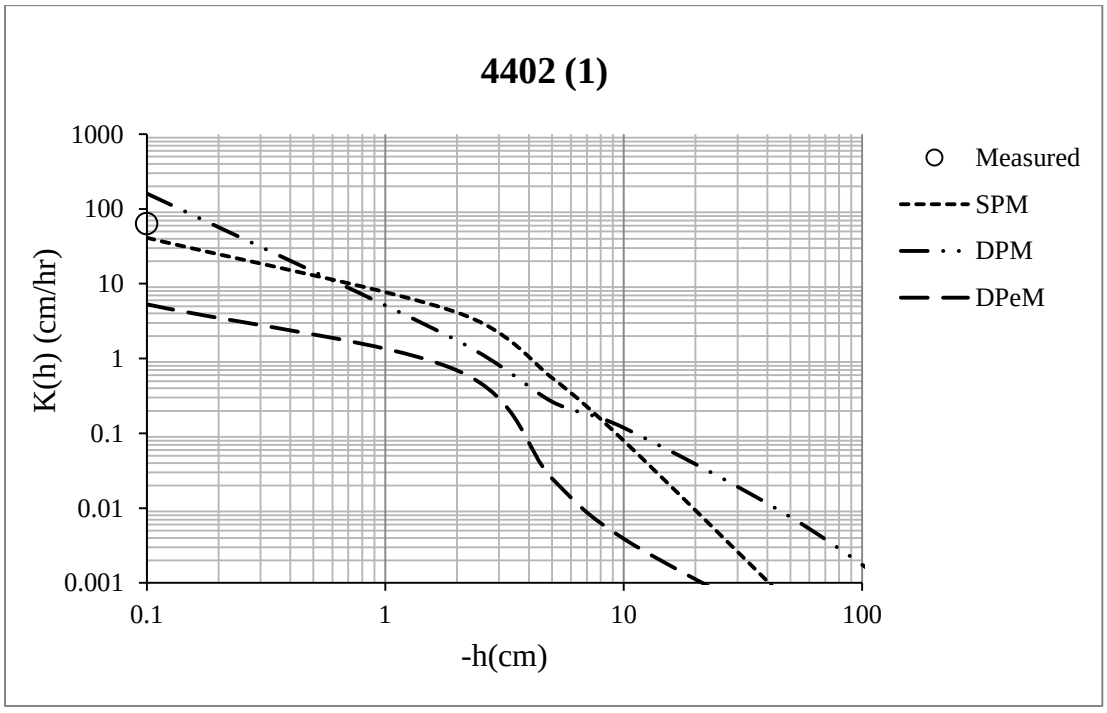
4402 (1)
K(h) (cm/hr)
1000
100
10
1
0.1
0.01
0.001
0.1
1
10
100
-h(cm)
Measured
SPM
DPM
DPeM

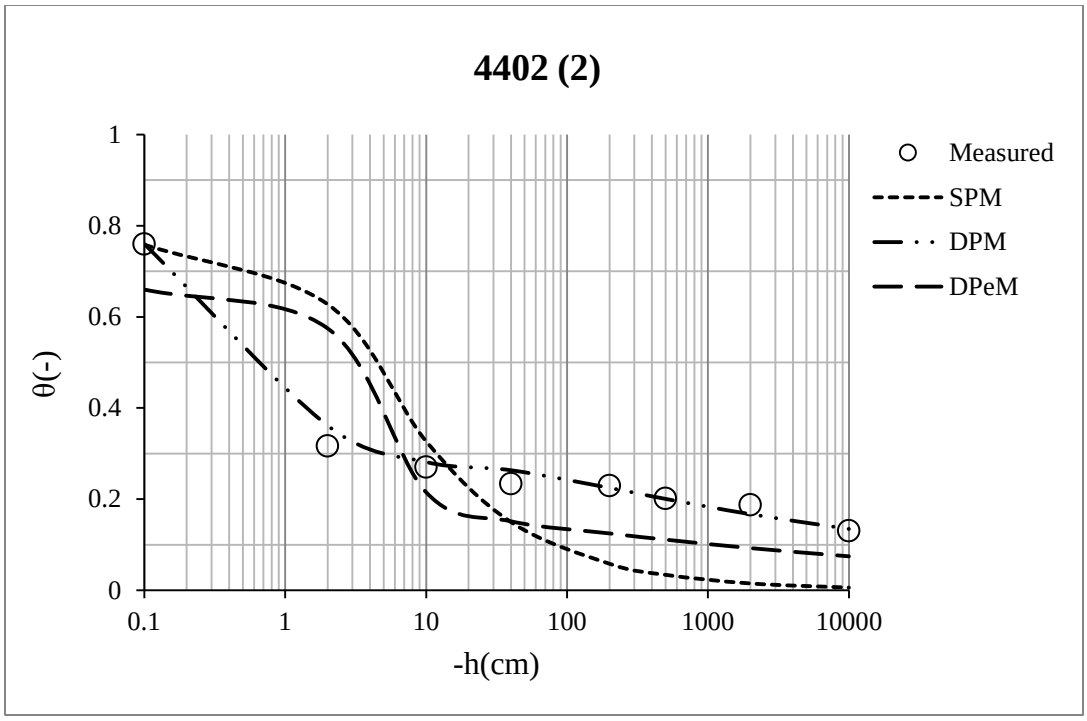
4402 (2)
θ(-)
1
0.8
0.6
0.4
0.2
0
0.1
1
10
100
1000
10000
-h(cm)
Measured
SPM
DPM
DPeM

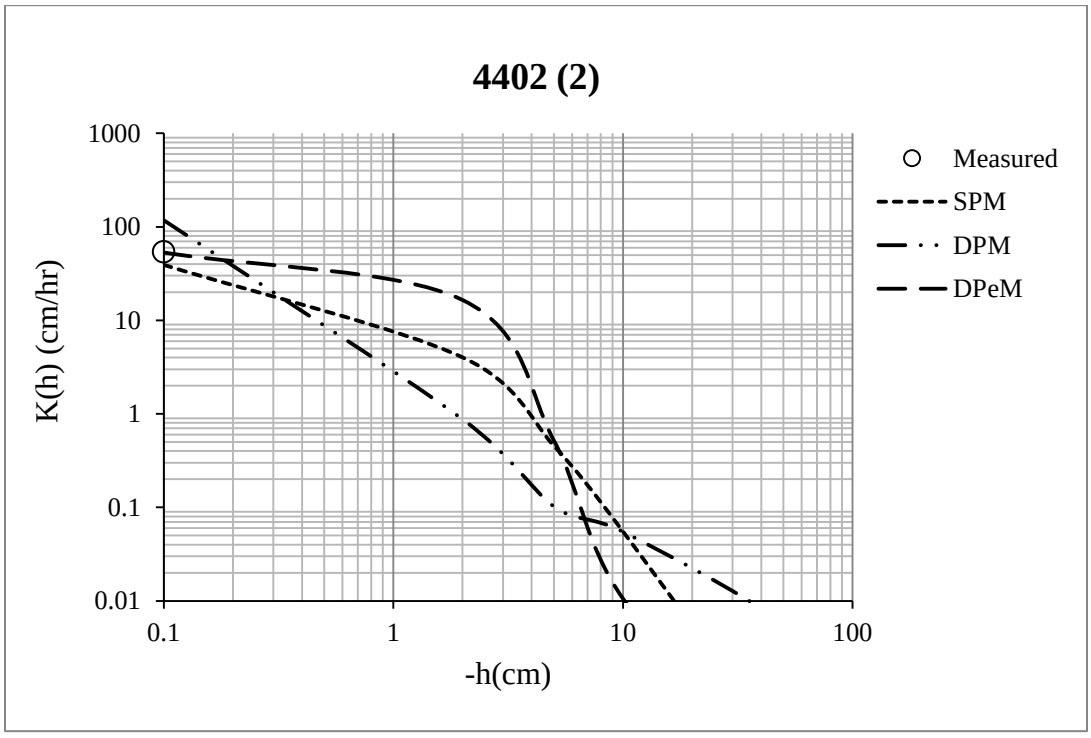
4402 (2)
K(h) (cm/hr)
1000
100
10
1
0.1
0.01
0.1
1
10
100
-h(cm)
Measured
SPM
DPM
DPeM

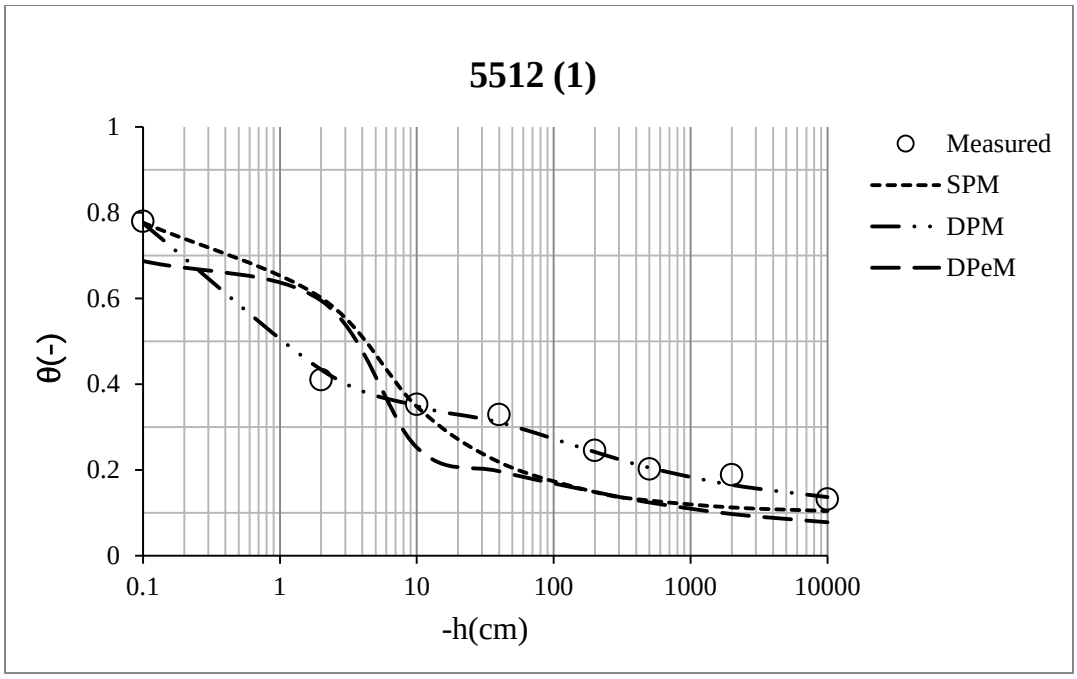
5512 (1)
θ(-)
1
0.8
0.6
0.4
0.2
0
0.1
1
10
100
1000
10000
-h(cm)
Measured
SPM
DPM
DPeM

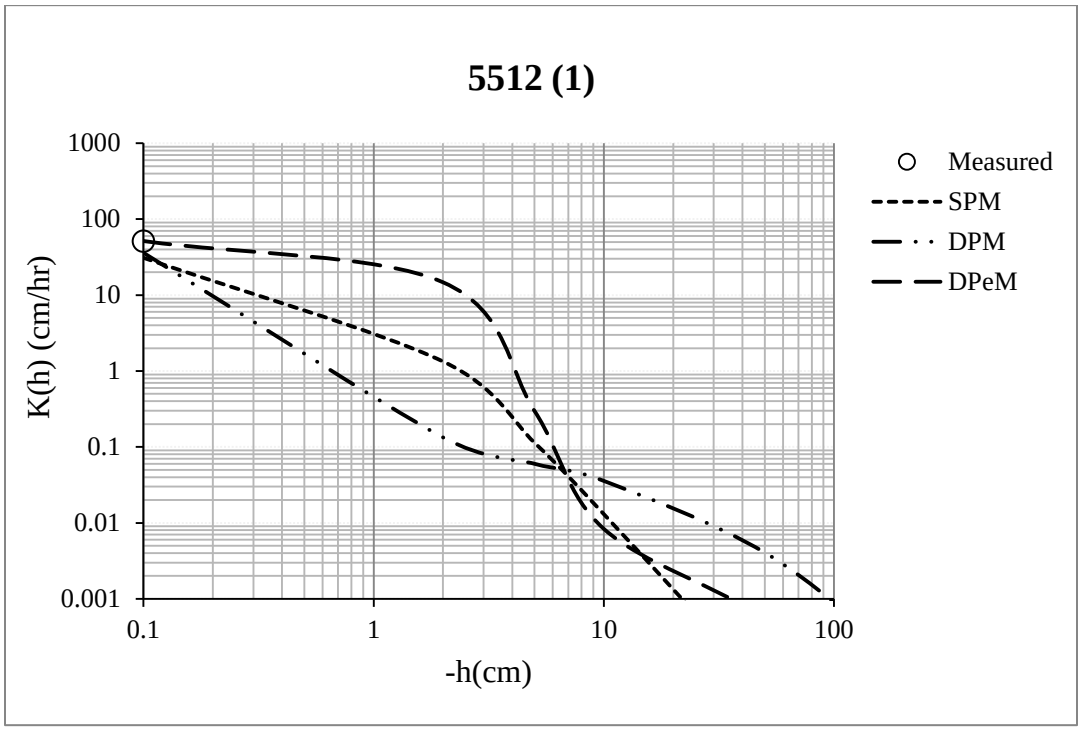
5512 (1)
K(h) (cm/hr)
1000
100
10
1
0.1
0.01
0.001
0.1
1
10
100
-h(cm)
Measured
SPM
DPM
DPeM

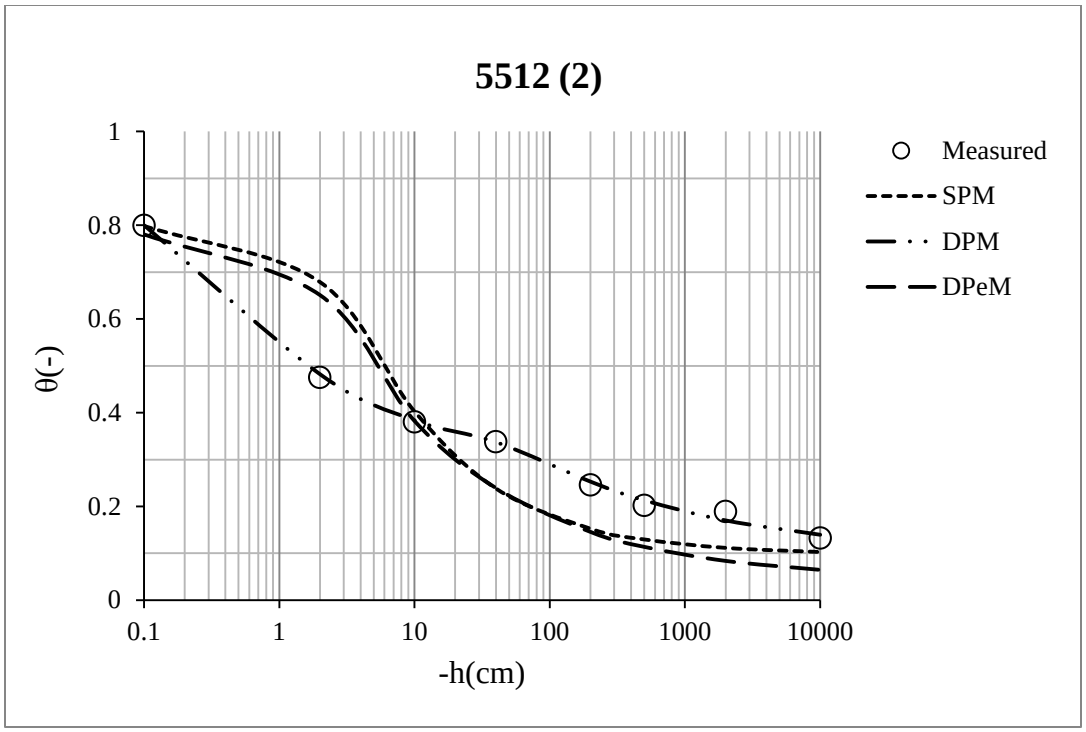
5512 (2)
θ(-)
-h(cm)
Measured
SPM
DPM
DPeM
1
0.8
0.6
0.4
0.2
0
0.1
1
10
100
1000
10000

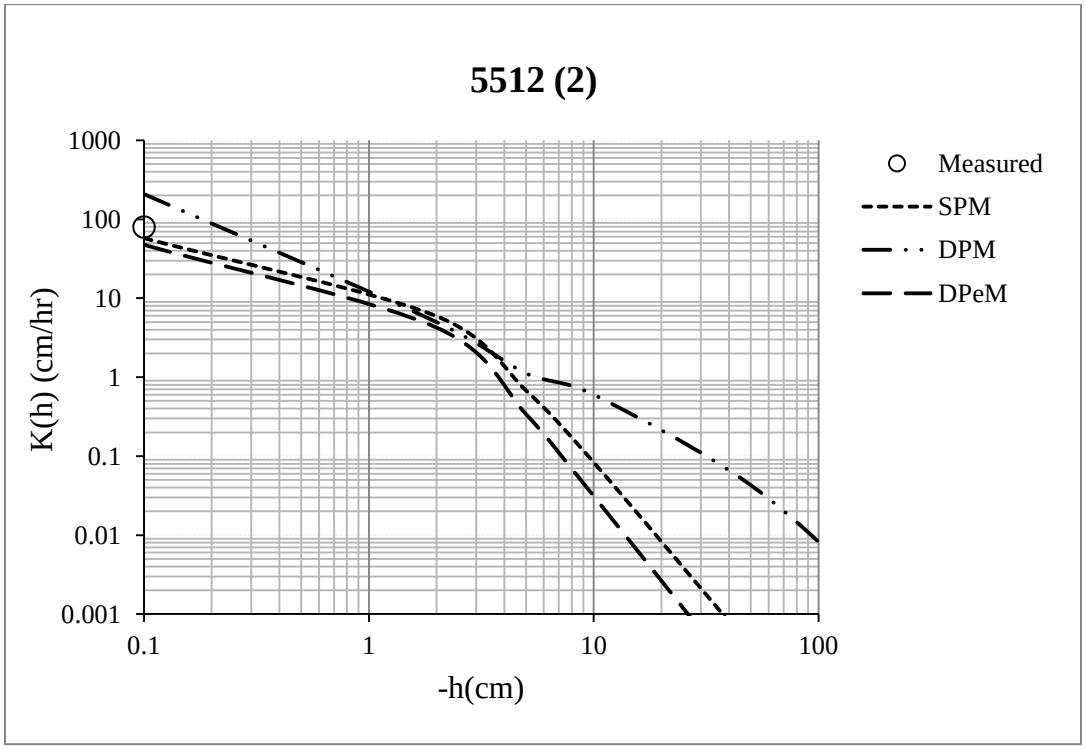
5512 (2)
K(h) (cm/hr)
-h(cm)
Measured
SPM
DPM
DPeM
1000
100
10
1
0.1
0.01
0.001
0.1
1
10
100

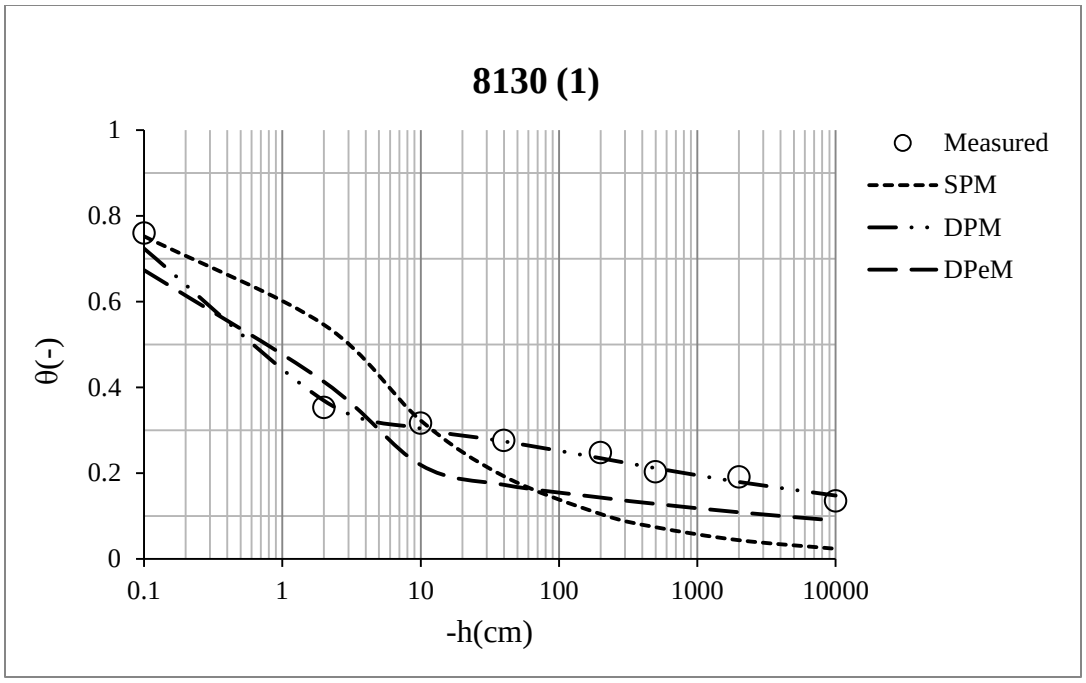
8130 (1)
θ(-)
1
0.8
0.6
0.4
0.2
0
0.1
1
10
100
1000
10000
-h(cm)
Measured
SPM
DPM
DPeM

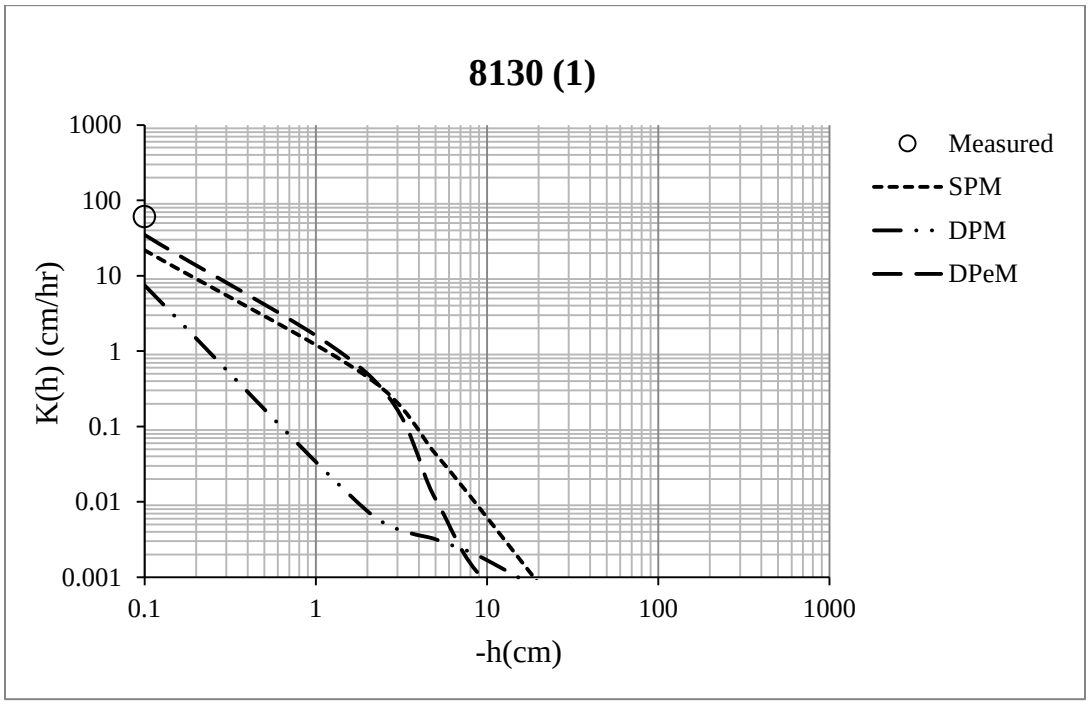
8130 (1)
K(h) (cm/hr)
1000
100
10
1
0.1
0.01
0.001
0.1
1
10
100
1000
-h(cm)
Measured
SPM
DPM
DPeM

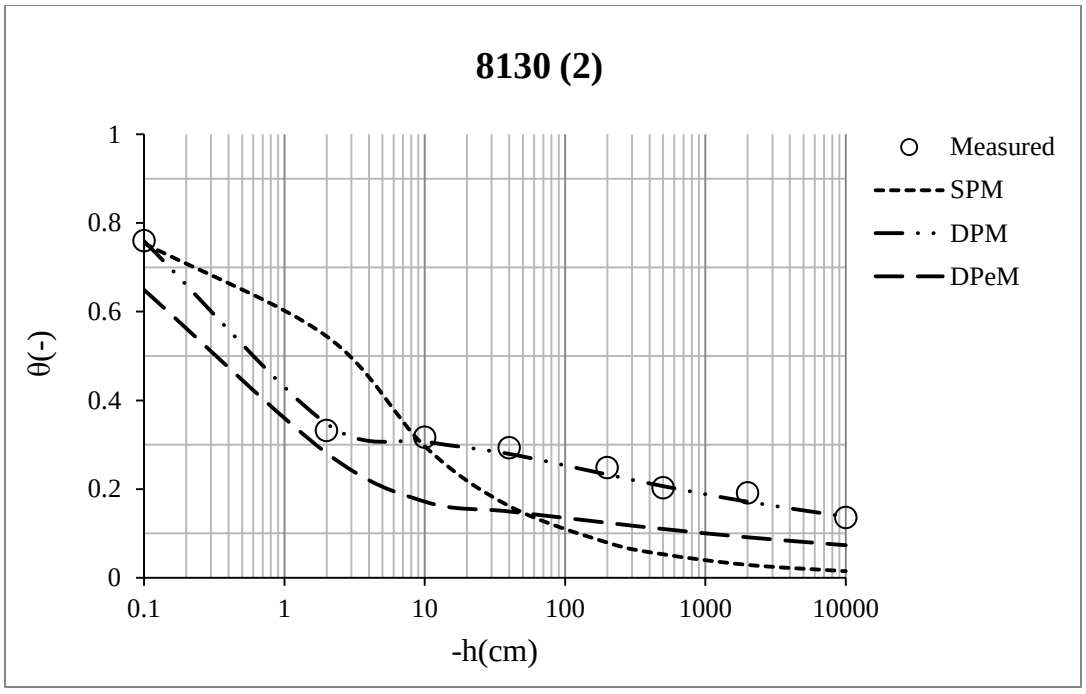
8130 (2)
θ(-)
1
0.8
0.6
0.4
0.2
0
0.1
1
10
100
1000
10000
-h(cm)
Measured
SPM
DPM
DPeM

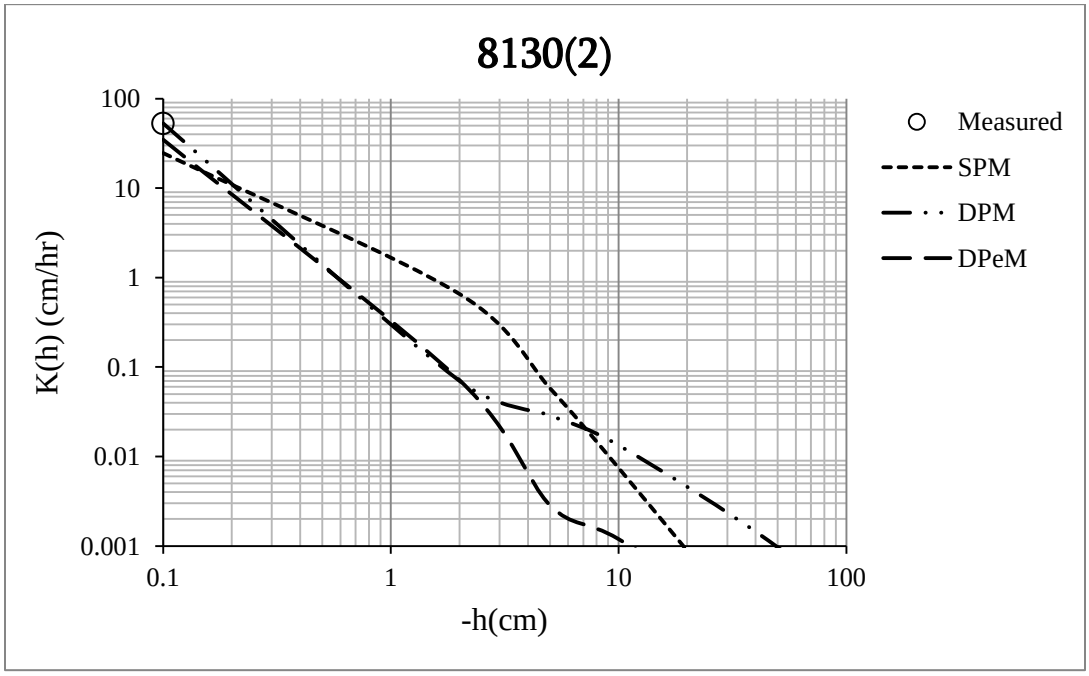
8130(2)
K(h) (cm/hr)
100
10
1
0.1
0.01
0.001
0.1
1
10
100
-h(cm)
Measured
SPM
DPM
DPeM